CHALMERS

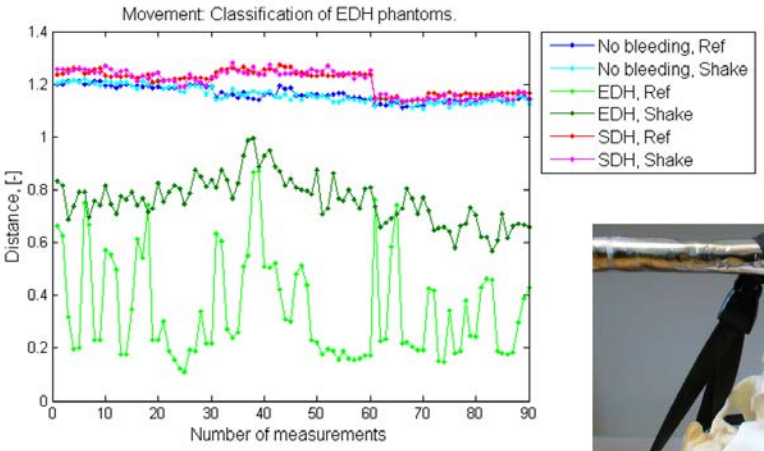

Detection of traumatic epidural and subdural haematomas in brain phantoms using microwave technology

Master's Thesis in Biomedical Engineering

Tora Dunås and Madeleine Kildal Schilliger

Department of Signals & Systems
Chalmers University of Technology
Gothenburg, Sweden June 3, 2013
Master's Thesis 2013:6

Abstract

Traumatic brain injury (TBI) is a worldwide problem with around 10 million serious incidences every year, whereof 22 000 in Sweden. The main causes are road traffic accidents, falls and violence. The most serious complication of a TBI is an intracranial haematoma, which is a bleeding inside the cranium that rapidly can cause fatal complications in the form of ischemia and increased intracranial pressure. A TBI is normally diagnosed at the hospital with computed tomography (CT). However, to be able to give faster and better medical care a portable diagnosis method is needed.

In this project, which is a cooperation between two engineering students and one medical student, the possibility to use microwave technology in the form of a microwave helmet (MWH) to detect intracranial bleedings was investigated. A network analyser with a built in switch was used together with a MWH consisting of twelve antennas. The measurements were performed on phantoms in a human cranium. Two types of common TBI bleedings, epidural and subdural haematomas with the volumes 20, 40 and 60 ml, were modelled. Interfering factors that may affect the measurements were also studied. The measurement data were analysed with a singular value decomposition based classifier. The analyses were focused on classifying phantoms with or without bleeding and with respect to type, volume and location of the bleeding.

Interferences such as a microwave radiation from an active mobile phone or person close to the measurement setup did not significantly affect the measurements. The interference factors that had a visible effect on the measurements were a person holding the measurement cables, presence of a wig of human hair around the cranium and moving the phantoms during the measurements.

The thirteen phantoms that were constructed were not enough to be able to say if the MWH together with the classifier can detect intracranial bleedings. Although some trends can be seen, for example manages the classifier to recognise the individual phantoms, which is an indication that it will be able to recognise bleedings with a larger test set. The interference factors that had a visible effect need to be investigated further and compensated for.

MWT seeems to be a promising technique to detect intracranial bleedins. However a larger data base is needed before it can be completely evaluated.

Sammanfattning

Traumatiska hjärnskador är ett stort problem världen över, med omkring 10 miljoner allvarliga fall varje år, varav 20 000 bara i Sverige. De huvudsakliga orsakerna är trafikolyckor, fallolyckor och misshandel. En av de farligaste komplikationerna av en traumatisk hjärnskada är en intrakraniell blödning. Det är blödningar innanför kraniet som kan ge dödliga komplikationer, så som ischemi och ökat intrakraniellt tryck. Vanligtvis diagnosticeras en traumatisk hjärnskada med hjälp av en CT på sjukhuset, men för att kunna ge snabbare och bättre medicinsk vård behövs en portabel diagnosmetod.

I detta projekt, som är ett samarbete mellan två ingenjörsstudenter och en läkarstudent, undersöktes möjligheten att använda mikrovågsteknik i form av en mikrovågshjälm för att diagnosticera intrakraniella blödningar. En nätverksanalysator med inbyggd switch användes tillsammans med en mikrovågshjälm bestående av tolv antenner för att utföra mätningarna. Mätningarna genomfördes på fantomer i ett mänskligt kranium. Två typer av vanliga blödningar vid traumatiska hjärnskador, epidural- och subduralhematom med volymerna 20, 40 och 60 ml, modellerades. Även störande faktorer som kan påverka mätningarna undersöktes. Mätdatan analyserades med hjälp av en klassificerare baserad på singulärvärdesuppdelning. Analyserna fokuserade på att klassificera fantomer med eller utan blödning, samt med avseende på typ, volym och placering av blödningen.

Störningar av mikrovågsstrålning från en aktiv mobiltelefon eller person som stod nära mätuppställningen gav ingen påverkan. Däremot påverkade störningar i form av en person som håller i mätkablarna, förekomst av en peruk med mänskligt hår runt kraniet och skakning av fantomen under mätningarna.

De tretton fantomerna som gjordes var inte tillräckligt många för att kunna avgöra om mikrovågshjälmen tillsammans med klassificeraren kan detektera blödningar. Vissa trender kunde dock ses, till exempel kunde klassificeraren känna igen individuella fantomer, vilket är en indikation på att den kommer kunna detektera blödningar med en större referensdatagrupp. Störningarna som hade en synlig påverkan behöver undersökas ytterligare och kompenseras för.

Mikrovågsteknik verkar vara lovande för att detektera intrakraniella blödnignar, dock behövs en större databas för att fullständigt kunna utvärdera tekniken.

Preface

Medfield Diagnostics has developed a microwave based product called Strokefinder R10 for diagnosing stroke patients and are right now in the clinical trials. This project investigates the Strokefinder further, to see if it also can be used to diagnose traumatic intracranial bleedings.

This project has mostly been carried out at MedTech West at Sahlgrenska University Hospital in Gothenburg. Measurements have been performed at Medfield Diagnostics and Chalmers University of Technology.

This project was a cooperation with medical student Philip Swahn, whom we would like to thank for his work with the phantoms.

We would also like to thank our supervisors Stefan Candefjord at MedTech West and Stefan Kidborg at Medfield Diagnostics for their help, support and great encouragement throughout the project.

Thanks to Medfield Diagnostics and Dag Jungenfelt, and especially thanks to Gustav Mårtensson and Johan Klingstedt that has helped us a lot with the measurement equipment. Thanks to MedTech West for providing us with a work place and nice work environment.

We would also like to thank Tora's examinator Andreas Fhager and Hana Dobsicek Trefna at the Biomedical Electromagnetics research group at Chalmers for help at the Microwave laboratory and with placement of orders, as well as Tomas McKelvey and Yinan Yu at the Signal Processing research group at Chalmers for providing the classifier used for analysis of the data. Thank to Madeleine's examinator Mats Gustafsson, at the department of Electrical and Information technology at Lund University, for his time.

We would also like to thank neurosurgeons Thomas Skoglund and Johan Ljungqvist at Sahlgrenska University Hospital for advise on the clinical aspects of the project.

Tora Dunås
Madeleine Kildal Schilliger
Gothenburg, June 2013

Contents

List of Figures

List of Tables

Nomenclature

CSF Cerebrospinal Fluid

CT Computed Tomography

DAI Diffuse Axonal Injury

EDH Epidural Haematoma

GCS Glasgow Coma Scale

ICH Intracerebral Haematoma

ICNIRP International Comission on Non-Ionizing Radiation Protection

ICP Intracranial Pressure

MRI Magnetic Resonance Imaging

MWH Microwave Helmet

MWT Microwave Technology

NIRS Near Infrared Spectroscopy

PNA Programmable Network Analyser

SAH Subarachnoid Haemorrhage

SAR Specific energy Absorption Rate

SDH Subdural Haematoma

SVD Singular Value Decomposition

TBI Traumatic Brain Injury

VNA Vector Network Analyser

Chapter 1

Introduction

Around 22 000 people in Sweden suffer every year from a traumatic brain injury (TBI), according to Kleiven et al. [1]. They based their study on data from the years 1987–2000. The incidence rate was stable in this time interval, but the distribution of causes changed, with a decreasing number of traffic accidents and an increasing number of fall accidents. Among these injured people around 800–900 died [2]. Men had a 2.1 times higher risk for head injuries [1] and 2.5 times more men died from TBI compared to women [2]. Children at the age 0–4 years, teenagers at the age 15–19 years and adults aged over 65 years are the most likely to get injured [3].

Worldwide around 10 million serious TBI occurs annually leading to mortality or hospitalisation [4, 5]. Around 57 million people worldwide are living with TBI–related disability [4]. Road traffic accidents are currently the leading cause of TBI in all parts of the world, resulting in 60 % of the injuries [5]. The rest are due to falls (20–30 %), violence (10 %) and a combination of work and sport related injuries (10 %).

The development of an intracranial haematoma is one of the most serious complications of TBI [6]. A haematoma is the general term for escaped and usually clotted blood and intracranial means it is located inside the cranium [7]. Two common intracranial heamatomas are epidural haematoma (EDH) and subdural haematoma (SDH) [8]. It is important to diagnose the traumatic brain injuries and the intracranial haematomas as early as possible to be able to give the best medical care and minimise the risk for permanent damage or death [6]. Today TBI is diagnosed by computed tomography (CT) at the hospital [8]. To be able to give better medical care a portable and faster diagnosis method that could be installed in an ambulance is desired. One promising technique to get faster diagnosis of TBI is microwave technology (MWT).

In this project a microwave helmet (MWH) with 12 antennas, developed at Chalmers University of Technology and Medfield Diagnostics, is used to investigate if MWT can be used as a diagnostic technique for TBI.

This project will continue from the results in the master thesis "Detecting traumatic intracranial bleedings in a brain phantom using microwave technology" by Malik Ahzaz Ahmad [9]. The results by Malik Ahmad show that bleedings could be detected by the MWH in a phantom using a human cranium. The results therefore show potential for the MWH to be able to detect TBI. Now it needs to be investigated further to see if the MWH works for even more realistic phantoms with different types of bleedings in different locations.

1.1 Aim

The aim of this project is to investigate if the MWH can be used to find and localise intracranial bleedings in a human cranium. The method will be a further development from the one used in the master thesis by Malik Ahmad [9]. This will be done by producing a larger number of more anatomically correct phantoms and performing more extensive analyses.

1.1.1 Research questions

- Is it possible to detect a bleeding in a phantom by using a MWH?
- Is it possible to approximate the volume of the bleeding?
- Is it possible to localise the bleeding and to distinguish between EDH and SDH?
- How large is the variation between the MWH measurements and between the measurements where the MWH has been taken off and on again, in relation to the variability for different types and sizes of the bleeding?
- Is it possible to model some anatomically parameters that are thought to give great variability in measurements on different patients, such as the the amount of hair?
- How sensitive is the system for different types of disturbances, such as radiation from mobile phones and shaking the system to simulate ambulance movement?

1.2 Delimitations

- The phantoms used will be of the solid type and made in the same way as in the master thesis by Malik Ahmad [9].

- The MWH provided by Medfield Diagnostics will be used for the measurements. No design changes will be done to the MWH.
- The analyses will be done with the provided in house classifier and no further developments will be performed.

1.3 Division of labor

This master's thesis is part of a collaboration between two engineering students, Tora Dunås and Madeleine Kildal Schilliger, and one medical student, Philip Swahn. Philip Swahn has been responsible for the anatomical design of the phantoms, whereas Tora Dunås and Madeleine Kildal Schilliger have been responsible for the dielectric measurements, MWH measurements and the data analysis.

All construction of the recipes and measurements have Tora Dunås and Madeleine Kildal Schilliger performed together. Tora Dunås has looked more at the raw data from the MWH measurements and Madeleine Kildal Schilliger has looked more at the dielectric data. The classifications have been divided between the two engineering students, but all the discussions have been made together.

Chapter 2

Theory

2.1 Anatomy of the brain

The central nervous system contains the spinal cord and the brain [7]. The brain consists of four main parts; the brain stem, the cerebellum, the diencephalon and the cerebrum, see Figure 2.1. The cerebrum is divided into different parts by shallow grooves on the surface of the brain, these parts are called lobes, see Figure 2.2. The five major lobes are the frontal, parietal, occipital and temporal lobes and the gyri of insula [7].

The brain consists of grey and white matter. Both the cerebrum and the cerebellum have an outer shell, cortex, consisting of grey matter and and inner part consisting of white matter [7]. The amount of white matter is slightly higher than the amuont of grey matter, as seen in Figure 2.3. The different types of matter are made up of different parts of the nerve cells. The nerve cells consists of a cell body, dendrites and an axon, see Figure 2.4 [7]. The cell body consists of a nucleus surrounded by cytoplasm containing the cellular organelles. The dendrites are sites where the cell can receive signals from other neurons. The axon is a long conductor that transmits nerve impulses away from the cell body. Some axons have myelin sheaths around them to increase the speed of an impulse. The speed is increased since the signal can jump in the gaps between the sheaths [7]. The grey matter consists of the cell bodies of the neurons and the white matter is the axons with the myelin sheaths, which gives the white colour [7].

The brain is protected by the skull, the cerebrospinal fluid (CSF) and the meninges [7]. The CSF is the fluid that the brain is covered with. CSF works as a cushion for the brain, but it also helps to nourish, remove waste products and transport hormones [7]. The meninges consist of the dura mater, which is the most external layer, the arachnoid mater that is the middle layer and the pia mater that is the inner layer, see Figure 2.5 [7].

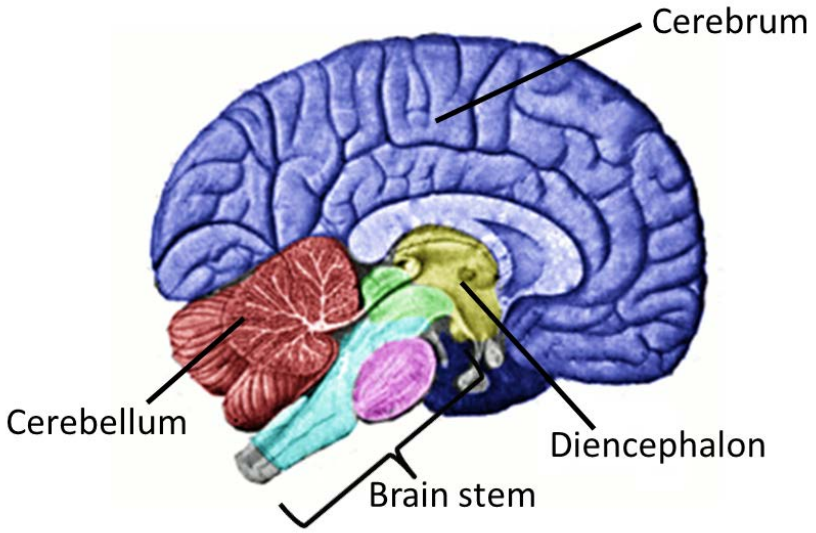

Figure 2.1: The main parts of the brain. (Source (2011-09-30): `http://en.wikipedia.org/wiki/File:Vertebrate-brain-regions_small.png`)

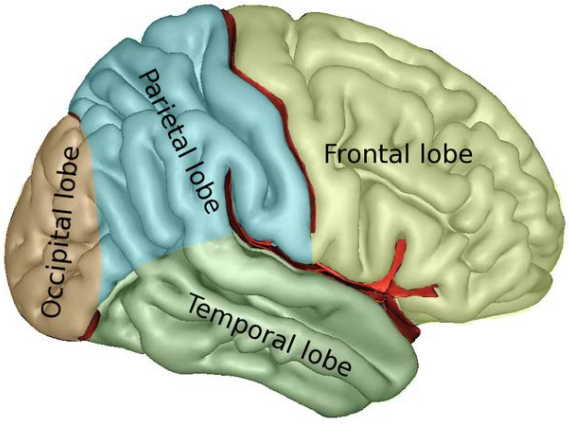

Figure 2.2: The different lobes of the brain. The gyri of insula lies in the middle of the brain and can not be seen in the figure. (Source: Sebastian023 (2012-09-02): `http://en.wikipedia.org/wiki/File:LobesCaptsLateral.png`)

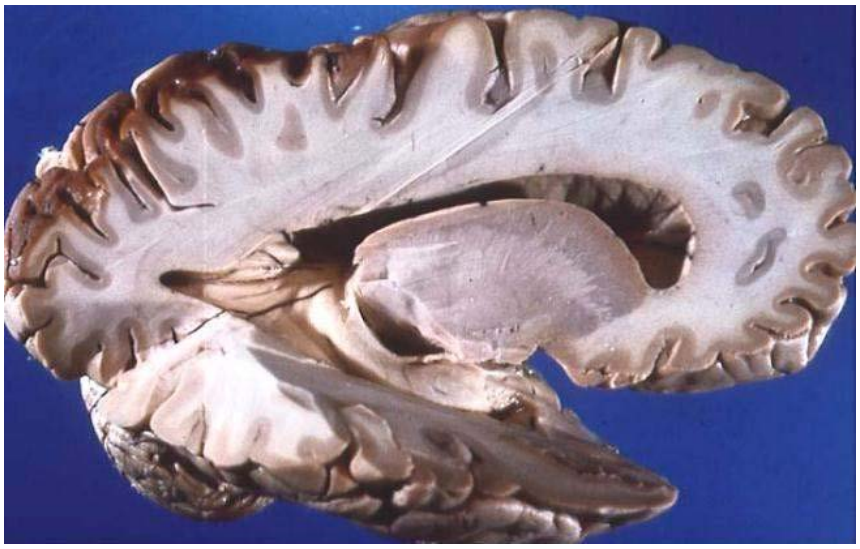

Figure 2.3: Lateral view of a dissected brain where the amount of white and grey matter can be seen. (Source: John A Beal, PhD Dep't. of Cellular Biology & Anatomy, Louisiana State University Health Sciences Center Shreveport (2005-11-30): `https://commons.wikimedia.org/wiki/File:Human_brain_right_dissected_lateral_view.JPG`)

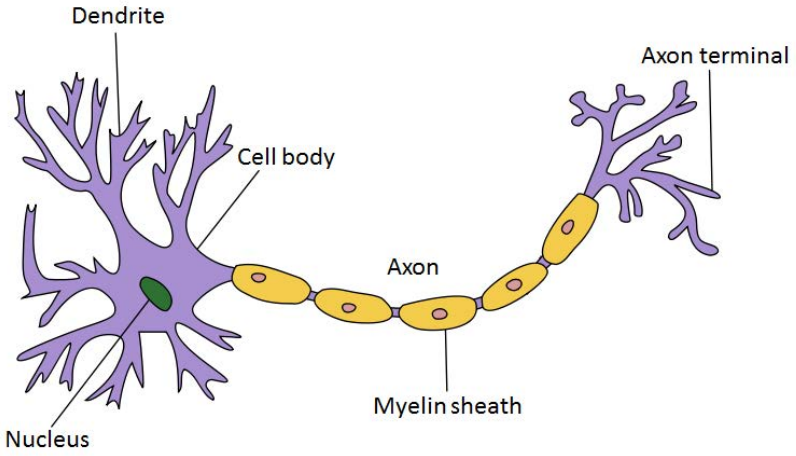

Figure 2.4: Schematic picture of a nerve cell. (Source: Quasar Jarosz at en.wikipedia (2009-08-11): `http://en.wikipedia.org/wiki/File:Neuron_Hand-tuned.svg`)

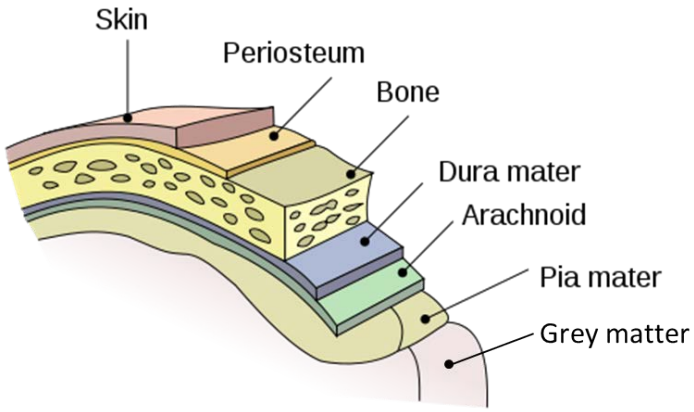

Figure 2.5: The meninges and other layers that protect the brain. (Source: "SVG by Mysid, original by SEER Development Team"(Retrieved 2013-01-30): `http://en.wikipedia.org/wiki/File:Meninges-en.svg`)

2.2 Traumatic brain injuries

TBI is a critical public health problem and a major cause of death and disability worldwide [5]. A TBI can occur when the head is subject to an external force, either as a direct hit, a penetrating force or a strong acceleration [8]. For infants, the most common cause of TBI is physical abuse, for small kids and elderly people it is fall accidents, for older kids sport injuries, and for teenagers and young adults traffic accidents [10].

The injuries can be divided into minor, mild, moderate and severe TBI depending on consciousness [10]. Mild injuries are the most common types, but they are also the least well understood, since they can cause severe problems for the patient even though the CT-image of the brain looks normal.

TBI can be divided into primary and secondary injuries [10]. Primary injuries, such as bleeding and tissue damage are caused by the force at the initial trauma and consist of physical damage on the brain tissue. Secondary injuries occur later on and include swelling, bleeding, ischemia, etc. This division is not absolute since TBI is a dynamic process. The primary injuries are considered irreversible, but secondary injuries can be prevented with good hospital care [10]. In the primary stage, the most common reasons of death is brain damage and loss of blood [11]. In the later stage, it is damages from increased intracranial pressure (ICP), lowered blood pressure and lowered oxygen level in the brain that is the main cause of death. When a TBI occurs, the pressure inside the skull increases which can cause a lot of different problems, such as cerebral herniation, which is an acute life

threatening condition were the brain is pressed out through openings in the cranium [11].

An injury that can be both primary and secondary is intracranial bleeding. It can be divided into extracerebral and intraaxial bleedings, where the former appears between the meningues outside of the brain (see Figure 2.5), and the later on the surface or deeper into the brain [8]. An EDH ia a bleeding that occurs between the skull and the dura mater, see Figure 2.6. If the bleeding occurs underneath the dura, above the arachnoid matter, it is an SDH, see Figure 2.6 [8]. These injuries are both common and dangerous, and since they are placed outside the brain, it is possible to evacuate them surgically in an acute stage. The blood in the EDH comes mainly from the arteries, and there are usually fractures in the skull close to the bleeding and the blood stays quite close to the site of injury [8]. SDH is mainly venous and it spreads out across the surface of the brain, but does not expand to the other hemisphere. Both EDH and SDH can be operated but the prognosis for EDH is better than for SDH [8]. EDH usually have a fast development while SDH have a slower progress [12]. SDH that becomes symptomatic within three days are classified as acute, within 21 days as subacute and if it takes longer time, it is chronic [12]. SDH usually origins from torsion of bridging veins that goes through the dura mater to transport blood away from the brain. EDH usually forms in the temporal and parietal lobes, see Figure 2.2, and is typically caused by a blow to the head that fractures the temporal bone, see Figure 2.7 [12].

Some other types of intracranial bleedings are subarachnoid haemorrhage (SAH), contusions, intracerebral haematoma (ICH) and diffuse axonal injury (DAI). SAH is a bleeding below the arachnoid matter and is, just as SDH and EDH, classified as extracerebral. SAH is usually caused by a bleeding contusion. A contusion is an injury on the surface of the brain that can be bleeding or non-bleeding and is usually located near bony outgrowth of the skull [8]. ICH is a bleeding inside the brain, usually quite superficial, see Figure 2.6. It occurs when blood vessels are torn, usually due to fast decelerations for example in traffic accidents [8]. In DAI the axons in the brain are torn due to shear stress. The shear stress usually occurs at the border between white and grey matter, since the tissue have different densities, and is due to acceleration, deceleration or rotation of the brain [8].

2.3 Diagnostic methods

For open injuries where the skull is penetrated, the existence of a TBI is obvious since it can be directly seen, but the severity and extent of the

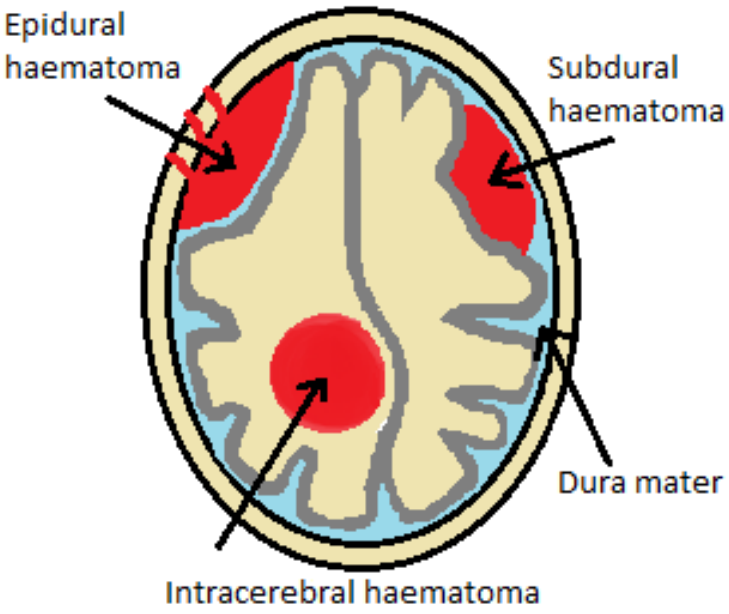

Figure 2.6: Sketch over the different bleeding types EDH, SDH and ICH. These are only examples and do not represent a real injury.

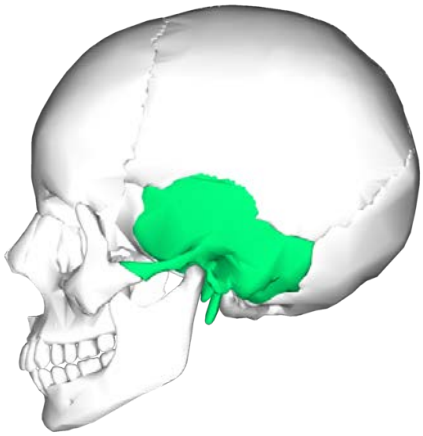

Figure 2.7: Position of the temporal bone (shown in green). (Source:21 January 2013 "BodyParts3D, ©The Database Center for Life Science licensed under CC Attribution-Share Alike 2.1 Japan.": `http://en.wikipedia.org/wiki/File:Temporal_bone_lateral5.png`)

injury still needs to be determined. For closed injuries, the diagnosis might be harder. If no injury can be seen on the surface of the head, internal damages might go unnoticed [10]. This is often the case for more severe injuries where the damage is underestimated and time is lost by sending the patient to the wrong hospital or department [13].

One way to determine the severity of a brain injury is by the Glascow Coma Scale (GCS) [8] where the motor response, verbal response and eye opening response is graded on a scale and summed to get a total score [14]. If the person is already intubated, or for some other reason not able to fully interact, it can be hard to obtain the GCS-score [8].

2.3.1 Computed tomography

To make a more detailed diagnosis, imaging of the brain is needed, this is done with CT. To perform a CT is a standard procedure for head injuries, but it is always a consideration if it should be done or not. Some risk factors that motivates the use of CT are if the patient is over 60 years old, have experienced amnesia, loss of consciousness or have an alcohol or drug problem [8].

In CT X-ray radiation is used to investigate the degree of attenuation in different areas of the body. Since this spectrum is quite wide and even small differences can be of interest, window functions can be applied to the image [8]. A window function enhances the contrast for values of attenuation close to that of the tissue of interest [15]. A window adapted for bone is used to find fractures in the skull, while a window adapted for brain tissue is used to study abnormalities inside the brain [8]. If the bleeding occurs close to the bone, it can be hard to distinguish with the brain window and in that case a soft tissue window can be useful [8]. A blood clot has a higher attenuation than the surrounding tissue and appears as a white dot on the CT. Unclotted blood does also appear white, but not as intense [16]. An oedema or ischemic region where the blood supply is reduced appears darker. An example of a CT image of a SDH can bee seen in Figure 2.8.

Another thing that is studied in the CT image is if the brain is shifted to one side, called the midline shift, see Figure 2.8. This shift is related to the ICP, the more shifted the brain is to one side, the larger the pressure is [16]. This relation is not absolute. If the bleeding is not restricted to one side of the head, or the blood is spreading out into a wider area, the ICP might be high without any noticeable midline shift [16].

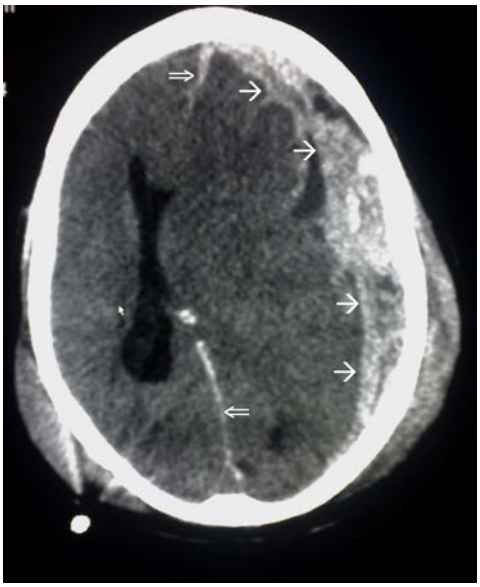

Figure 2.8: CT scan showing the spread of a SDH (single arrows) and a midline shift (double arrows). (Source:2007-06-24 17:16 Glitzy queen00 at Wikipedia: `http://en.wikipedia.org/wiki/File:Trauma_subdural_arrows.jpg`)

2.3.2 Magnetic resonance imaging

If the CT does not give any clear result or the long term effects are of interest, magnetic resonance imaging (MRI) is used. It has a higher sensitivity and gives a more detailed picture [16]. MRI is also better at imaging injuries in the inner parts of the brain. The reason it is not used in the acute cases is that it takes longer time than a CT and is usually not available on short notice [16].

To see how the injury has affected the brain function of the patient, the physiology of the brain, such as the metabolism and blood flow, must be examined. This can be done in many ways, such as functional MRI, perfusion CT or proton emission tomography (PET) [16].

2.3.3 Near infrared spectroscopy

The Infrascanner is a new technology that is based on the near infrared spectroscopy (NIRS) technique [17]. Light with a wavelength of 808 nm is used to detect traumatic haematomas in the head [17]. The technique is based on the principle that the higher concentration of haemoglobin in the haematoma absorbs more light than the normal brain tissue. The absorption of the different sides of the head are compared to each other. In normal

condition head is assumed to be symmetrical, so if there is a great enough difference it could indicate a haematoma [17]. The sensor device consists of a NIRS diode laser and a detector that measures the reflected light intensity [17]. The penetration depth is 2–3 cm and measurable width is around 2 cm [17]. The exam lasts for 3 min and four predefined points at opposite positions on each side of the head is examined using a handheld device.

2.3.4 Ultrasound

Ultrasound is normally not used in diagnosing TBI, since human bones attenuates the sound waves too much [18]. Instead it can be used during brain surgery and the removal of deep seated haematomas [19]. In brain surgery the problem with the bone is avoided, since parts of the cranium is removed during the surgery. It is possible to detect a midline shift with ultrasound, by using transcranial colour-coded duplex sonography (TCCS) through the thinner temporal bone in the head, see Figure 2.7 [20].

2.4 Microwave technology

Another future technique that can be used to detect TBI is MWT. This section explains what MWT is, how it works, how it is used and some safety guidelines that needs to be considered when using it.

2.4.1 Microwaves

Microwaves are electromagnetic radiation with a wavelength of between 1 mm and 1 m in vacuum, which corresponds to a frequency of 300 MHz to 300 GHz, the wavelength in air is practically the same [21]. Electromagnetic waves have one electric and one magnetic component, perpendicular to each other. The waves make up an electric and a magnetic field, and the propagation of these fields depends on the dielectric properties of the medium. This field propagation can be described by Maxwell's equations, see Equation (2.1)–(2.4) [21].

$$\nabla \times \mathbf{E} = \frac{-\partial \mathbf{B}}{\partial t} - \mathbf{M} \qquad \text{Faraday's Law of induction} \qquad (2.1)$$

$$\nabla \times \mathbf{H} = \mathbf{J} + \frac{\partial \mathbf{D}}{\partial t} \qquad \text{Ampere's Law} \qquad (2.2)$$

$$\nabla \cdot \mathbf{D} = \rho \qquad \text{Gauss's Law for electricity} \qquad (2.3)$$

$$\nabla \cdot \mathbf{B} = 0 \qquad \text{Gauss's Law for magnetism} \qquad (2.4)$$

E and **H** are the electric and magnetic field respectively, **D** and **B** the electric and magnetic flux density, **J** and **M** the electric and magnetic current density and ρ the total charge density [21]. To relate these equations to the properties of the material in which the field propagates, these constitutive relations are needed

$$\mathbf{D} = \epsilon\mathbf{E} \tag{2.5}$$

$$\mathbf{B} = \mu\mathbf{H} \tag{2.6}$$

$$\mathbf{J} = \sigma\mathbf{E}, \tag{2.7}$$

where ϵ is the permittivity, μ the permeability and σ the conductivity of the material. These three properties are usually refered to as the dielectric properties of the material. Equation (2.8) is the continuity equation that follows from Maxwells equation, this equation is particularly important for non-linear materials [21].

$$\nabla \cdot \mathbf{J} = -\frac{\partial \rho}{\partial t} \tag{2.8}$$

When a dielectric material is exposed to an electric field, the atoms and molecules of the material are polarised, creating a dipole moment that increases the electric flux [21]. For free space, Equation (2.5) looks like $\mathbf{D} = \epsilon_0\mathbf{E}$ where $\epsilon_0 = 8.854 \cdot 10^{-12}\,\mathrm{F\,m^{-1}}$, for other media the permittivity is a complex number

$$\epsilon = \epsilon' - j\epsilon'', \tag{2.9}$$

where the imaginary part accounts for heat loss due to damping of the vibrating dipole moments. The conductivity σ does also impact the material loss [21]. If an $e^{j\omega t}$ time dependency is assumed, all time derivatives in the Equations (2.1), (2.2) and (2.8) can be replaced by $j\omega$, where ω is the angular frequency $\omega = 2\pi f\,\mathrm{rad\,s^{-1}}$.

The conductivity of a material can be calculated from the imaginary part of the permittivity and the angular frequency as

$$\sigma = \omega\epsilon''. \tag{2.10}$$

The complex relative permittivity $\hat{\epsilon}$ can be expressed as

$$\hat{\epsilon} = \frac{\epsilon' - j\epsilon''}{\epsilon_0} = \epsilon_r - \frac{j\epsilon''}{\epsilon_0}\ \text{[21]}. \tag{2.11}$$

This can be calculated for different tissues from the 4-Cole–Cole dispersion model, see Equation (2.12), using the parameters from Gabriel et al. [22].

$$\hat{\epsilon}(\omega) = \epsilon_\infty + \sum_{n=1}^{4} \frac{\Delta\epsilon_n}{1 + (j\omega\tau_n)^{(1-\alpha_n)}} + \frac{\sigma_i}{j\omega\epsilon_0} \tag{2.12}$$

Where τ is the relaxation time of the material, ϵ_∞ the permittivity at high frequencies ($\omega\tau \gg 1$), $\Delta\epsilon_n = \epsilon_\infty - \epsilon_s$ the difference between permittivity at high and low frequencies ($\omega\tau \ll 1$), α the broadening of the dispersion area and σ_i the static ionic conductivity [22]. The conductivity σ of the material can then be calculated from the imaginary part of $\hat{\epsilon}$, using Equation (2.10). The dielectric properties for different tissues, calculated from the 4–Cole–Cole dispersion model using the parameters from Gabriel et al. [22] and Kaatze [23], can be seen in Figure 2.9.

The propagation of plane electromagnetic waves in lossless medium can be described by the propagation constant k and the wave impedance η, see Equations (2.13) and (2.14) where λ is the wavelength and v the speed of the wave [21].

$$k = \frac{2\pi}{\lambda} = \frac{\omega}{v} = \omega\sqrt{\epsilon\mu} \tag{2.13}$$

$$\eta = \frac{\omega\mu}{k} = \sqrt{\frac{\mu}{\epsilon}} \tag{2.14}$$

When a plane electromagnetic wave is travelling through lossy medium, the conductivity comes into account and the propagation constant and wave impedance becomes complex. The complex propagation constant is denoted γ and is defined by Equation (2.15). The wave impedance, η, is redefined by Equation (2.16) [21].

$$\gamma = j\omega\sqrt{\epsilon'\mu}\sqrt{1 - j\frac{\sigma}{\omega\epsilon'}} \tag{2.15}$$

$$\eta = \frac{j\omega\mu}{\gamma} = \sqrt{\frac{\mu}{\epsilon - j\frac{\sigma}{\omega}}} \tag{2.16}$$

The wave impedance, η, relates the electric and magnetic field strengths to each other. In free space the intrinsic impedance is denoted η_0, see Equation (2.17), where $\sigma = 0$ [21].

$$\eta_0 = \sqrt{\frac{\mu_0}{\epsilon_0}} \approx 377\Omega \tag{2.17}$$

The case when an electromagnetic wave E_i comes in normal to a material border is illustrated in Figure 2.10a. Some part, E_t, of the wave will propagate into material 2, but some, E_r, will be reflected at the border and continue to travel in material 1, but in the backward direction [24]. In an object with several material borders this phenomenon will happen at each border. The electromagnetic wave will scatter according to Snell's law if it has an oblique incidence to the border, see Figure 2.10b and Equation (2.18) and (2.19).

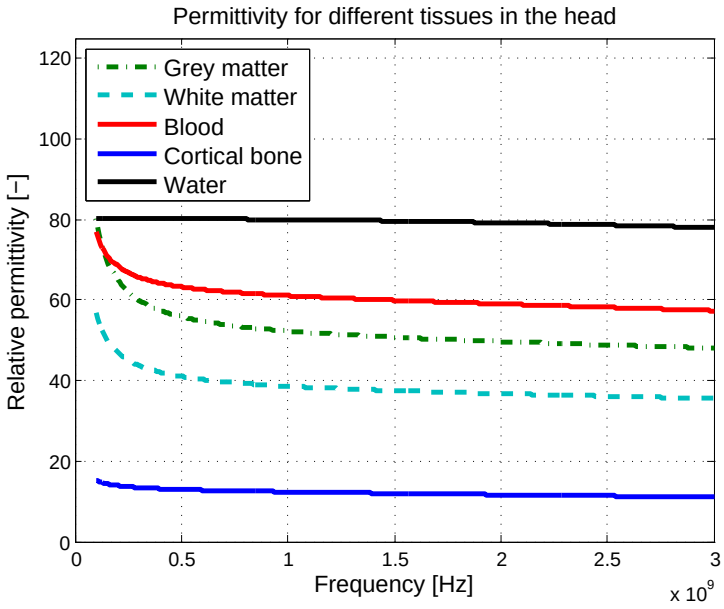

(a) Relative permittivity

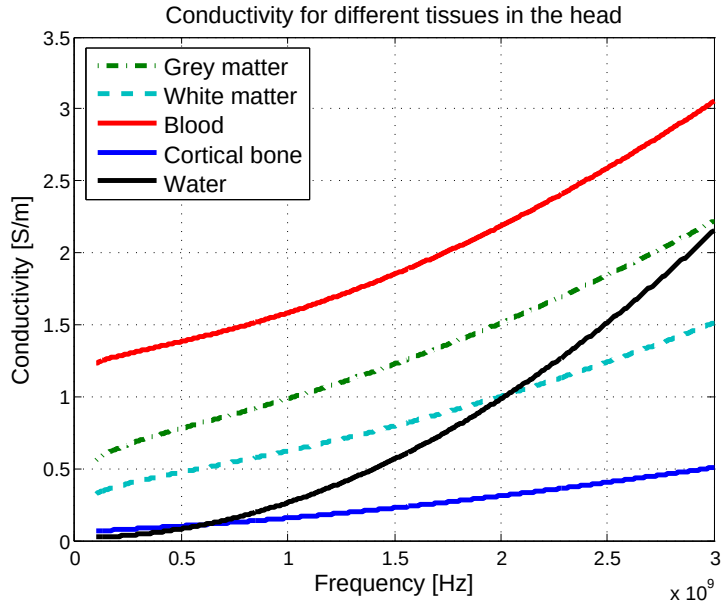

(b) Conductivity

Figure 2.9: Dielectric properties for different tissues in the head. Calculated with the 4-Cole–Cole dispersion model using the parameters from Gabriel et al. [22] and Kaatze [23].

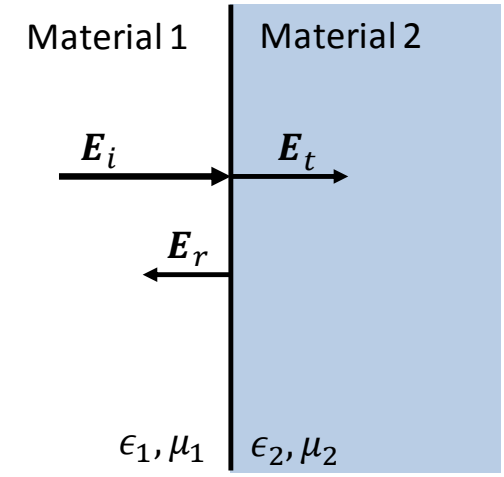

(a) Electromagnetic wave with normal incidence at a material border.

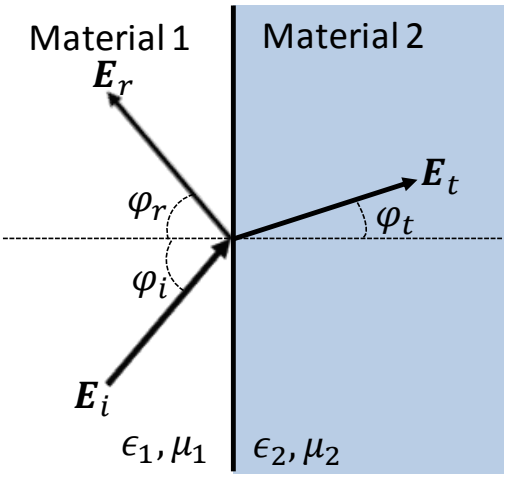

(b) Electromagnetic wave with oblique incidence at a material border.

Figure 2.10: Electromagnetic wave at a material border. 2.10a: Electromagnetic wave with normal incidence that is reflected and transmitted through a material border. 2.10b: Electromagnetic wave with an oblique incidence that is scattering at a material border. E_i, E_t and E_r are the incident, transmitted and reflected wave. ϵ and μ are the permittivity and permeability of the materials. φ_i, φ_r and φ_t are the angles for the incident, reflected and transmitted waves.

$$\varphi_i = \varphi_r \tag{2.18}$$

$$k_1 \sin(\varphi_i) = k_2 \sin(\varphi_t) \tag{2.19}$$

Where φ_i, φ_r and φ_t are the angles for the incident, reflected and transmitted waves. The propagation constants k_1 and k_2 are defined by Equation (2.13) and are the constants for material 1 and material 2, respectively.

The amount of reflection can be expressed with the reflection coefficient Γ. The reflection coefficient is the ratio between the incident and the reflected wave, see Equation (2.20) [24].

$$\Gamma = \frac{E_r}{E_i} = \frac{\eta - \eta_0}{\eta + \eta_0} \tag{2.20}$$

The return loss is the magnitude of the reflection coefficient expressed in dB, see Equation (2.21) [25]. The return loss is how many dB:s that the reflected signal is below the incident signal. The return loss is always denoted as a positive number, so therefore an extra minus sign is added in Equation (2.21) [25].

$$\text{Loss}_{\text{return}} = -20 \cdot \log_{10}(|\Gamma|) \tag{2.21}$$

The transmission T is how much of the signal that is transmitted through the medium and is calculated with Equation (2.22) [21].

$$T = 1 + \Gamma = \frac{2\eta}{\eta + \eta_0} \tag{2.22}$$

The magnitude of the transmitted voltage will be lower than the incident voltage for tissue, and the material will then exhibit insertion loss. The insertion loss is the magnitude of the transmission coefficient expressed in dB, see Equation (2.23) [25]. Also here a minus sign is added to the equation to get a positive dB-number on the loss.

$$\text{Loss}_{\text{insertion}} = -20 \cdot \log_{10}(|T|) \tag{2.23}$$

It is not only the amplitude of the reflected and transmitted signals that matters, the phase may also contain some information about the materials. The phase of a wave is a relative property, i.e. it can only be defined in relation to another wave of the same wavelength. When the microwave signal is transmitted through a material, it might be shifted in comparison to its original propagation, due to difference in propagation speed [21]. This shift is described as an angle θ, which is illustrated in Figure 2.11.

In lossy media there is a limitation of how deep the electromagnetic waves can penetrate, this can be described by the skin depth, δ_s [21]. The

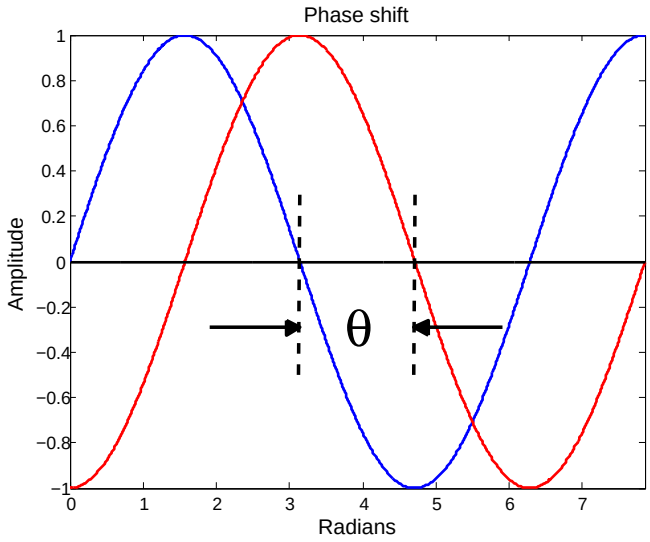

Figure 2.11: Illustration of a $\pi/2$ phase shift.

skin depth for lossy materials can be calculated by using Equation (2.24), where γ is the value from Equation (2.15). In lossless materials, the skin depth goes towards infinity [21]. The skin depth for different tissues, calculated from the 4–Cole–Cole dispersion model using the parameters from Gabriel et al. [22] and Kaatze [23], can be seen in Figure 2.12.

$$\delta_s = \frac{1}{Re\{\gamma\}} \tag{2.24}$$

When measuring with the MWH, electromagnetic waves will be sent from an antenna and go through different materials with different dielectric properties, see Figure 2.9, in the phantom. The waves will scatter at the interface between the borders of the different materials, some part of the waves will be reflected and some will propagate through the medium and be transmitted to the other side. The scattering comes from the fact that the electromagnetic waves in the MWH will in most cases be incident at an angle to the border. The waves will also be attenuated since tissue is a lossy medium [22] and there will be a change in amplitude and phase of the waves. The skin depth of the electromagnetic waves will be different depending on what frequency they have, so some waves will penetrate deep and some will not penetrate so deep.

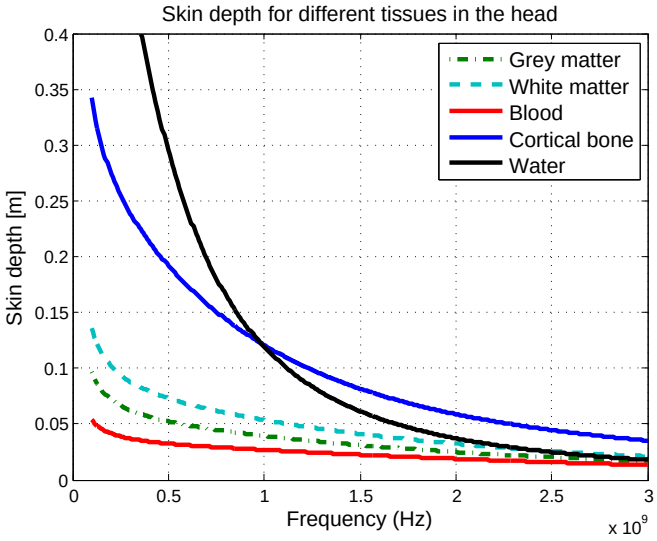

Figure 2.12: Skin depth for different tissues in the head. Calculated with the 4–Cole–Cole dispersion model using the parameters from Gabriel et al. [22] and Kaatze [23].

2.4.2 Scattering parameters

Scattering parameters (S-parameters) are used in two-port networks to get a measure of how much of the signal that is transmitted and reflected between the two ports [26]. The origin of the scattering parameters can be seen in Figure 2.13. An electromagnetic wave a_1 comes in to port 1 in the two-port network and some part of it is reflected, the reflection coefficient is denoted as S_{11} [26]. But some part of the wave is also transmitted through the network to the other port, this transmission coefficient is denoted S_{21}. On the other port another wave a_2 is incoming. This wave will also be divided into reflected and transmitted parts, with the reflection and transmission coefficients S_{22} and S_{12}. This relationship can be written in a system of equations, see Equation (2.25) [26]. The matrix in this system of equations is called the scattering matrix and is made up of the scattering parameters S_{11}, S_{12}, S_{21} and S_{22}.

$$\begin{pmatrix} b_1 \\ b_2 \end{pmatrix} = \begin{pmatrix} S_{11} & S_{12} \\ S_{21} & S_{22} \end{pmatrix} \begin{pmatrix} a_1 \\ a_2 \end{pmatrix} \tag{2.25}$$

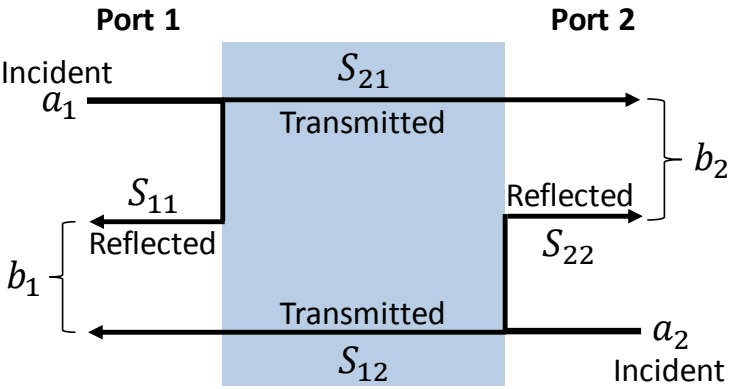

Figure 2.13: Illustration of the S-parameters.

2.4.3 Applications

MWT has been used since World War II, when the radar was developed. The field is now expanding quickly and the most common use of MWT is in wireless networks and communication systems, mobile phones do for example work in the microwave domain [21]. Microwave ovens do, as implied by the name, also use MWT. One advantage of data transmission at higher frequencies is that it gives higher band width, which means higher data rate [21].

There are two types of MWT used in medicine; therapeutic and diagnostic. Therapeutic MWT does generally refer to thermotherapy where microwaves are used to heat the tissue. This can be used to kill cells in tumours, since they are less resistive to temperatures between 42 °C and 45 °C [27]. It can also be used to coagulate tissue during surgery and to sterilise wounds and speed up wound healing.

In thermography the thermal radiation, i.e. heat, emitted from the body is measured [27]. Heat is a form of electromagnetic radiation in the microwave range. Since cancer cells have a higher metabolism and induces an increased blood flow, the temperature is slightly higher than in healthy tissue. It is possible to detect a tumour by measuring the difference in temperature for two equivalent areas [27].

It is possible to get information about a material by sending microwaves through it and observing the signal on the other side [28]. If a set of antennas is used, where one is transmitting a microwave signal that is detected by the other antennas, differences in conductivity and permittivity in the material can be detected. With this technique, it might be possible to detect and localise a bleeding in the brain. The transmitted signal will spread through

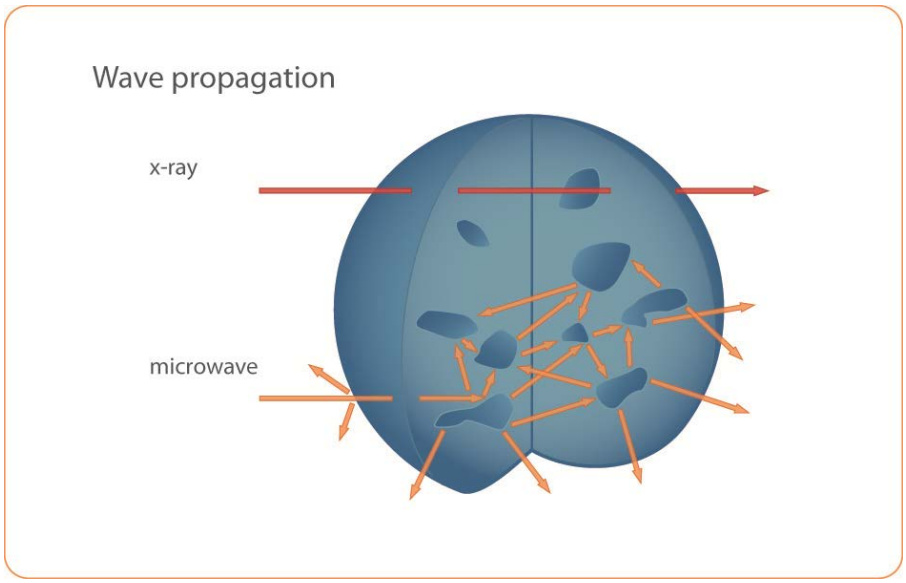

Figure 2.14: Microwaves propagating through an area consisting of different tissues. (With kind permission: Medfield Diagnostics, `http://www.medfielddiagnostics.com/technology/`)

the material and in the process their amplitude and phase will change, see Figure 2.14. By measuring this change of wave properties, an image of the tissue can be formed, although not in real time [28].

2.4.4 Patch Antennas

The antennas used in the MWH are patch antennas. Patch antennas are antennas made out of a metallic patch on top of a dielectric substrate on top of a ground plane. Patch antennas are favourable due to the small size, the light weight and that they are easy and cheap to manufacture [29]. The length L of a normal rectangular patch antenna, see Figure 2.15, is around half a wavelength. The thickness of the antenna is then usually just a fraction of a wavelength [30].

The electric field for a rectangular patch antenna can be seen in Figure 2.15. The E-fields that extend a small distance around the sides of the patch are called fringing fields [30]. One way to model the radiation of the patch antenna is to see the area around the patch with the fringing fields as the effective radiating area.

The size has been reduced, in the patch antenna used for the MWH, by choosing a triangular patch and also use a shorting wall that connects the patch with the ground plane, see Figure 2.16 [29]. The bandwidth for the

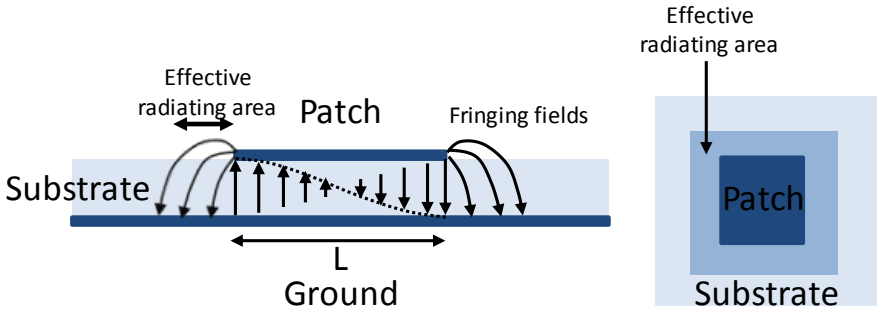

Figure 2.15: E-field for a rectangular patch antenna seen from the side and from above.

patch antenna used in the MWH is increased by introducing a V-shaped slot in the patch [29]. The triangular patch antenna can then be seen as two triangular patch antennas, one smaller and one bigger. The two patches will then have two different resonance frequencies and by using both of them a larger bandwidth can be obtained.

2.4.5 Safety guidelines

The Internal Commission on Non-Ionizing Radiation Protection (ICNIRP) have the task to investigate the dangers that may be associated with non-ionising radiation. They have put up some restriction and guidelines for electromagnetic fields in different frequency regions [31, 32].

For the frequency region relevant for the MWH there are restrictions on the specific energy absorption rate (SAR). The maximum SAR values are defined from how much temperature increase the human tissue can withstand without damage, which is 1° C [31]. For the head the maximal SAR value is 10 W kg^{-1} for occupational exposure and 2 W kg^{-1} for general public exposure [31]. The SAR value is calculated by taking the averaged absorbed effect in 10 g of continuous tissue [31]. The maximum SAR value from the MWH can be calculated by assuming that all the microwave radiation from the MWH ends up in 10 g of the tissue in the head. This means a SAR value of SAR=0.001 W/0.01 kg = 0.1 W kg^{-1}, since the MWH sends out a maximal effect of 1 mW per antenna, and only one antenna is sending at the time. This is far below the allowed SAR value. A GSM 900 mobile phone has an average power output of 250 mW [33], which gives a SAR value of 25 W kg^{-1}.

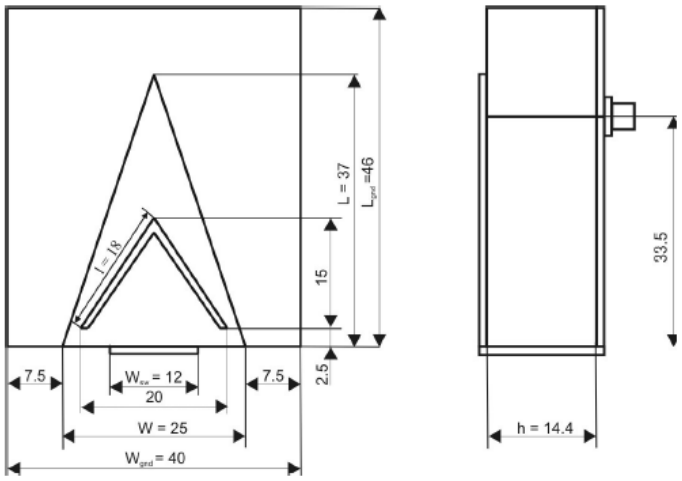

Figure 2.16: The dimensions for the triangular patch antenna used in the MWH. (With kind permission: H. Trefná and M. Persson, "Antenna Array Design for Brain Monitoring" (2008))

2.5 Data analysis

The data from the MWH was analysed and classified with Singular Value Decomposition (SVD). The t–test was used for some of the dielectric data to show that there was a difference between them.

2.5.1 Singular value decomposition

Any $m \times n$ matrix, A, can be factorised as

$$A = USV^T, \tag{2.26}$$

with $S = \begin{pmatrix} D & 0 \\ 0 & 0 \end{pmatrix}$ where D is a diagonal $r \times r$ matrix with $r = rank(A)$, containing the positive singular values of A in descending order. The singular values are the square roots of the eigenvalues for A^TA [34]. U and V are $m \times m$ and $n \times n$ orthogonal matrices consisting of the eigenvectors corresponding to the eigenvalues from AA^T and A^TA respectively. The columns of U and V are called left and right singular vectors of A. S is uniquely determined by A, but U and V are not [34].

In the analysis, a variant of SVD called reduced SVD is used. It is a more compact version that can be used if A contains rows or columns that only contains zeros [34]. In this case, only the r first columns of U and V are used. Since S only have r non–zero entries, the result is the same as

for regular SVD, but can be written as $A = U_r D V_r^T$ where U_r and V_r are the reduced matrices. SVD can be used to estimate the rank of a matrix by counting the number of non–zero singular values. Roundoff errors from the row reduction shows up as extremely small singular values, so if those are removed, it is possible to get rid of the redundant information in the matrix [34].

2.5.2 T–test

The t–test can be performed to see if two independent and normally distributed samples differ from each other [35]. The two samples $\overline{X}$ and $\overline{Y}$ have the means μ_X, μ_Y and equal variances.

The statistic in Equation (2.27) follows a t–distribution with $m + n - 2$ degrees of freedom, where m and n are the sample sizes of X and Y respectively [35].

$$t = \frac{(\overline{X} - \overline{Y}) - (\mu_X - \mu_Y)}{s_p \sqrt{\frac{1}{n} + \frac{1}{m}}} \tag{2.27}$$

The variance can be estimated with the pooled sample variance s_p^2 that is defined in Equation (2.28) [35].

$$s_p^2 = \frac{(n-1)s_x^2 + (m-1)s_Y^2}{m + n - 2} \tag{2.28}$$

Where s_X^2 and s_Y^2 are the standard deviations for X and Y. The test statistic for testing the null hypothesis $H_0 : \mu_X = \mu_Y$ is

$$t = \frac{\overline{X} - \overline{Y}}{s_p \sqrt{\frac{1}{n} + \frac{1}{m}}}. \tag{2.29}$$

The probability of falsely rejecting the null hypothesis is defined as the p–value. Therefore, the smaller the p–value is, the more likely it is that the null hypothesis could be rejected and that the two samples have unequal means [35].

Chapter 3
Method

This chapter explains in detail how the project was carried out, with the creation of the phantoms, the MWH measurements, measurements of the dielectric properties of the phantoms and the data analyses of the MWH data.

3.1 Experimental setup

3.1.1 Dielectric measurements

The measurements on the dielectric properties were performed in the Microwave laboratory at the department Signal and Systems at Chalmers University of Technology. A programmable network analyser (PNA Series Network Analyzer, 10 MHz–20 GHz, Agilent Technologies E8362B) was used to transmit and receive the microwave signals. A dielectric probe (Dielectric Probe Kit, Agilent Technologies 85070E) was connected to the PNA to measure the dielectric properties. The probe was connected to the PNA by using a test-cable (Test-Cable, Hochfrequenztechnik, Rosenberger) and an adapter (Adapter Kit, Precision 3.5 mm, Agilent Technologies 83059K). The whole measurement setup is shown in Figure 3.1.

3.1.2 Microwave helmet measurements

The measurements with the MWH were done in the laboratory at Medfield Diagnostics. A Strokefinder R10 (Medfield Diagnostics) was used together with a MWH to perform the measurements. The 12 ports at the Strokefinder were connected with cables to the 12 antennas on the MWH, see Figure 3.2. The Strokefinder consists of a vector network analyser (VNA) and a mechanical switching box.

The MWH was a research prototype developed by Medfield Diagnostics in collaboration with Chalmers. It consisted of 12 patch antennas, see Figure 2.16 and 3.3, attached to a plastic helmet, see Figure 3.4. Each

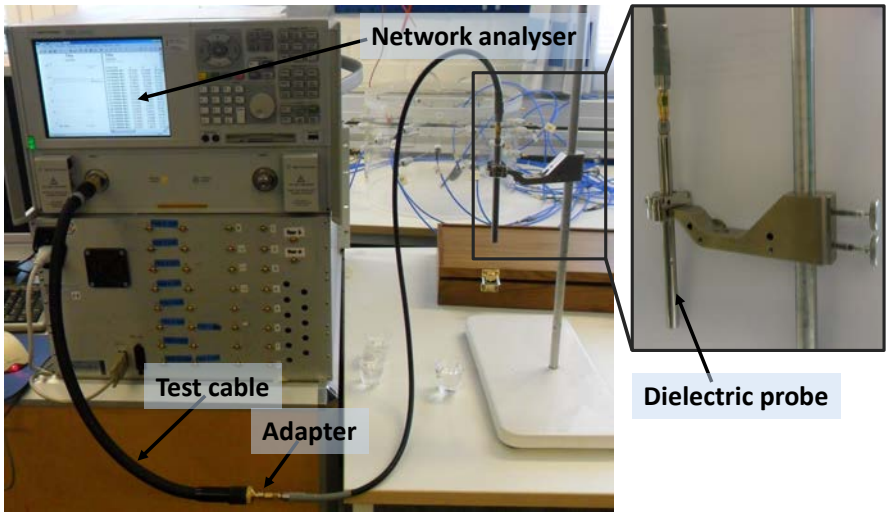

Figure 3.1: Measurement setup for the dielectric probe at Chalmers.

antenna had a plastic covering for hygienic purposes. For better connection between the phantom and antennas, plastic bags with water were attached to the antennas.

The frequency interval used was 0.1–3 GHz. The corresponding wave lengths in vacuum are 3 m to 10 cm and in grey matter 0.3 m to 0.01 m. The skin depths in grey matter for these frequencies are 2–10 cm, with 2 cm corresponding to the highest frequency of 3 GHz, see Figure 2.12.

3.2 Phantom construction

In total thirteen phantoms were made, nine with bleeding and four without. After the four first phantoms there was a time gap of about three weeks before the rest of the phantoms were created. All phantoms were produced during a period of nine weeks.

The phantom used to model the head consisted of a human cranium filled with a mass of deionised water, sugar (Garant), salt (Jozo salt with iodine) and fine powder agar (Sigma-Aldrich, W201201). The cranium had been cut into two halves in a transverse plane, see Figure 4.1a. The water was usually measured with a graduated cylinder and the rest of the measurements where done with a measuring set for cooking. The phantom mass was supposed to mimic the dielectric properties for the grey matter of the brain. Another similar mass with the dielectric properties of blood was used

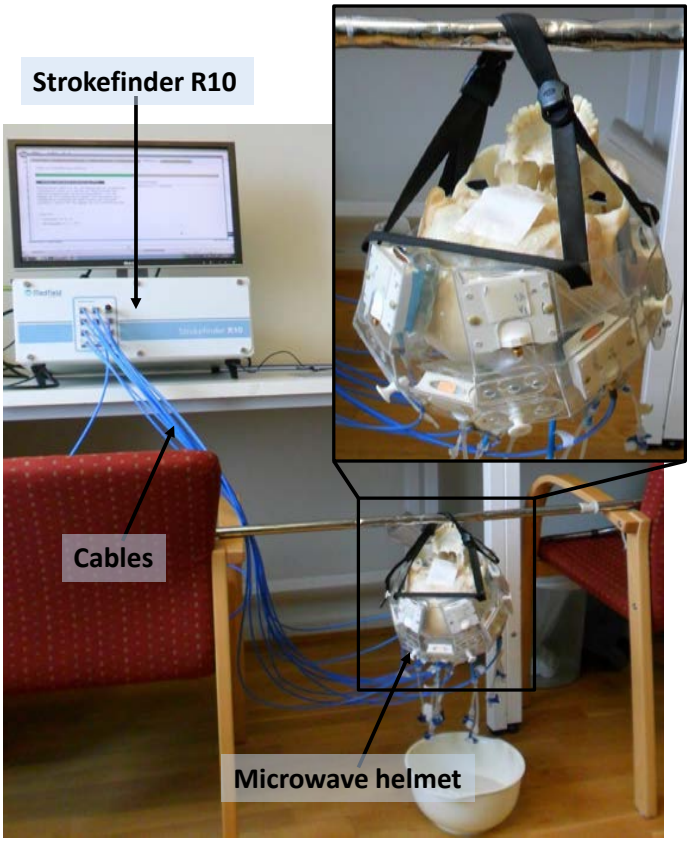

Figure 3.2: Measurement setup at Medfield Diagnostics.

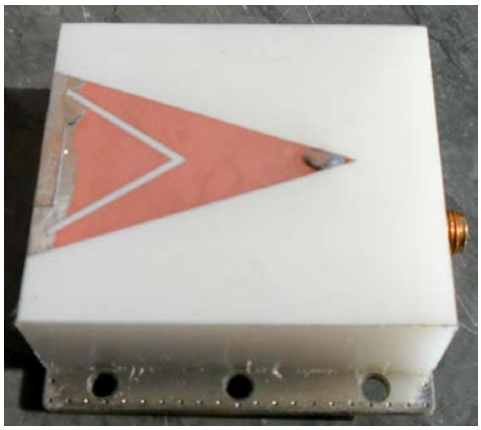

Figure 3.3: One of the patch antennas used in the MWH.

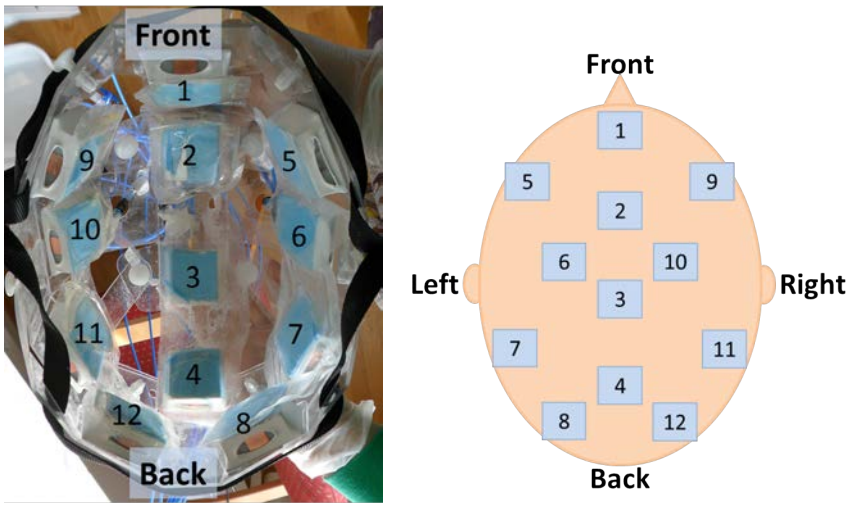

(a) Inside of the MWH with antenna numbering. **(b)** Antenna placement in the MWH, seen from above.

Figure 3.4: The MWH used to perform the measurements (3.4a) and a schematic figure of the MWH related to the head (3.4b). The numbers indicates the numbering of the antennas, antenna number 8 and 12 were not used in the measurements.

to model the bleeding. The recipes for the phantom masses were based on the recipes created by Malik Ahmad [9], see Table 3.1a and 3.2a. The dielectric properties were measured with the dielectric probe at the Chalmers laboratory. Despite many tries, the results by Malik Ahmad could not be reproduced. The recipe for blood was therefore altered to get the right properties, see Table 3.2b. After the first four phantoms were produced, it was discovered that the permittivity for the grey matter did not match the previous results, and was too close to the properties of the blood. Therefore a new recipe was developed, see Table 3.1b.

Two type of bleedings (EDH and SDH), two locations (left and right) and three volumes (20, 40 and 60 ml) were investigated. The choices of volumes were supported by a study by Robertson et. al [36], where the volume distribution of 83 cases of intracranial heamatomas were declared. One of the reference phantoms was made in the same way as a SDH, but with grey matter phantom mass in the bleeding. This was done to see if the bleeding production method impacts the result more than the difference in dielectric properties.

The phantom solution was prepared by first dissolving the salt in the water and then adding the sugar. The solution needed to be heated to

Grey mass	Vol%	Volume
Battery water	57.9	1447.5 ml
Salt	0.1	2.5 ml
Sugar	36	900 ml
Agar	6	150 ml

(a) Recipe 1 for the grey matter phantom mass.

Grey mass	Vol%	Volume
Battery water	50.1	1252.5 ml
Salt	0.1	2.5 ml
Sugar	43.8	1095 ml
Agar	6	150 ml

(b) Recipe 2 for the grey matter phantom mass.

Table 3.1: The two recipes for grey matter phantom masses. Recipe 1 (3.1a) is the recipe from Malik Ahmad [9]. The volumes are calculated for 100 vol% = 2.5 l, which was the amount needed to fill the cranium.

around 50 °C for the sugar to dissolve properly. 0.3 vol% formalin (37 wt.% in water) was added to the grey matter phantom solution to avoid bacterial growth in the cranium. For the blood phantom solution the colour was added at this stage. Then the agar was added and the mixture was heated to between 70 °C and 80 °C.

The EDH was prepared by shielding off the area where the bleeding should be placed, using tape and plastic wrapping, see Figure 3.6a. This area was filled with blood phantom mass, see Figure 3.6b. When the bleeding had solidified, the shielding was removed and the cranium was joined together. To avoid leaking of the agar-mass, the two parts of the cranium were joined together with fabric tape and covered with several layers of plastic wrapping. The SDH was prepared after the cranium parts had been joined together. The cranium was then tilted about 30° to the side and the desired amount of blood phantom mass was added to form a haematoma at the surface of the brain, see Figure 3.5. When the bleedings had solidified, a grey matter phantom solution was made and the cranium was filled up with the new phantom mass.

The phantoms were usually made the day before the MWH measurements were performed. Two of the phantoms were made three days before the MWH measurements. All the phantoms rested and solidified over night in room temperature and a water bath. The water bath kept the phan-

Blood	Vol%	Volume
Battery water	68	204 ml
Salt 10% solution	2	6 ml
Sugar	26	78 ml
Red food colour	1	3 ml
Agar	3	9 ml

(a) Recipe 1 for the blood phantom mass.

Blood	Vol%	Volume
Battery water	66	198 ml
Salt	1	3 ml
Sugar	26	78 ml
Red food colour	1	3 ml
Agar	6	18 ml

(b) Recipe 2 for the blood phantom mass.

Table 3.2: The two recipes for blood phantom masses. Recipe 1 (3.2a) is the recipe from Malik Ahmad [9]. The volumes are calculated for 100 vol% = 3 dl, all phantoms are made with blood recipe 2 (3.2b).

tom mass from leaking out of the cranium. After the microwave measurements were completed, the cranium was opened and the phantom was photographed, removed from the cranium, sliced and checked for air-bubbles. This was difficult to do for the EDH, since the bleeding was more separated from the rest of the phantom and fell off when it was removed from the cranium.

3.3 Dielectric measurements

3.3.1 Phantoms

The dielectric properties were measured for each phantom, both with and without agar. Two liquid samples from each phantom solution were removed before the addition of agar and stored until they could be measured one to four days later. For the solid blood phantom mass, more mass than needed was prepared, and some of the leftovers were saved for dielectric measurements. For the grey matter, two slices of the solid phantom were used for the measurements.

The dielectric properties were measured once a week at the Chalmers

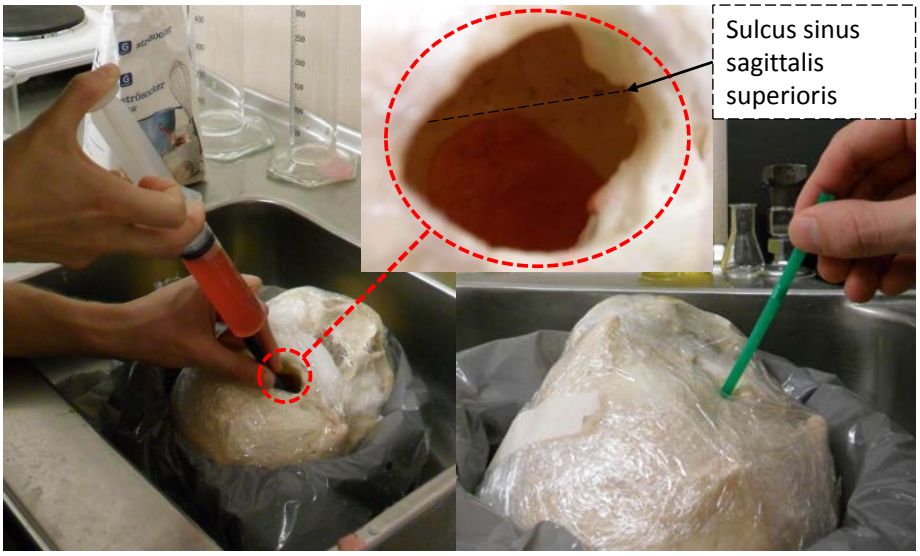

Figure 3.5: Placing a SDH in the cranium. The bleeding does not cross the sulcus sinus sagittalis superioris, which is the groove that separates the brain hemispheres.

laboratory, two measurements were done for each of the liquid samples and five times each for the solid samples. More measurements were needed for the solid sample since it was harder to get good measurements, because of the risk of air or water pockets between the phantom sample and the probe. There might also be some variations over the areas if the phantom mass was not completely homogeneous. The output from the dielectric probe were the real and imaginary parts of the complex relative permittivity ϵ_r' and ϵ_r''. From the latter the conductivity can be calculated using Equation (2.10) with $\epsilon_r'' = \epsilon''/\epsilon_0$, i.e. $\sigma = \omega\epsilon_r''\epsilon_0$. The data therefore had to be processed in Matlab before it could be visualised.

3.3.2 Coagulated blood measurements

Since the blood in real patient haematomas are partly coagulated, an experiment to evaluate the difference in dielectric properties between coagulated and uncoagulated blood was performed. Pig blood was bought frozen at the store (S.O. Larsson at Saluhallen in Gothenburg, from Skövde Slakteri AB).

Ten samples were taken from the 1 kg thawed pig blood. The dielectric properties were measured 6 times on these samples at body temperature

(a) Preparation for EDH.

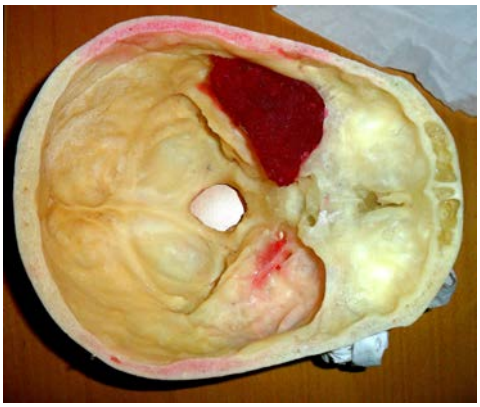

(b) EDH in cranium.

Figure 3.6: The cranium seen from above during EDH production.

(37 °C). Afterwards were the samples heated up to around 70 °C so the blood started to coagulate. When a clot had formed at the bottom of the sample, it was cooled down to body temperature. The clot samples were then measured six times each with the dielectric probe.

3.4 Microwave helmet measurements

When the phantom had solidified completely, by resting over night in room temperature, the plastic wrapping was removed. The fabric tape was kept around the skull to keep the upper part of the skull in place. The cranium was wiped off on the outside with a cloth to remove excess phantom mass and reduce stickiness. A piece of tape was attached to the foramen magnum to avoid evaporation.

The MWH was prepared by attaching the cables to the antennas. Only 10 of the antennas were used, since the two neck antennas, number 8 and 12

in Figure 3.4 and 3.2, did not get a good connection with the cranium since it was quite small. The two ports that weren't used were terminated with a 50 Ω load to avoid interference. Water bags were attached to the antennas to get a better connection between the antennas and the skull. The bags were partly filled with water and air bubbles were removed before the cranium was placed in the MWH. Afterwards more water was added until the cranium was fixated. The MWH with the phantom was hung on a metal rod between two chairs, see Figure 3.2.

The position of the MWH relative the bleedings can be seen in the schematic picture in Figure 3.7. The EDH were always placed at the same location by the temporal bone, SDH varied more in location and were sometimes positioned more to the front and sometimes more to the back.

3.4.1 Ordinary measurements

30 measurements were performed in ten sets of three. After every third measurement the water bags were emptied, the cranium was lifted a few centimetres and the position was adjusted. The water bags were refilled and the measurements continued. This was done to simulate the variation in position of the MWH on the patients head and between different measurements on the same patient.

3.4.2 Interfering factors

Person close and holding the cables

The impact of a persons close to the measurement setup was investigated by doing 30 measurements with a person standing close the MWH, see Figure 3.8a. This is interesting to investigate for the possibility to use the MWH in an ambulance where the space is limited. Another 30 measurements were performed with a person holding the cables, see Figure 3.8b, and then yet another 30 measurements were performed, where the person was standing more than 1 m from the setup, as a reference to the other measurements. All these three types of measurements were randomised among each other. These experiments were only performed for the first four phantoms.

Phone

The impact of a mobile phone (HTC Wildfire S) signal was also investigated. The mobile phone calls in the GSM network with a frequency around 900 MHz [21], which is in the frequency interval used for the MWH measurements. This was done by doing 30 measurements with a calling mobile phone close to the MWH, see Figure 3.8c. The mobile phone was calling

another mobile phone in the same room that did not answer. As a reference to these measurements, 30 measurements were performed with the mobile phone in flight mode close to the MWH. All these 60 measurements were performed in a randomised manner to minimise time dependent errors.

Hair

For the last nine phantoms, the impact of hair was investigated by putting a wig with real human hair on the cranium. 30 measurements were performed in the same way as the ordinary measurements, with the cranium being repositioned after every three measurements. The position of the cranium with the wig in the MWH can bee seen in see Figure 3.9.

Movement

The impact of movement was investigated by doing 30 measurements when the MWH was put into movement, by rocking it back and forth, and compare these to 30 measurements without movement, see Figure 3.8d. These 60 measurements were performed in a randomised manner to minimise the time dependent errors.

3.5 Data analysis

3.5.1 Dielectric measurements

The dielectric probe gave unstable results below 0.5 GHz and those values can therefore not be trusted. All the t–tests and mean value calculations are therefore done in the frequency interval 0.5–3 GHz.

Phantoms

The mean values from all the measurements (liquid and solid for both grey matter and blood phantom samples) for each phantom sample were first calculated. After this the mean values for the relative permittivity and conductivity from all the phantom samples were calculated. Reference values for grey matter and blood were calculated in Matlab by using the 4-Cole-Cole dispersion model, see Equation (2.12), together with the parameters for grey matter and blood from Gabriel et al. [22].

The difference in dielectric properties between the grey matter and the blood phantom masses were calculated for all the bleeding phantoms individually. This was defined as the contrast in the phantom. The contrast was calculated for each phantom individually and then the mean value and standard deviation (SD) was calculated for all the phantoms together.

Liquid and solid phantoms

A t–test, see Section 2.5.2, was performed to see if the mean values of the dielectric properties for the liquid phantom solutions differed from the solid phantom masses. The data was preprocessed by integrating each measurement over the whole frequency region, with the Matlab function `trapz`. By doing this one value could be obtained for each measurement. To be able to perform the t–test the data had to be normally distributed, which was tested for all the group of values with the Matlab function `lillietest`. The data in the two groups also had to have the same variance, which was tested with the Matlab function `vartest2`. The only data that was normally distributed was grey matter phantom mass with recipe 2, therefore the t–test was only performed on this group. The p–value was calculated with the Matlab function `ttest2`. The values for the frequencies below 0.5 GHz were not used, since the dielectric probe wasn't reliable in that frequency region.

Coagulated blood measurements

A t–test was performed in the same way as for the liquid and solid phantom samples, using the data for the coagulated and uncoagulated blood. The mean value from all the uncoagulated blood measurements were first calculated for each sample. After this the mean values for the relative permittivity and conductivity from all the samples were calculated. The same procedure was used for the measurements on the coagulated blood samples. Since the shape of the curves were equal in all groups (in the frequency interval 0.5–3 GHz), the difference in mean value could be calculated. This mean value was calculated by taking the mean over these frequencies for one group and divide by the mean over these frequencies for another group, which gave a value for the offset between the two groups.

3.5.2 Microwave helmet measurements

For data analysis an in-house classifier, made by Professor Tomas McKelvey and Yinan Yu at Chalmers University of Technology, was used. The phantoms were divided into groups depending on location, type and size of bleeding, and each property was analysed independently. The measurement data for each group of phantoms formed a data sets. The data sets were presented as a 2D–matrix where each column corresponded to one measurement, containing all other variables, which can be as many as 30 000. The data were preprocessed by taking the natural logarithm and the 2–norm of the raw data.

The classifier uses SVD, see Section 2.5.1, to calculate a subspace U, see Equation (2.26), for each data set. The distance from the data point that should be classified to each subspace is calculated using the 2–norm. The classifier returns a scalar describing which subspace is closest, a vector with the distances to each subspace and the matrix describing the subspaces.

The data from the group of phantoms that should be classified is divided into a training set and a test set. The training set is used to create the subspace of the class, and the test set is the data that is classified. The data from the other groups of phantoms are used to create the subspaces of the other classes, one for each class. When the first test set has been classified, a new test set is formed from the training data. The rest of the training data, together with the previous test set forms the new training set and a new subspace is calculated. This is called cross-validation, in this case, k–fold cross-validation is used. This means that the dataset is randomly divided into k number of subsets. One of these subsets are used as the test set while the rest is used as the training set, this is repeated for all k subsets. In all results presented, five–fold cross–validation is used.

The ordinary measurements were done in groups of three were the phantom was moved in between. Care was taken in the analysis that measurements from the same three measurement groups were in the same test sets, since they were so alike.

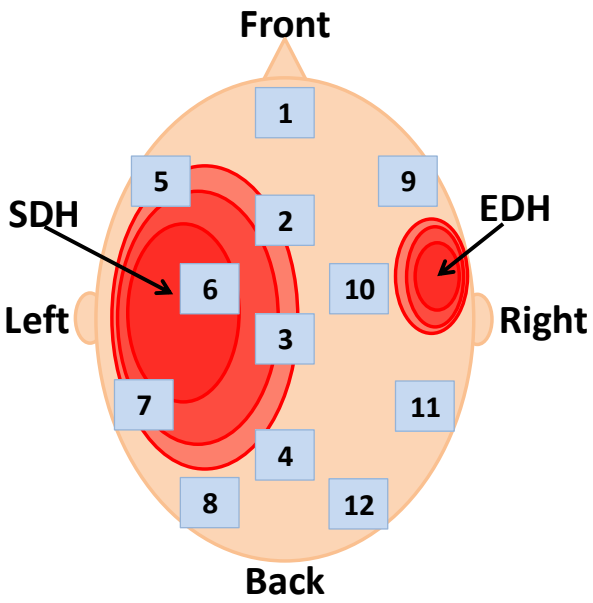

(a) Seen from above.

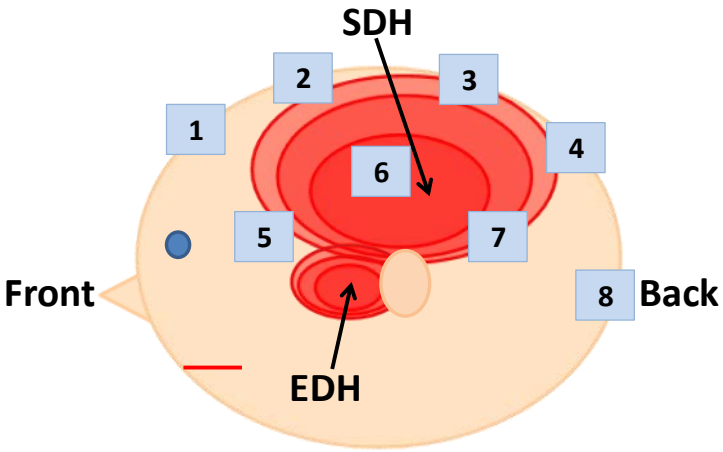

(b) Seen from the left side.

Figure 3.7: Schematic figures of the positions of the bleedings relative the antennas in the microwave helmet. SDH and EDH denotes the subdural and epidural haematomas, and the circles show the different volumes. The numbers indicate the antenna numbering in the MWH.

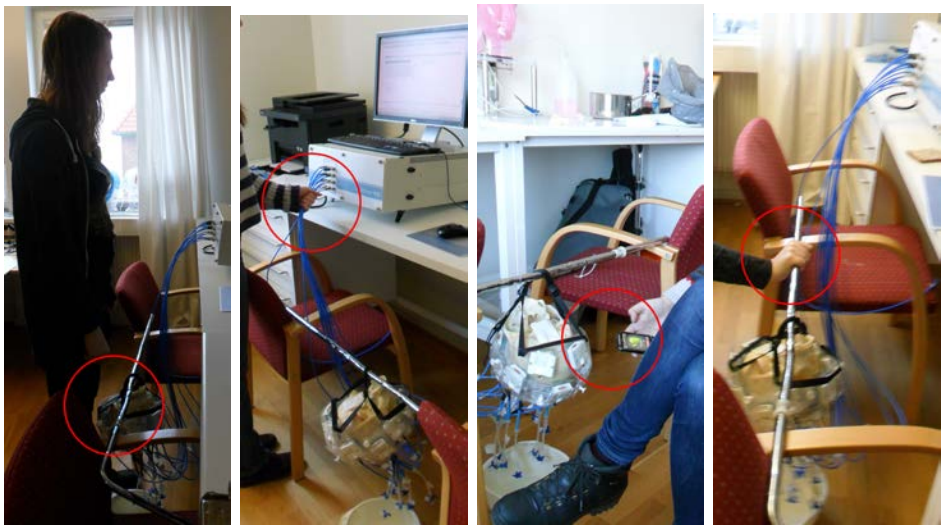

(a) Close. **(b)** Holding. **(c)** Phone. **(d)** Shaking.

Figure 3.8: Different types of measurements with the MWH. 3.8a: Person standing close to the MWH. 3.8b: Person holding the cables. 3.8c: A calling mobile phone close to the MWH during measurements. 3.8d: Shaking the MWH during measurements.

Figure 3.9: Cranium with wig placed in the MWH for measurements of the impact from hair.

Chapter 4
Result

4.1 Phantoms

The produced phantoms are listed in chronological order in Table 4.1. For a more detailed list, see Appendix B and for anatomical analyses, see the master's thesis by Philip Swahn [37].

Number	Phantom name	Recipe
1	Ref_0ml_1	1
2	Ref_0ml_2	1
3	SDH_40ml_Right	1
4	SDH_60ml_Left	1
5	SDH_20ml_Right	2
6	SDH_60ml_Right	2
7	EDH_40ml_Right	2
8	EDH_20ml_Left	2
9	Ref_0ml_3	2
10	SDH_40ml_Left	2
11	EDH_60ml_Left	2
12	SDH_20ml_Left	2
13	Ref_0ml_4	2

Table 4.1: List of phantoms in chronological order, EDH and SDH indicates epidural or subdural haematoma. The name also includes the volume and location of the bleeding. The phantoms named Ref are reference phantoms without bleeding, and they are numbered for identification. A more detailed list can be found in Appendix B.

The bleeding mass in the phantoms was usually more stiff than the grey matter phantom mass. No visible air pockets could be seen between the grey matter mass and the bleeding mass, but they were clearly separated. Non of the phantoms filled the entire cranium at the solid state since there were some leakage, both out of the phantom and into smaller cavities in

the cranium, during the process of solidification. This caused an air gap at the location of the cerebellum. Figure 4.1a and 4.1b shows a 60 ml SDH phantom and Figure 4.1c shows a 40 ml EDH phantom. The EDH was not covered by any of the antennas, which can bee seen in Figure 4.1d. This means that non of the direct signal pathways will go through the EDH. Some of the signal will still go through the EDH, due to the scattering, but not as much as for the SDH that was covered by several antennas.

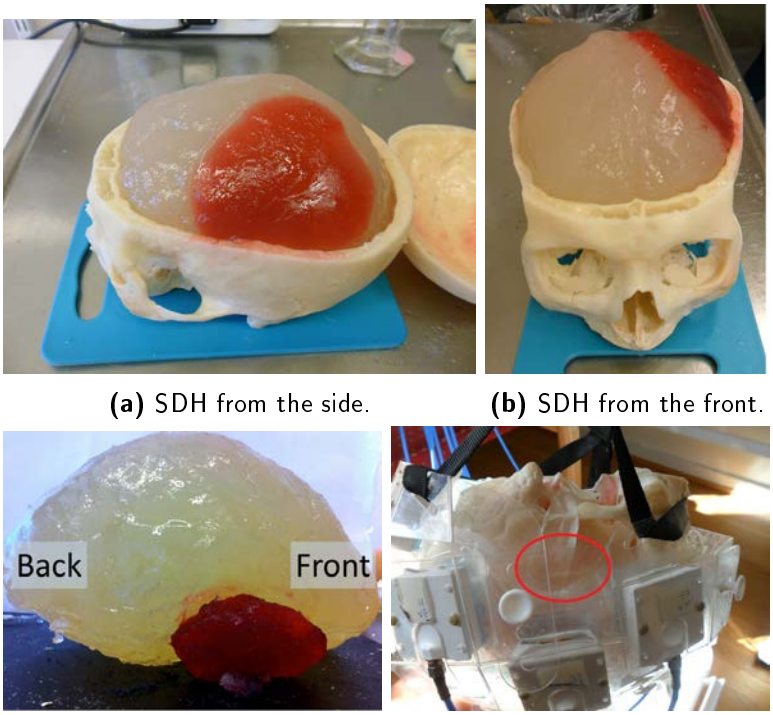

(a) SDH from the side. **(b)** SDH from the front.

(c) EDH with volume 40 ml. **(d)** Phantom in MWH.

Figure 4.1: Examples of EDH and SDH phantoms. 4.1a and 4.1b: Example of 60 ml SDH phantom (phantom 4). 4.1c: Example of 40 ml EDH phantom without skull (phantom 7), 4.1d: Phantom in MWH, the red circle indicates the location of an EDH, which is not covered by any of the antennas. All phantom numbers refer to Table 4.1.

4.2 Dielectric properties

4.2.1 Phantoms

The dielectric properties for all the phantoms can be seen in Figure 4.2. Due to practical reasons the dielectric properties for all the phantoms could not be measured at the same day as the MWH measurements were performed. The maximum number of days between the MWH measurements and the dielectric measurements were three days. No visible change could be seen on the phantoms over these days. To further determine if the dielectric properties in a phantom did change over a few days, the dielectric properties on one phantom were measured every day for a week. The result was that the calibration of the dielectric probe changed more between the days than the dielectric properties of the phantom.

The phantoms differed in consistency, even though the same procedure and recipe had been used each time. However, the consistency did not effect the dielectric properties, since they still had the same amount of sugar, salt and water.

The amount of formalin (0.3 vol%) that was added to the phantoms did not significantly affect either the permittivity (p–value of 0.22) or the conductivity (p–value of 0.36), when five samples were tested.

The effect on the dielectric properties when adding food colour was also tested. No clear effect could be seen when four samples of water and food colour were tested. Unfortunately the t–test couldn't be performed since the data wasn't normally distributed. The difference in mean could be calculated and was less than 1 % for the permittivity and conductivity between the two cases (water and water with food colour).

The temperature does affect the permittivity and conductivity. This was tested by measuring a sample of water ones every ten degrees in the interval 20–80 °C. Both the relative permittivity and conductivity goes down with increasing temperature in the frequency region 0.5–3 GHz. It is therefore important to measure the dielectric properties at the same temperature as the MWH measurements have been done, which was around 21–23 °C.

Contrast in bleeding phantoms

The mean contrasts in dielectric properties between the grey matter and blood in the bleeding phantoms are shown in Table 4.2.

4.2.2 Grey matter and blood recipes

The dielectric properties for the two grey matter recipes and the two blood recipes are shown in Figure 4.3 and 4.4 respectively. The results by Malik

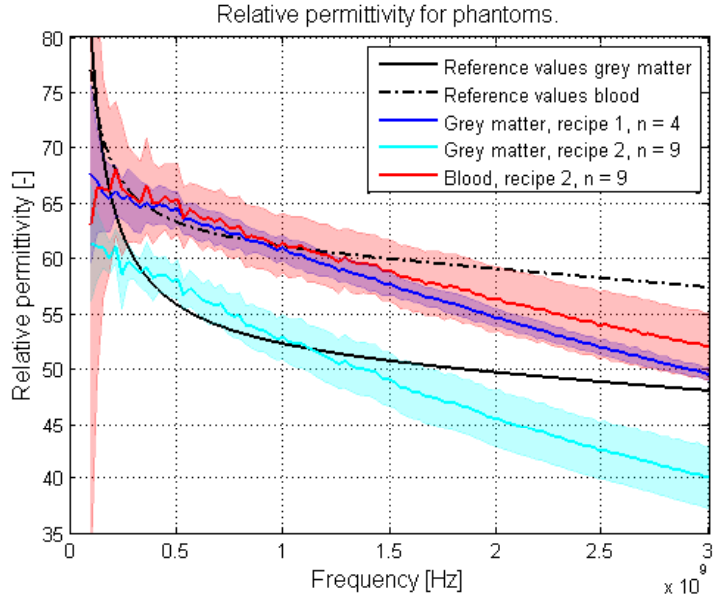

(a) Relative permittivity.

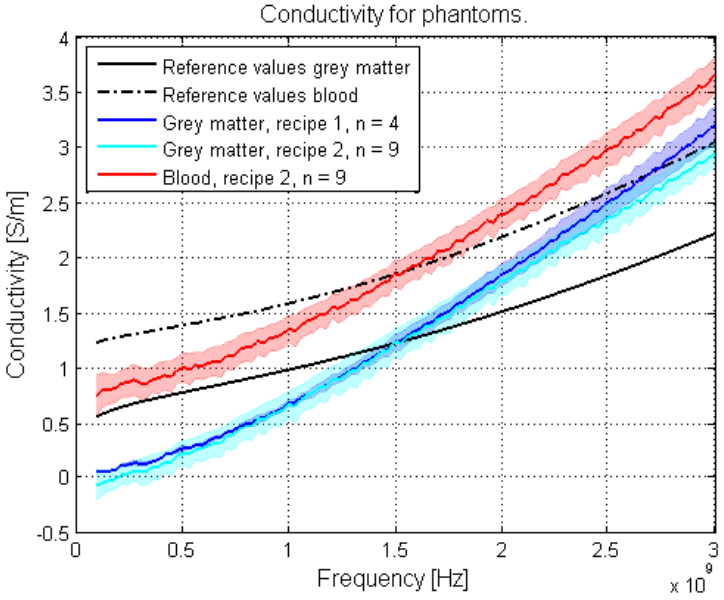

(b) Conductivity.

Figure 4.2: Relative permittivity (4.2a) and conductivity (4.2b) for all the phantoms. The measurements are done on solid grey matter and blood phantom masses. The shadows indicate the standard deviation from the mean value (the solid lines). The reference values are calculated from the 4-Cole–Cole dispersion model [22].

	Relative contrast (mean ± SD) [%]
Reference values	15
Phantoms, grey matter recipe 1, n = 2	6 ± 3
Phantoms, grey matter recipe 2, n = 7	17 ± 6

(a) Relative Permittivity

	Relative contrast (mean ± SD) [%]
Reference values	33
Phantoms, grey matter recipe 1, n = 2	37 ± 1
Phantoms, grey matter recipe 2, n = 7	34 ± 4

(b) Conductivity

Table 4.2: Relative contrast in dielectric properties between solid grey matter and blood phantom masses. All recipes can be found in Table 3.1a, 3.1b and 3.2b. The reference values are calculated from the 4-Cole–Cole dispersion model [22].

Ahmad [9] are also shown in the figures.

4.2.3 Liquid and solid phantoms

The permittivity of the solid phantoms that contains agar are significantly different from the ones without agar ($p<0.05$). The permittivity for the solid phantom are 6 % lower than the permittivity of the liquid phantoms, see Table 4.3. The conductivity for the solution is not significantly affected by the agar.

	t-test p–value	Mean value difference [%]
Relative Permittivity, n = 9	0.02	6 ± 1
Conductivity, n = 9	0.78	-

Table 4.3: Difference in relative permittivity and conductivity between solid and liquid phantom masses in the frequency interval 0.5–3 GHz.

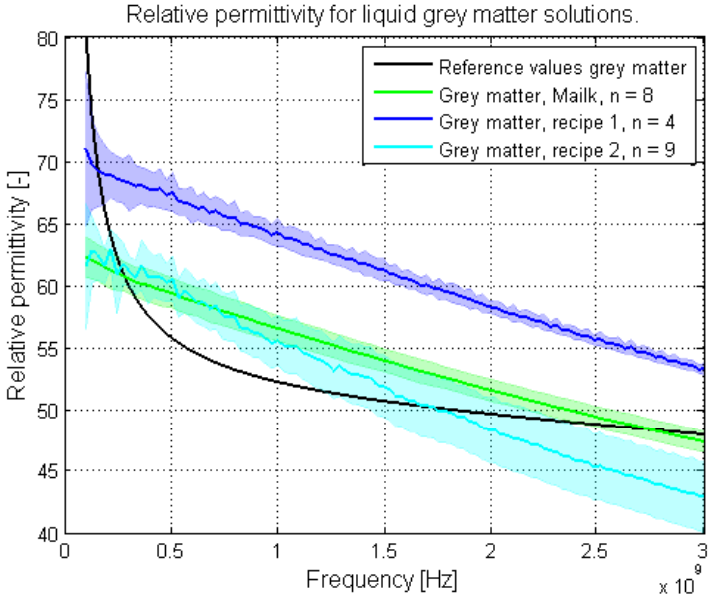

(a) Relative permittivity.

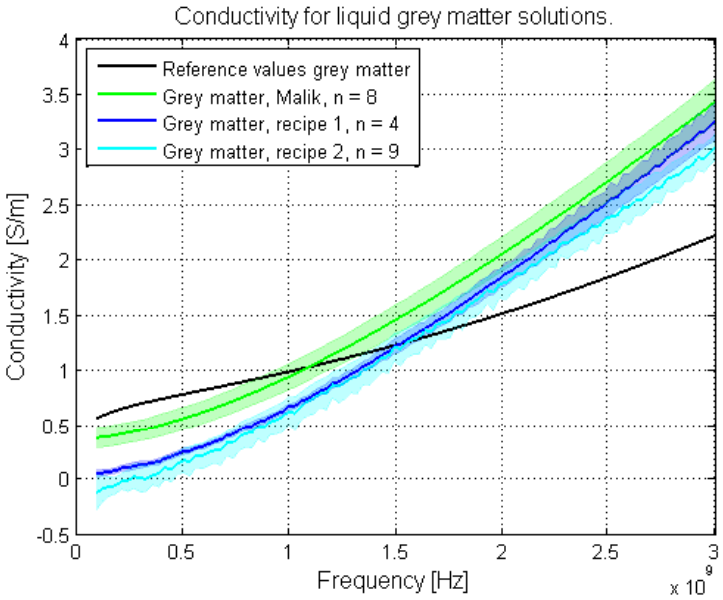

(b) Conductivity.

Figure 4.3: Relative permittivity (4.3a) and conductivity (4.3b) for the liquid grey matter phantom solutions together with the data from Malik Ahmad [9]. The shadows indicate the standard deviation from the mean value (the solid lines). The reference values are calculated from the 4-Cole–Cole dispersion model [22].

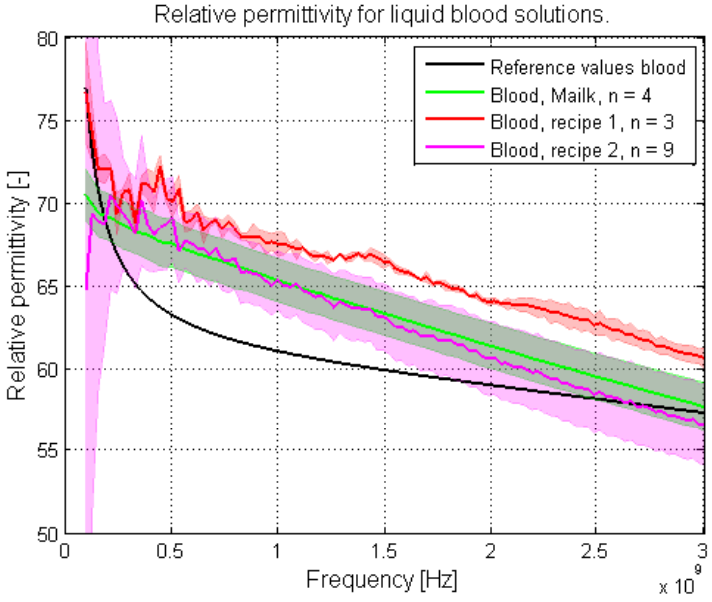

(a) Relative permittivity.

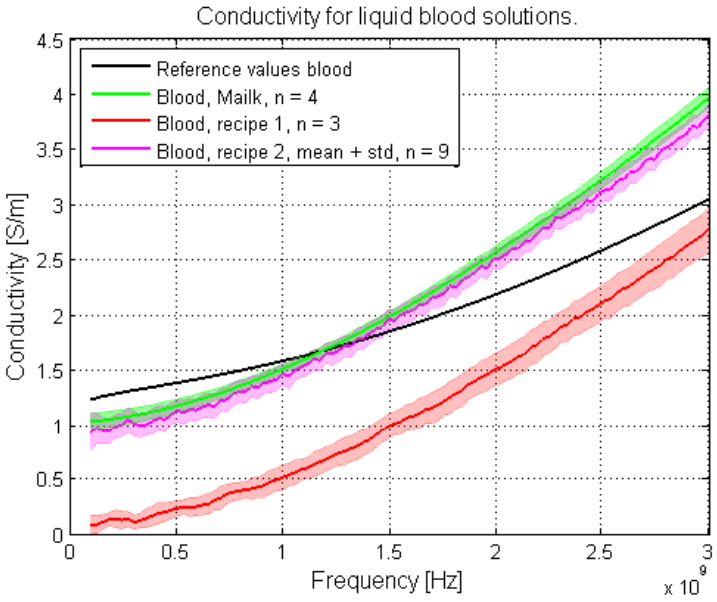

(b) Conductivity.

Figure 4.4: Relative permittivity (4.4a) and conductivity (4.4b) for the liquid blood phantom solutions together with the data from Malik Ahmad [9]. The shadows indicate the standard deviation from the mean value (the solid lines). The reference values are calculated from the 4-Cole-Cole dispersion model [22].

4.2.4 Coagulated blood measurements

Measurements on relative permittivity and conductivity were performed on pig blood to see the impact of coagulation, see Figure 4.5. The permittivity for uncoagulated blood and coagulated blood differed ($p<0.05$). The mean value for the permittivity was 2 % lower for coagulated 37 °C blood than for uncoagulated 37° C blood and the standard deviation was 2 %. The conductivity for the uncoagulated and coagulated blood did not differ significantly.

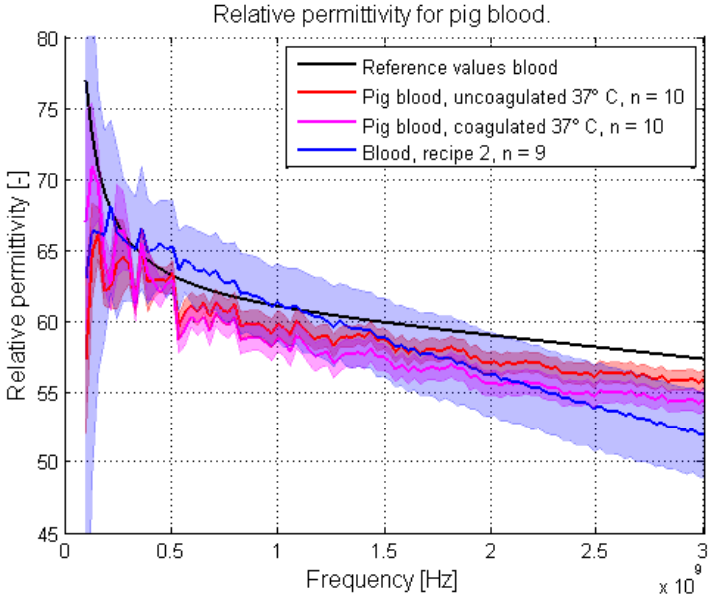

(a) Relative permittivity.

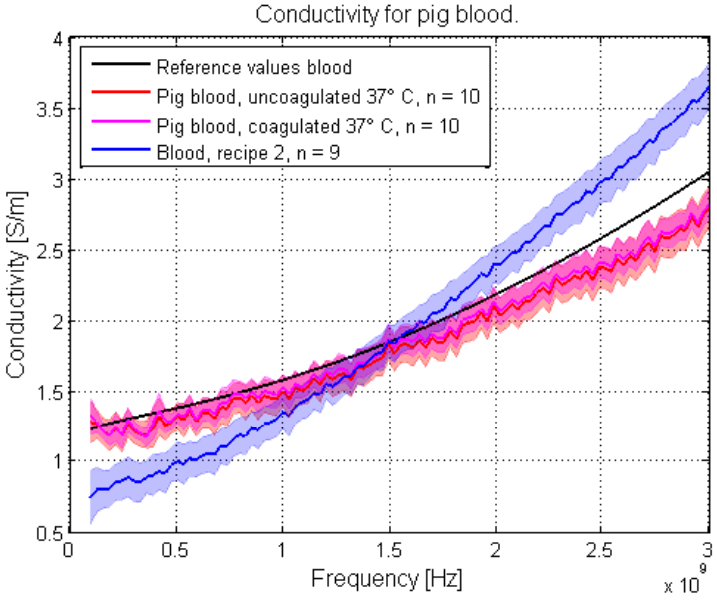

(b) Conductivity.

Figure 4.5: Relative permittivity (4.5a) and conductivity (4.5b) for uncoagulated and coagulated pig blood measurements. The blood had been coagulated by heating it up to over 70° C. The shadows indicate the standard deviation from the mean value (the solid lines). The reference values are calculated from the 4-Cole–Cole dispersion model [22].

4.3 Microwave helmet

The MWH that was used for the measurements works best between 0.5–1.7 GHz. Below 0.5 GHz, the transmission is very low, as seen in Figure 4.6a and 4.6b. Above 1.7 GHz, the transmission is divided into two groups of lines, see Figure 4.6b. These groups are seen for all transmission coefficients and originates from different calibrations where some internal changes have occurred in between. This difference is due to bad isolation in some of the switches, witch causes the transmission to takes place inside the machine rather than between the antennas. Therefore the analyses are performed in the interval previously mentioned.

There were some problems with bad cable connections and noisy signals. Both cables and ports were swapped to try to get the best signals. Two of the antennas on the MWH (8 and 12) were not connected to the Strokefinder R10 and are therefore not included in the analyses. Another antenna (number 1) had to be excluded because of some problems with bad connection and very high reflection.

Due to some unexpected problems with the equipment, the data from phantom 5 and phantom 6 in Table 4.1 could not be used due to artefacts in data. The transmission signal for these measurements were about 40 dB higher than usual, resulting in positive values. The same thing occurred for the movement data from phantom 4.

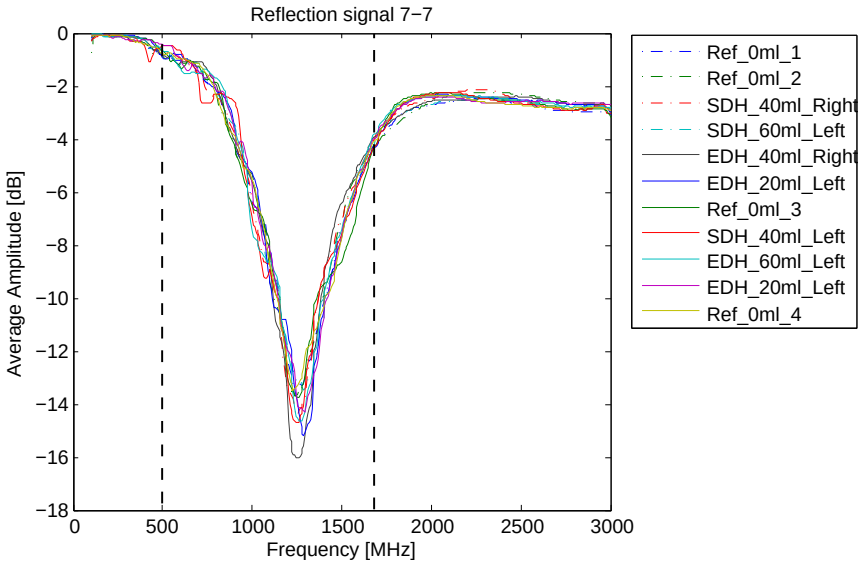

(a) Reflection coefficient for antenna number 7 for all phantoms.

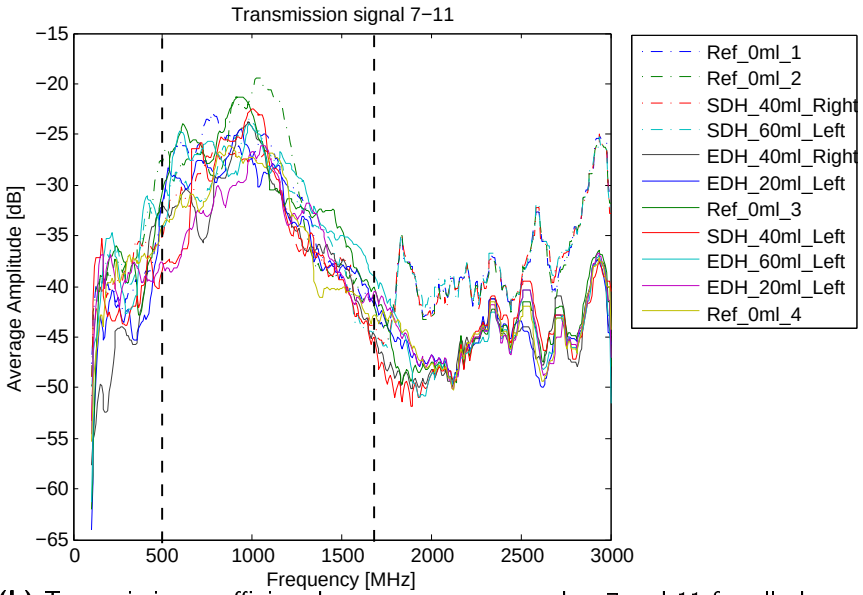

(b) Transmission coefficient between antenna number 7 and 11 for all phantoms.

Figure 4.6: Reflection (4.6a) and transmission (4.6b) coefficients for all phantoms. The selected frequency interval is marked with vertical black lines. 4.6a: For frequencies below 0.5 GHz, the reflection is close to total, i. e. no signal is transmitted. 4.6b: The signal over 1.7 GHz depends on the calibration, which drowns any possible useful information. The Matlab function `mag2db` is used to convert the data to dB. An one–dimensional median filter with order 15 is applied to the signals with the Matlab function `medfilt1`.

4.4 Data analysis

The distances in the classification plots are the 2–norm of the distances from the measurement point to the subspaces calculated by the classifier. A small distance means that the measurement point is close to that subspace, and the probability is high that it belongs to the corresponding class, provided that the distance to the other classes are larger.

The measurements were done in sets of three, with a total of ten sets for each phantom. In Figure 4.7, non bleeding phantoms are classified to the two classes non bleeding and bleeding phantoms. It is easy to distinguish the groups of three measurement points in the figure since the measurements are ordered chronologically. The phantoms are also chronologically ordered, and it is possible to distinguish between the different phantoms that are classified. In Figure 4.7 the data points corresponding to different phantoms are separated by lines to visualise this. In the rest of the plots, these lines are not used. The last phantom in Figure 4.7, (phantom 13, see Table 4.1) is the one that was made in the same way as a SDH. As seen in the figure, this phantom is not closer to the bleeding class than the other phantoms.

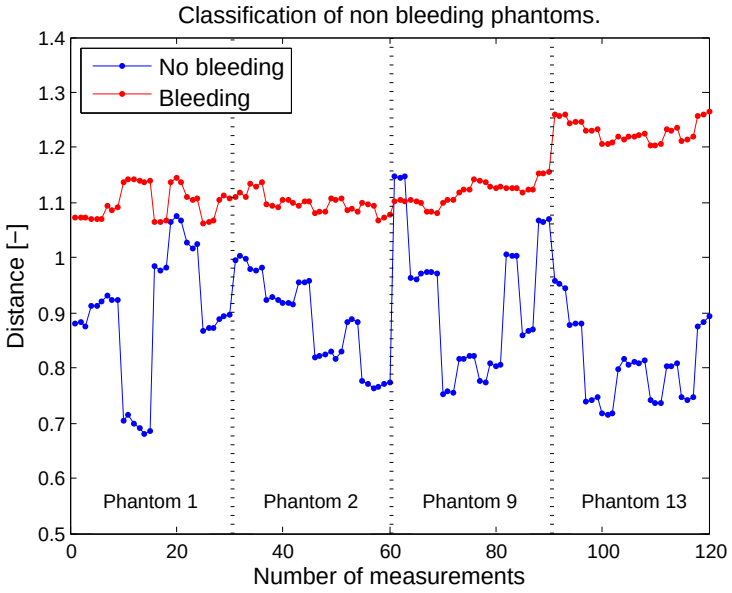

Figure 4.7: Classification of non bleeding phantoms and all measurement points (30 points for each phantom). The phantoms are classified in chronological order with the non bleeding phantoms: 1, 2, 9, 13 and bleeding phantoms: 3, 4, 7, 8, 10, 11, 12 from Table 4.1.

Only one point from each of these groups of three is used for the clas-

sifications, in all cases except for the interference data. This means a total of ten points per phantom, where the phantom orders are specified in the caption. All the classifications are done with data from the frequency region 0.5–1.7 GHz.

4.4.1 Non bleeding and bleeding phantoms

Figure 4.8 shows the classification results of non bleeding and bleeding phantoms. Four non bleeding phantoms are used in the non bleeding class and seven bleeding phantoms are used in the bleeding class. It can be seen that the classification is 100 % correct in the bleeding case and almost 100 % in the non bleeding case. There are bigger variations between the distances belonging to the same phantom than between the different phantoms. These strong results were only obtained when data from the classified phantoms were included in the training data.

Classifying a phantom that is not in the trainingset

Table 4.4a shows the result from the classification of one phantom at the time that is completely left out of the training set. The phantoms were classified to two classes; non bleeding and bleeding phantoms. The number of phantoms were the same in each class. If the size was uneven, the smallest distance was obtained to the class with the largest number of phantoms. The bleeding phantoms that were used were the phantoms with the permittivity contrast closest to the reference values calculated from the 4-Cole–Cole dispersion model (see Equation (2.12)), using the parameters from Gabriel et al. [22].

The results show that the classifier manages to classify the non bleeding phantoms with grey matter recipe 1 to the non bleeding phantom class and almost all the bleeding phantoms with grey matter recipe 2 to the bleeding class. But it does not manage to classify the non bleeding phantoms with the grey matter recipe 2 correct or the bleeding phantoms with grey matter recipe 1. When the same analysis were done in the frequency intervals 100–300 MHz and 2.5–3 GHz where the information content of the signal should be much lower, similar results were obtained, but the distances were different.

4.4.2 Epidural and subdural haematomas

Figure 4.9 shows the classification results of non bleeding, EDH and SDH phantoms. The classifier manages to classify all the phantoms 100 % correct. Only the phantoms made with grey matter recipe 2 were used for these analysis. It is possible to see some trends here. In Figure 4.9a, the

Phantom name and number	Mean distance ± SD to non bleeding phantoms [–]	Mean distance ± SD to bleeding phantoms [–]	Correct classification [%]
1: Ref_0ml_1	**1.21 ± 0.02**	1.26 ± 0.02	100
2: Ref_0ml_2	**1.20 ± 0.02**	1.27 ± 0.02	100
9: Ref_0ml_3	1.28 ± 0.02	**1.23 ± 0.03**	0
13: Ref_0ml_4	1.32 ± 0.01	**1.31 ± 0.03**	20

(a) Non bleeding phantoms.

Phantom name and number	Mean distance ± SD to non bleeding phantoms [–]	Mean distance ± SD to bleeding phantoms [–]	Correct classification [%]
3: SDH_40ml_Right	**1.12 ± 0.02**	1.20 ± 0.01	0
4: SDH_60ml_Left	**1.15 ± 0.02**	1.23 ± 0.02	0
7: EDH_40ml_Right	1.18 ± 0.02	1.18 ± 0.03	80
8: EDH_20ml_Left	1.19 ± 0.02	1.19 ± 0.02	50
10: SDH_40ml_Left	1.17 ± 0.02	**1.11 ± 0.02**	100
11: EDH_60ml_Left	1.13 ± 0.02	**1.10 ± 0.02**	100
12: SDH_20ml_Left	1.15 ± 0.01	**1.11 ± 0.01**	100

(b) Bleeding phantoms.

Table 4.4: In Table 4.4a and Table 4.4b is one non bleeding phantom and one bleeding phantom at a time left out of the training data respectively. The bold marked numbers indicate the smallest distance to a class. The phantoms in the training sets were the non bleeding phantoms: 1, 2, 9, 13 and bleeding phantoms: 8, 10, 11, 12 from Table 4.1. When a non bleeding phantom was taken out of the training data was also phantom number 8 taken out so the sets had equal size. When a bleeding phantom was taken out of the training data was phantom number 7 added to the bleeding set so the two sets had equal size.

non bleeding phantoms are closer to the EDH class than the SDH class. The same trend can be seen in the other figures, where the EDH phantoms lie equally close to the SDH class and the non bleeding class, see Figure 4.9b. The SDH phantoms are also closer to the EDH class than the non bleeding class, see Figure 4.9c. When the same analysis were performed in the frequency interval 2500–3000 MHz, a similar trend could be seen, but the variations were larger and the classes were more mixed together.

4.4.3 Volume of bleedings

Classification by volume is shown in Figure 4.10. It is possible to classify the phantoms to the correct group, but the distance to the other subspaces does not seem to reflect the sizes of the bleedings. The order in which the distance to the classes arranges themselves vary between the phantoms. Both 0 ml and 20 ml are for some phantoms closest to 60 ml, and 60 ml classification is closest to the 0 ml class.

4.4.4 Left and right bleedings

To analyse the location of the bleedings, the order of the antennas was mirrored to make it look like the bleeding was located on the other side. One phantom was removed from the training set and both the mirrored and non-mirrored versions were classified against both a non-bleeding class and two classes with left-sided and right-sided bleedings. This classification did only give a correct result for left-sided bleedings. Instead the analysis were done in the same way as for the other properties, where the classified phantom was part of the training set, the result of this can bee seen in Figure 4.11. The classifier manages to classify the phantoms almost 100 % correct when the phantoms are in the training set.

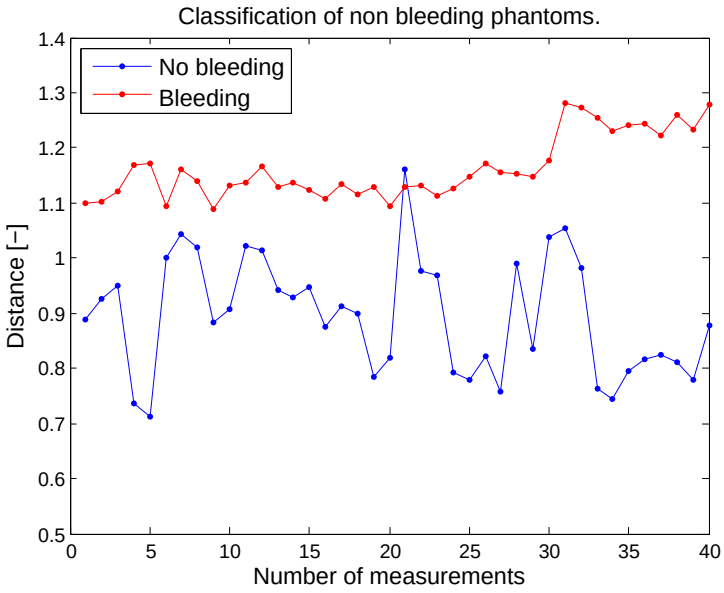

(a) Non bleeding phantoms.

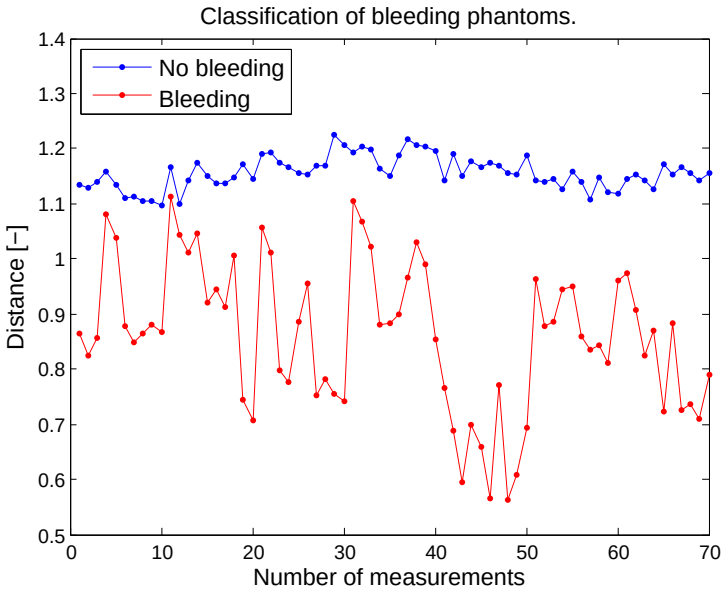

(b) Bleeding phantoms.

Figure 4.8: Classification of non bleeding (4.8a) and bleeding phantoms (4.8b). The phantoms are classified in chronological order with the non bleeding phantoms: 1, 2, 9, 13 and bleeding phantoms: 3, 4, 7, 8, 10, 11, 12 from Table 4.1.

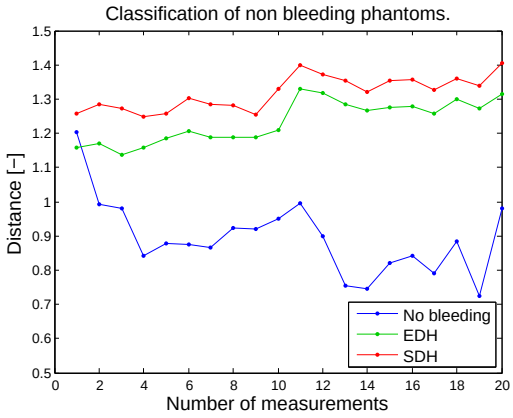

(a) Non bleeding phantoms.

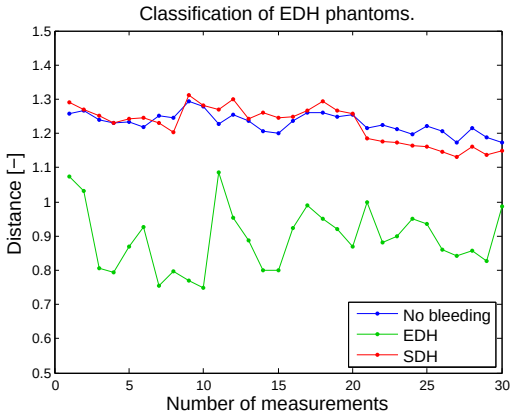

(b) EDH phantoms.

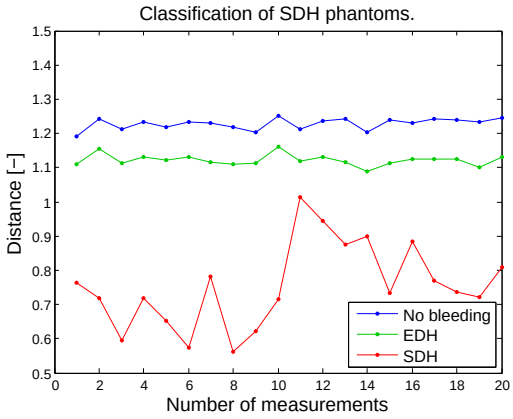

(c) SDH phantoms.

Figure 4.9: Classification of non bleeding (4.9a), EDH phantoms (4.9b) and SDH phantoms (4.9c).The phantoms are classified in chronological order with the non bleeding phantoms: 9, 13, EDH phantoms: 7, 8, 11 and SDH phantoms: 10, 12 from Table 4.1.

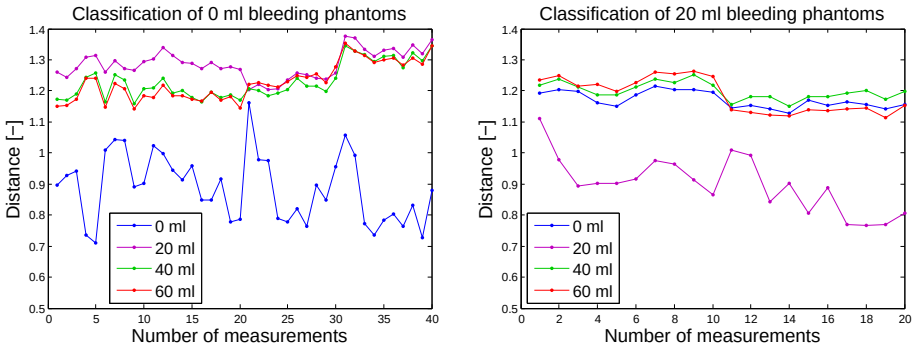

(a) Classification of non bleeding (0 ml) phantoms.

(b) Classification of 20 ml bleeding phantoms.

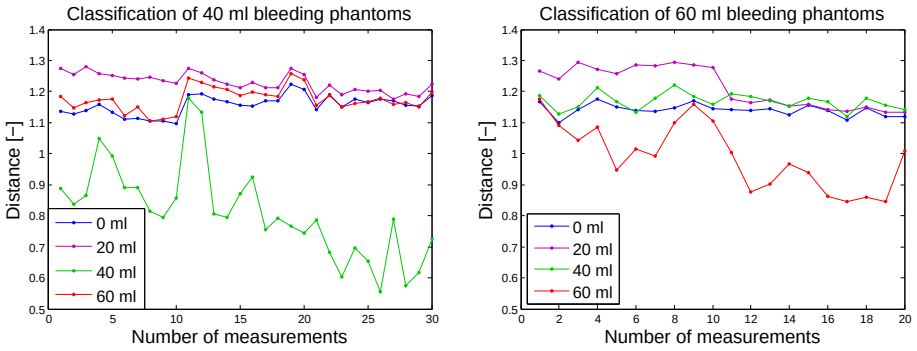

(c) Classification of 40 ml bleeding phantoms.

(d) Classification of 60 ml bleeding phantoms.

Figure 4.10: Classification with respect to volume. The phantoms are classified in chronological order with the non bleeding (0 ml) phantoms: 1, 2, 9, 13, 20 ml: phantoms 8, 12, 40 ml: phantoms 3, 7, 10 and 60 ml phantoms: 4, 11 from Table 4.1.

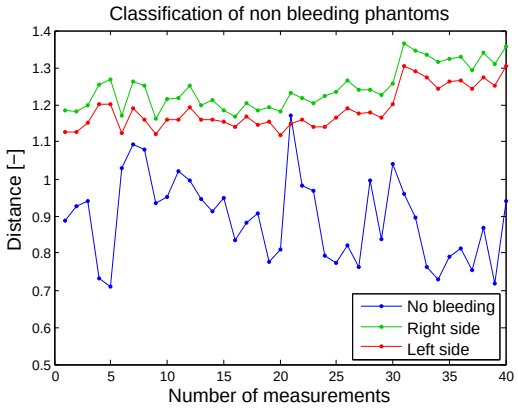

(a) Classification of non bleeding phantoms.

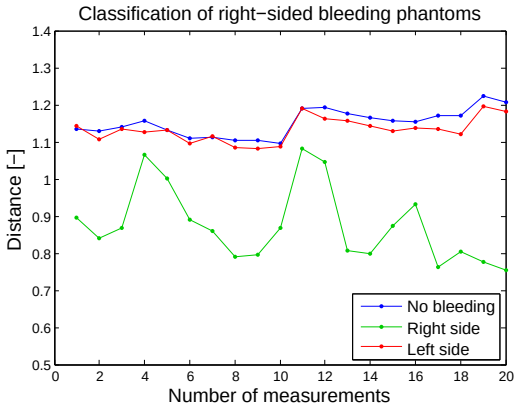

(b) Classification of right-sided bleeding phantoms.

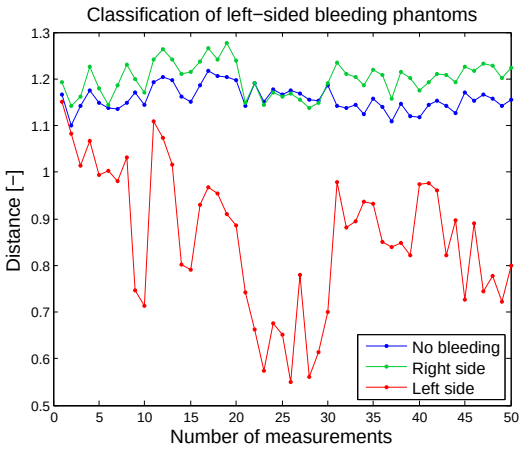

(c) Classification of left-sided bleeding phantoms.

Figure 4.11: Classification with respect to location of the bleeding. The phantoms are classified in chronological order with the non bleeding phantoms: 1, 2, 9, 13, right sided bleeding phantoms: 3, 7 and left sided bleeding phantoms: 4, 8, 10, 11, 12 from Table 4.1.

4.4.5 Interfering factors

Person close

Figure 4.12 shows the classification of bleeding phantoms with interference from a person close to the measurement setup. Table 4.5 shows a summary of the classifications of bleeding and non bleeding phantom classes with this interference. There is no clear difference between the reference and when a person is standing close to the measurement setup.

Holding the cables

Figure 4.13 shows the classification of bleeding phantoms with interference from a person holding the cables during the measurements. Table 4.6 shows a summary of the classification of bleeding and non bleeding phantom classes with this interference. There is a difference between the mean values for the reference and the interference data, where the interference data lies closer to the other subspaces. The standard deviation is also larger for the reference values.

Phone call

Figure 4.14 shows an example of the interference from a calling mobile phone close to the phantom during the measurements. The example is from classification of non bleeding phantoms to the three classes; no bleeding, EDH and SDH phantoms. Table 4.7 presents a summary of the classification of the interference from a calling mobile phone. The mean distances are approximately the same for the reference values as for the calling phone values.

Hair

Figure 4.15 shows the interference from hair around the phantoms during measurements. The example is from classification of SDH phantoms to the three classes; no bleeding, EDH and SDH phantoms. The reference values in this classification are the ordinary measurements. Just like in the ordinary measurements, the phantoms were repositioned between the measurements, which gives an extra variability. Table 4.8 shows a summary of the interference from hair on the phantoms. The classification of the phantoms with hair was closer to the other subspaces than the reference and the classifier did not manage to classify all the phantoms correctly.

Movement

Figure 4.16 shows an example of how shaking the phantoms during measurements affects the classification. The example is from the classification of the EDH phantoms to the three classes; non bleeding, EDH and SDH phantoms. A summary of the effect of movement on the classification is shown in Table 4.9. All the shaking values lie generally closer to the other classes than the reference values, but the classification is still made correctly in all the cases. Another interesting thing that can be seen, is that the standard deviation is smaller for the shaking phantom values than the reference values. The raw data from the movement experiments were studied and compared to the reference data and no obvious differences could be found.

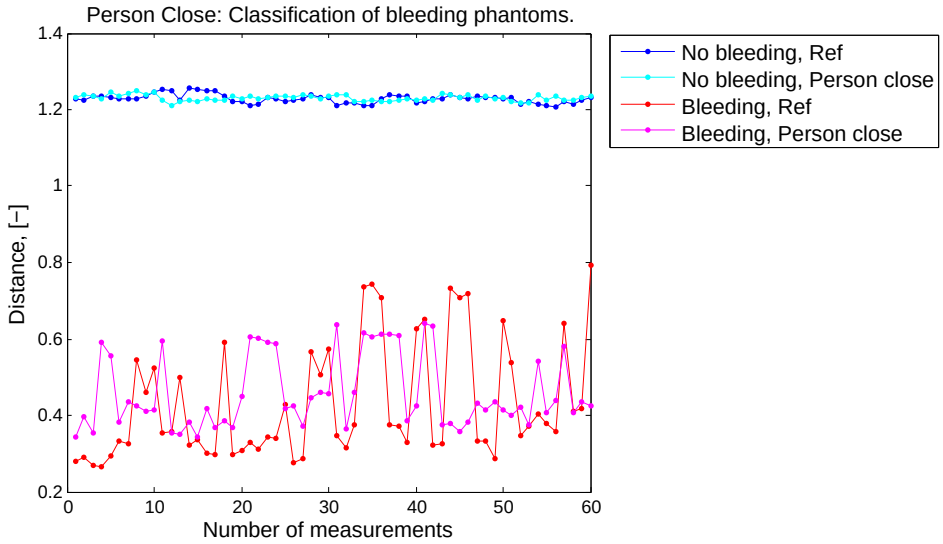

Figure 4.12: Classification of bleeding phantoms with person close to the MWH during measurements. The training data comes from reference measurements with a person far away from the setup.

Phantoms	Mean distance ± SD to reference non bleeding subspace [–]	Mean distance ± SD to reference bleeding subspace [–]	Correct classification [%]
Non bleeding reference	**0.44 ± 0.14**	1.24 ± 0.03	100
Non bleeding person close	**0.48 ± 0.09**	1.24 ± 0.03	100
Bleeding reference	1.23 ± 0.01	**0.43 ± 0.15**	100
Bleeding person close	1.23 ± 0.01	**0.46 ± 0.10**	100

Table 4.5: Classification of phantoms with a person close to the MWH during the measurements. The interference are classified relative the reference measurements. The classes are made up of the following phantoms, non bleeding phantoms: 1, 2 and bleeding phantoms: 3, 4 from Table 4.1. Figure 4.12 shows an example of how the bleeding phantom classification looks like.

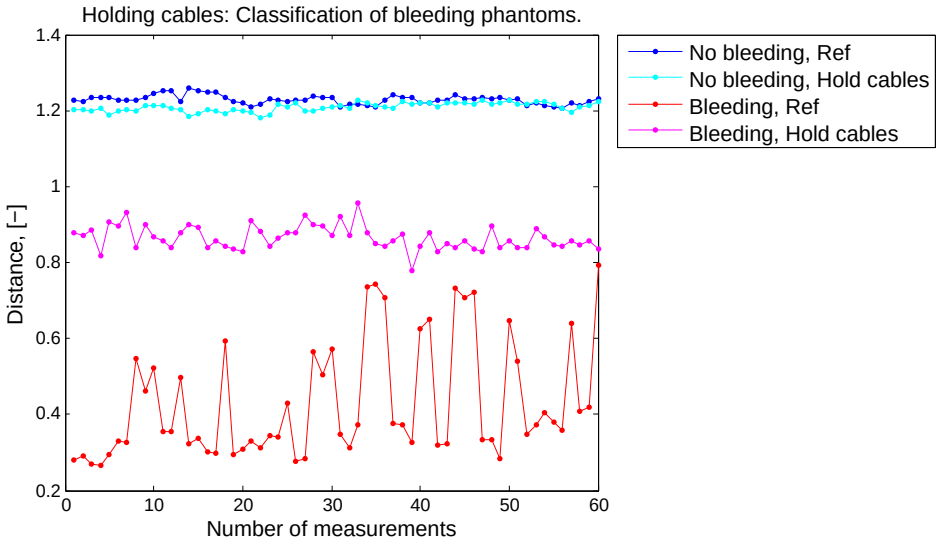

Figure 4.13: Classification of bleeding phantoms with a person holding the cables to the MWH during measurements. The training data comes from reference measurements.

Phantoms	Mean distance ± SD to reference non bleeding subspace [–]	Mean distance ± SD to reference bleeding subspace [–]	Correct classification [%]
Non bleeding reference	**0.44 ± 0.14**	1.24 ± 0.03	100
Non bleeding hold cables	**0.91 ± 0.02**	1.23 ± 0.03	100
Bleeding reference	1.23 ± 0.01	**0.43 ± 0.15**	100
Bleeding hold cables	1.21 ± 0.01	**0.87 ± 0.03**	100

Table 4.6: Classification of phantoms with a person holding the cables during the measurements. The interference are classified relative the reference measurements. The classes are made up of the following phantoms, non bleeding phantoms: 1, 2, bleeding phantoms: 3, 4 from Table 4.1. Figure 4.13 shows an example of how the bleeding phantom classification looks like.

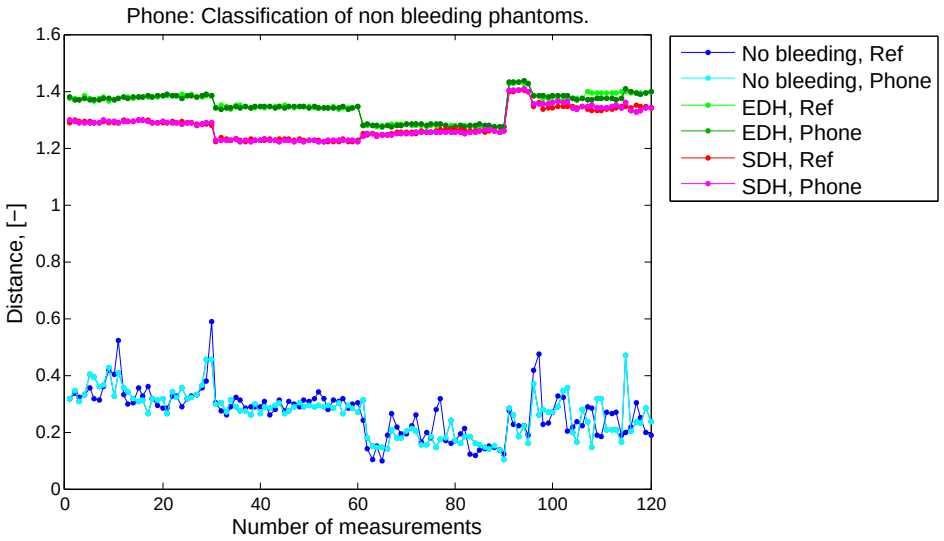

Figure 4.14: Classification of non bleeding phantoms with a calling mobile phone and reference (phone in flight mode) non bleeding phantoms.

Phantoms	Mean distance ± SD to reference non bleeding subspace [–]	Mean distance ± SD to reference EDH subspace [–]	Mean distance ± SD to reference SDH subspace [–]	Correct classification [%]
Non bleeding reference	**0.27 ± 0.08**	1.35 ± 0.05	1.28 ± 0.05	100
Non bleeding call	**0.26 ± 0.08**	1.35 ± 0.05	1.28 ± 0.05	100
EDH reference	1.21 ± 0.03	**0.20 ± 0.08**	1.22 ± 0.05	100
EDH call	1.21 ± 0.03	**0.19 ± 0.06**	1.22 ± 0.05	100
SDH reference	1.20 ± 0.02	1.27 ± 0.03	**0.23 ± 0.06**	100
SDH call	1.20 ± 0.02	1.27 ± 0.03	**0.22 ± 0.06**	100

Table 4.7: Classification of phantoms with a calling mobile phone close to the phantom during the measurements. The reference measurements are done with a mobile phone in flight mode close to the phantoms. The classes are made up of the following phantoms, non bleeding phantoms: 1, 2, 9, 13, EDH phantoms: 8, 11 and SDH phantoms: 3, 10, 12 from Table 4.1. Figure 4.14 shows an example of how the non bleeding phantom classification looks like.

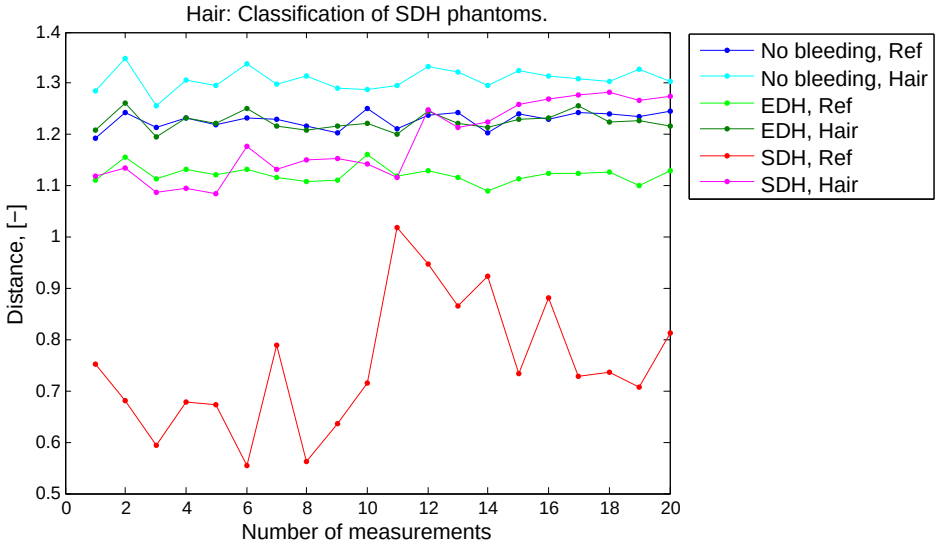

Figure 4.15: Classification of SDH phantoms with a wig. The training data comes from reference measurements with phantoms without wig.

Phantoms	Mean distance ± SD to reference non bleeding subspace [–]	Mean distance ± SD to reference EDH subspace [–]	Mean distance ± SD to reference SDH subspace [–]	Correct classification [%]
Non bleeding reference	**0.87 ± 12**	1.23 ± 0.06	1.32 ± 0.05	95
Non bleeding with hair	**1.23 ± 0.07**	1.29 ± 0.06	1.36 ± 0.04	50
EDH reference	1.23 ± 0.03	**0.92 ± 0.09**	1.23 ± 0.05	100
EDH with hair	1.30 ± 0.04	**1.16 ± 0.04**	1.30 ± 0.05	100
SDH reference	1.23 ± 0.02	1.12 ± 0.02	**0.75 ± 0.13**	100
SDH with hair	1.31 ± 0.02	1.23 ± 0.02	**1.19 ± 0.07**	60

Table 4.8: Classification of phantoms with a wig. The reference measurements are done without the wig, and the measurements using the wig are classified relative those. The classes are made up of the following phantoms, non bleeding phantoms: 9, 13, EDH phantoms: 7, 8, 11 and SDH phantoms: 10, 12 from Table 4.1. Figure 4.15 shows an example of how the SDH phantom classification looks like.

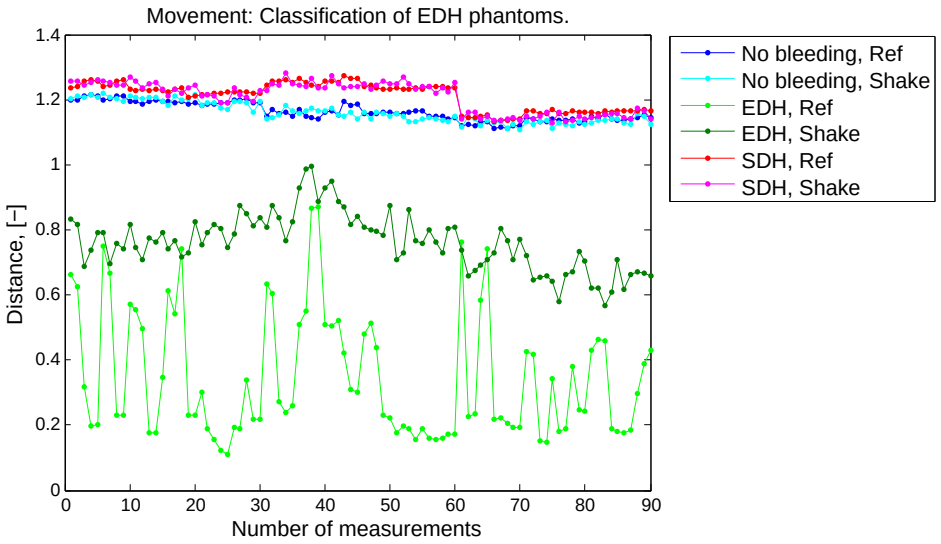

Figure 4.16: Classification of EDH phantoms with and without movement. The training data comes from reference measurements with no shaking phantoms.

Phantoms	Mean distance ± SD to reference non bleeding subspace [–]	Mean distance ± SD to reference EDH subspace [–]	Mean distance ± SD to reference SDH subspace [–]	Correct classification [%]
No bleeding reference	**0.46 ± 0.20**	1.27 ± 0.05	1.23 ± 0.05	100
No bleeding shake	**0.73 ± 0.22**	1.27 ± 0.04	1.23 ± 0.04	100
EDH reference	1.16 ± 0.03	**0.35 ± 0.19**	1.21 ± 0.04	100
EDH shake	1.16 ± 0.03	**0.76 ± 0.09**	1.21 ± 0.05	100
SDH reference	1.14 ± 0.03	1.22 ± 0.03	**0.31 ± 0.13**	100
SDH shake	1.14 ± 0.02	1.22 ± 0.04	**0.78 ± 0.10**	100

Table 4.9: Classification of shaking phantoms. The reference measurements are done with still phantoms, and the shaking phantoms are classified relative those. The classes are made up of the following phantoms, non bleeding phantoms: 1, 2, 9, 13, EDH phantoms: 7, 8, 11 and SDH phantoms: 3, 10, 12 from Table 4.1. Figure 4.16 shows an example of how the EDH phantom classification looks like.

Chapter 5
Discussion

5.1 Phantoms

Two types of bleedings were modelled, EDH and SDH. They were chosen since they are both common, dangerous and extracerebral, which make them operable in an acute stage. The brain consists of both white and grey matter, surrounded by CSF and meninges. The phantoms on the other hand consisted only of grey matter. To add extra layers, such as white matter or meninges, would be both complicated and add an extra factor of variation between the phantoms. The anatomy of the brain is similar between different persons and not all layers have to be included, since they will contribute in a similar way for all the patients. Grey matter was selected even though the amount of white matter in the brain is higher. The reason is that the difference in permittivity between blood and grey matter is smaller than the difference between blood and white matter. The MWH seems to detect symmetry differences in the brain, rather than borders between materials. So if a bleeding placed in grey matter can be detected, it can also be detected in white matter.

Several ways to produce the bleedings were tested, the ones that were finally selected were recommended by neurosurgeons Thomas Skoglund and Johan Ljungqvist at Sahlgrenska University Hospital. These methods were chosen since the phantoms were easy to construct and reproduce and the neurosurgeons thought they looked realistic.

Even if the phantoms were produced in the same way, the consistency differed between them. Some were very soft and collapsed when they were removed from the cranium and others were very solid. This has to do with the temperature of the mass. The temperature was monitored with a simple thermometer and it was hard to keep an even temperature throughout the mass. The consistency was evaluated by eye, and the speed with which it solidified depended on how much and for how long the mixture was heated. The bleeding was usually more solid than the rest of the brain. The rea-

son was that a smaller amount of phantom mass heats up and cools down quicker, due to higher surface to volume ratio. The consistency affects how easy it is to measure the dielectric properties, but is not thought to affect the dielectric properties much. Even if there would be an effect from the consistency, it would be smaller than the change in dielectric properties between liquid and solid phantom mass, which for the permittivity was 6 %.

The EDH does usually spread out more and have a larger area in the real cases than they did in the phantoms. It can be hard for the MWH to detect the EDH in the phantoms, since no antenna was covering it, see Figure 4.1d. It could therefore be interesting to change the design of the MWH to also cover the temporal bone where the EDH often is positioned. This would probably make it easier to detect the EDH.

After the first set of phantoms were finished, some discolouration on the cranium was noticed. A yeast infection was suspected due to the high sugar content of the mass and insufficient drying of the cranium. The cranium was put in a formaline bath and carefully cleaned. From then on formaline was put into the phantom mass to avoid further bacterial growth. The condition of the cranium was changed during the period of measurements. There were some cracks when the project started, but both the number and size increased during the measurement period and the thin cartilage in for example the nose was lost during the cleaning. Non of this should affect the results significantly, since the cartilage in the face was so thin and no antenna was placed there. A human cranium contains a lot of small natural cavities which made it hard to remove all excess phantom mass. There was therefore a risk that old dried phantom mass was still present when the next phantom was produced. The amount was very small and would therefore have no influence on the measurements.

The air gap in the phantoms at the location of the cerebellum was inevitable. The same thing appeared for all phantoms and the antennas close to this region were not used during the measurements, so this should not be a big problem.

5.2 Dielectric properties

5.2.1 Phantoms

It was hard to create recipes for grey matter and blood that had exactly the right relative permittivity and conductivity over the whole frequency range, see Figure 4.2. The shape of the permittivity and conductivity curves are not the same as for the reference values, which means that a certain target frequency had to be chosen where the reference values were matched. This was due to the chosen phantom recipes that can not fully replicate

the dielectric properties for grey matter and blood in the whole frequency range. In the curves the mean value for blood and grey matter phantom mass are the same as the reference values at 1 GHz for the relative permittivity and 1.5 GHz for the conductivity. How much the electromagnetic waves scatter, reflect and transmit through the phantom has to do with the difference in dielectric properties between the grey matter and the blood phantom masses. Even though the slope of the curves are not the same as the references, the difference between the means of blood and grey matter is approximately the same for the permittivity and conductivity. Therefore it can be assumed that the recipes works as models for grey matter and blood.

The variations between the phantoms are probably due to the fact that it is not exactly the same amount of each ingredient in every phantom, even though care was taken to be as precise as possible. If it would have been possible to measure the dielectric properties during the phantom making could more even results be obtained. Another change that was noticed during the measurements were the differences in the calibration of the dielectric probe. A new calibration was done every day, but the water measurements differed each day, even though it had the same temperature. This may have affected the dielectric property measurements with a few percent. The number of days between the creation of the phantoms and the dielectric measurements may also have affected the properties. The effect is probably not be that big, due to the fact that the phantom mass samples were covered in plastic wrapping and stored in the refrigerator until the day of the dielectric measurements.

In some of the dielectric graphs the conductivity goes below zero, see Figure 4.2. This is due to the uncertainties for the dielectric probe measurements at frequencies below 0.5 GHz.

The small amount of food colour and formalin used in the phantom masses do not affect the dielectric properties and can therefore be replaced with deionised water in the recipes. The food colour was practical to use to be able to see where the bleeding was located in the phantom.

Contrast in bleeding phantoms

The mean contrast in relative permittivity between the grey matter and blood phantom masses in the bleeding phantoms, see Table 4.2a, are a little bit higher than for the reference values. There is a quite big standard deviation, so some phantoms have a difference in permittivity that may be harder to see than what it actually is in a real brain, especially the case with the bleeding phantoms done with grey matter recipe 1. These differences may also make the classification harder, because the MWH data will differ

between different phantoms.

5.2.2 Grey matter and blood recipes

Differences between the grey matter and blood phantom solution results from recipe 1, and the results from Malik Ahmad [9] in Figure 4.3 and 4.4, may be due to method differences. Malik Ahmad had for example the possibility to measure the dielectric properties during the construction of the phantom solutions.

5.2.3 Liquid and solid phantoms

The results for liquid and solid phantom masses makes it possible to create new recipes from liquid solutions. If six percent agar is added the permittivity will decrease with six percent and no effect will be seen on the conductivity, see Table 4.3. Only the phantoms with grey matter recipe 2 could be used for these calculations, since the other phantom groups were not normally distributed over all frequency points. If these other phantoms, 22 in a total, were taken into account for the calculations of the mean value change, the result become the same. This indicates that the results are correct. Another indication that the results are valid is that experiments where agar was added to water gave the same result.

5.2.4 Coagulated blood measurements

The haematoma usually consists of clotted blood. Since the dielectric properties for blood from Gabriel et al. [22] are given for liquid 37 °C blood, it is interesting to see if the dielectric properties are the same for coagulated blood. It is very hard to mimic the coagulation process in the body and therefore the pig blood was coagulated by heat. These results, see Figure 4.5, can only be used as an indication for how the coagulation will affect the dielectric properties and more extended experiments have to be made to get certain results. The coagulated blood was shown to the neurosurgeons Thomas Skoglund and Johan Ljungqvist at Sahlgrenska University Hospital. They said it had similar consistency as blood in a haematoma in the brain. In this result the effect of the coagulation is small and the differences between the blood mass phantoms and the reference values for blood are larger than the effect of the coagulated blood is.

The information from the store was that no additives or special treatment procedures had been performed except freezing. However, the neurosurgeon Johan Ljungqvist thought that the pig blood may have been treated in some way, since it did not coagulate naturally. This could also be part of the explanation why the pig blood had lower permittivity and conductivity

than the reference values. Other reasons may be temperature variations in the pig blood samples, differences in method or differences in the dielectric probes used.

5.3 Microwave helmet

There were some problems with the measurement equipment. Several of the antennas gave weak or shaky signals, the error often built up during the measurements and the severity could not be seen until afterwards. This problem was present for most of the phantoms and on the same antennas, but worsened during the progress of the project. At one point, something happened inside the network analyser which made the old calibration files useless. What happened was that the isolation in one of the mechanical switches was changed, causing a large part of the signal to go directly from the transmitting port to the receiving port without going through the phantom. When the system was recalibrated, this leakage was compensated for, but the original problem was still present. Two phantoms were measured before this problem was discovered. The data from the deviant phantoms were normalised after recalibration, but they did still differ to much from the rest of the data to be able to use. Unfortunately the bleedings of both phantoms were placed on the right side, which means that only two right sided bleedings were left. It is hard to say if this change affected the classification since each phantom was measured only on one day. The differences between the first group of phantoms done with grey matter recipe 1, and the second group done with recipe 2, may be due to either the differences in dielectric properties or the change in the measurement equipment.

The skin depth in grey matter for the frequencies used in these measurements are only a few centimetres, see Figure 2.12. This means that a major part of the signal is lost before it reaches the antennas on the opposite side of the head. This might make it harder to find a bleeding deeper in the brain. However, if the MWH is compared to the Infrascanner, which uses a much shorter wavelength (808 nm), the skin depth of the MWH is much longer. Another problem with the Infrascanner is that a lot of practice is needed to perform the measurement, since the measurement sequence is done by hand. Only a few places on the head are measured, so if the bleeding is located somewhere else, or deeper into the brain, it would go unnoticed.

5.4 Data analysis

When analyses were done for frequencies outside the chosen interval, similar results were obtained. This is of course not good, since it indicates that the

classifier focuses on things outside the phantoms. Since the classifier at this point only seems to recognise the individual phantoms, rather than the bleedings, this was not really a surprising result. The interval is limited since the differences outside the frequency interval come from uninteresting factors.

The analysis in this project were done with an in-house classifier, no changes have been made to it and no extensive preprocessing of the data have been performed. There might be better ways to find the sought patterns in the data, but since this project focused on the phantoms, there was no time to develop a new method of classification.

The ordinary measurements were performed in groups of three, where the variation between the groups were much larger than within the groups, see Figure 4.7. This means that there is a greater variation between how the phantom was placed in the MWH and how the water bags were filled, than between the individual MWH measurements. The variation was calculated as the ratio between the mean of the standard deviation for all the phantoms and the mean of the standard deviation for each group of three measurements. It is not possible to compare them directly, since the number of measurements is much higher for the phantoms than for the smaller groups. The distance from one measurement point to the class it belongs to depends on the data in the training set and is therefore a very imprecise measurement from the beginning. To take the standard deviation of these values makes it even more imprecise since the class it is compared to is not the same for all points, due to the five–fold cross–validation. It is therefore difficult to evaluate this effect, but illustrates how the measurements are related.

Several k–values for the cross–validation were tested, generally larger values gave better results, since more of the data was put into the training set. However, a relatively small k–value was chosen to avoid the risk of over–training the classifier.

One of the reference phantoms was made as a SDH, but with the same batch of grey matter phantom mass for both the bleeding and the grey matter phantom parts. The distance from this phantom to the bleeding class is actually larger than for the other phantoms, see phantom 13 in Figure 4.7. This is probably due to the low permittivity for this phantom compared to the other reference phantoms, see Table B.1, and it indicates that the difference in dielectric properties is more important than the construction process.

The reason that only one measurement was used from each group of three for the analysis was that it might be easier for the classifier to see other, less obvious trends when this group–of–three trend is removed. Since the difference between the groups are much larger than within the group,

not much of the information are lost in this process. In the case when all three measurements were used, they were put in the same training set. The reason for this was that if one of them were in the training set and another one in the test set, the classifier may recognise these similarities instead of the properties of the bleeding.

5.4.1 Non bleeding and bleeding phantoms

The classifier manages to classify almost 100 % correct when some of the measurement points from the phantoms that were classified were part of the training data, see Figure 4.8. The classifier does not manage to classify all the phantoms correctly when leaving one phantom out of the training data, see Table 4.4. This indicates that the classifier manages to recognise individual phantoms, but it is not possible to tell if it can detect the bleedings. It also means that the measurements for each phantom are more similar to each other than different phantoms in the same class. This depends on the differences between the phantoms, such as the contrast in permittivity and conductivity between the bleeding and the grey matter, recipe, calibration, the dielectric properties for the phantom, the location of the bleeding and the connections between the antennas and the cables etc.

It is also possible to see that the first bleeding phantoms, phantoms number 3 and 4, lie closer to the non bleeding phantom set than the phantoms made with grey matter recipe 2, see Figure 4.8a. This can also be seen in the non bleeding phantom classification in Figure 4.8b, where the two first phantoms, phantom number 1 and 2, lie closer to the non bleeding phantom class than for the other phantoms. This may either be due to the recipe changes that were made between these groups of phantoms or the new calibration. It is hard to know which one of these factors that are the main contributor to the change. In the non bleeding phantom class were 50 % old phantoms made with recipe 1 and the old calibration, compared to 30 % of the phantoms in the bleeding class. This may make it easier to classify the old phantoms to the non bleeding class and phantoms with recipe 2 to the bleeding class. This argument is also supported by the results where one phantom is left out of the training set, see Table 4.4.

The classification for leave one phantom out is almost the same in the low and high frequency regions as in the chosen interval. This can be partly explained by the possibility that the classifier differ the phantom measurements between the old and the new phantoms. In between which both the recipe and calibration of the equipment was changed, as well as the hardware problem that occurred. Classes with even sizes had to be used in the case where one phantom at the time was left out of the training data. If the classes were not even in size, the classifier always gave the smallest

distance to the class with the largest number of phantoms. The classification became the same for uneven and even class sizes if the classification was done with measurement points from phantoms in the training data. This indicate that the classification keeps information in the subspace that is specific for the individual phantoms and not just the group of phantoms. Therefore it is not that important to have even class data size when classifying phantoms that are also in the training data.

There are too few phantoms made, to be able to say if the classifier manages to classify bleedings and non bleedings correctly. More phantoms would have to be made, especially phantoms that have equal size and location of the bleeding, since it is very hard for the classifier to find the common factor between the phantoms when they differ so much from each other. That is also one of the problems in the real case with real patients where the intracranial bleedings are all different from each other. Large training data sets are therefore needed to achieve high detection accuracy. This also means that phantoms made in this project are realistic, since they are not exactly the same.

Some analysis of the raw data were performed, where the mean phase and amplitude of the signal between two antennas were plotted. This was done for all phantoms and a couple of antenna pairs. The signals from bleeding and non bleeding phantoms were compared, but no obvious trends could be seen. This was a very simple analysis, and there might still be a lot of information in the phase, but it can not be seen with bare eye in these analysis.

5.4.2 Epidural and subdural haematomas

For EDH and SDH, only the phantoms made with grey matter recipe 2 were used, which removes the largest uncertainty factors. The classification of the non bleeding phantoms lie closer to the EDH class than the SDH class, see Figure 4.9. This may be due to the shape and location of the EDH in the phantom. In EDH, the bleeding had a smaller area and was not covered by any antennas, see Figure 4.1d and Figur 3.7, which can make the EDH phantoms look less like a bleeding phantom than the SDH phantoms.

This is the only case where it was possible to remove the old phantoms and still have enough data in all classes. Both volume and location had one class containing only one old and one new phantom. If the old one had been removed, only one phantom would have been left in the class. For bleeding and non bleeding, it would be possible to remove the old phantoms, but then the bleeding class would be more than twice the size of the non bleeding class, which might effect the possibility to make an adequate classification. In the EDH and SDH case, as well as for volume and location, the number

of phantoms in each subset was too small to leave a phantom out of the training set.

5.4.3 Volume of bleedings

As in the other cases it was possible to make a correct classification if data from the classified phantom was part of the training set, but there was no trend in the distances to the other subspaces. In many cases there was no obvious order in which the other subsets should arrange themselves, but in this case there was. A non bleeding phantom should optimally be closest to the subspace of the smallest bleeding, and furthest from the largest one. If this had been the case, it might have been possible to estimate the size of the bleeding even if no bleeding of the same size is present in the training set. In the real world, bleedings do not come in discrete sizes, they have different sizes, forms and locations. It is therefore good that there are variations between the phantoms, also inside the classes, but to get a full span of the class, the number of phantoms needs to be much larger, with more replicas of each type of bleeding.

5.4.4 Left and right bleedings

When the data was reversed to resemble bleedings on the other side of the head, the classifier found a much larger difference between if the data had been reversed or not, than between the two locations of the bleeding. The reason for this is probably that the antennas and their connections have different characteristics. The classifier did therefore recognise if the data had been modified.

Since both the phantoms that had to be removed due to hardware problems had the bleeding on the right side, and the number of right sided bleedings were lower to begin with, only two of the seven bleedings were placed on the right side. Since most of the bleedings were placed on the left side, it contained mostly unreversed data, while the right class consisted mostly of reversed data. Therefore all reversed data was classified to the right sided class, and the unreversed to the left sided. Even if it is desirable to see a difference between right and left sided bleedings, the difference to the non bleeding phantom class should be larger, but this can not be seen in the results, see Figure 4.11.

5.4.5 Interfering factors

Person close

There was no impact on the measurements when a person was standing close to the measurement setup, see Figure 4.12 and Table 4.5. This corresponds well to the expectation since there still was no direct contact with the measurement setup. This result means that this part would not be a problem in an ambulance.

Holding the cables

There was a change in the results when a person was holding the cables during the measurements, but there were still no problem with the classification, see Figure 4.13 and Table 4.6. This is probably due to the fact that the cables are not well enough isolated and the ground is then changed. This change in the ground makes the measurement signals differ from the reference. The standard deviation for the reference data is higher than for the interference data. This might have to do with the fact that the data that is sent in to the classifier is logarithmised. The classification was also done without logarithming the data, which gave a slightly larger standard deviation, but did not completely explain the difference in standard deviation.

Phone call

It can be seen that there is no effect from a calling mobile phone close to the measurement setup, see Figure 4.14 and Table 4.7. Therefore no care must be taken to turn off the patients phone before performing the measurements.

Hair

The hair measurements were performed in another way, due to practical reasons. The results can therefore not be compared to the other interfering results. In these experiments, the phantoms were moved between the measurements and classified against the ordinary measurements done a couple of hours before. This means that there are at least two interferences that are shown in this graph; the movement and the hair. There is also a possible time interference. However a comparison between reference measurements done in the morning and in the afternoon indicate that the time factor should not have a large impact. All these interferences may together make it hard to classify all the phantoms correctly. It can be seen in Figure 4.15 and Table 4.8 that it is harder to classify the hair phantoms than the regular phantoms.

It is interesting to test this effect further and maybe with different thickness of the hair. The hair probably makes it harder to get a good connection between the MWH and the phantom, since it is easier to get air pockets. The results indicate that the hair can make it harder to classify phantoms.

Movement

It can be seen in the results that the movement has an effect on the classification, see Figure 4.16 and Table 4.9. The classification of the movement measurements gets closer to the other subspaces than the reference measurements. These results are done without changing position of the phantoms between the measurements, so together with that effect it may build up together and be hard to classify the phantoms.

The influence of the movement was tested by rocking the MWH and phantom back and forth. The shaking in an actual ambulance is probably smaller than the tested movement. A damping mechanism could be used in the future to reduce the effect even further. The results only show that there is an effect but it does not say if the effect is so big that it can disguise a bleeding. Figure 4.16 indicates that it is still possible to make a correct classification.

5.5 Future work

There are a lot of things that needs to be further investigated with the MWH technique.

- Designing more realistic phantoms with white matter, meningues and blood vessels.
- Adapting recipes so the dielectric properties come closer to the reference values over the whole frequency range.
- Look more carefully at the phase of the raw data and see if any useful information is hidden there.
- Analyse different combination of antennas to focus more on deviations from the symmetry of the brain.
- Evaluate the obtained data with another classifier.
- Make a larger number of phantoms to get a larger database for better classifications.
- Make phantoms with different cranium sizes and forms.

- Test how different thickness and amount of hair affects the measurements.
- Do more extensive tests on the movement interference.

Chapter 6
Conclusion

It was not possible to obtain the correct dielectric properties over the whole frequency range, and hard to repeat the results, even though the same recipes were used. Despite this, the contrasts in the phantoms were generally close to the real differences, which indicates that the phantoms were still a valid model.

The methods to produce the EDH and SDH phantoms were fine since they were easy to reproduce and gave realistic looking bleedings. These methods can therefore be used in the future to produce more phantoms.

The best thing would have been if all the phantoms had been measured on the same day in a randomised manner. This could not be done, since only one cranium was available.

The amount of data from the MWH measurements was very large, with each measurement containing over 30 000 variables. It is therefore not that simple to find the relevant trends in the data, and a lot of effort needs to be put into the analysis.

It was possible to classify a phantom that was in the training set, but harder if the phantom was not in the training set. This indicates that the classifier can identify the individual phantoms. To be able to find the larger trends, such as the presence and type of bleedings, a lot more phantoms and a lot more measurements needs to be done. The trend that can be seen in the analysis for EDH and SDH is very positive, since it corresponds well to the expectations.

In the analysis of the interfering factors, it can be seen that hair, movement and holding the cables have impact on the classification, while just standing close to the device or using a mobile phone does not. On the other hand it is not clear if these impacts are large enough to disguise a bleeding, since the classifications in almost all cases were successful.

Overall MWT seems to be a promising technique for detecting intracranial bleedings, however a much larger set of measurement data needs to be obtained before it could be completely evaluated.

Bibliography

[1] S. Kleiven, P. M. Peloso, and H. Holst, "The epidemiology of head injuries in Sweden from 1987 to 2000," *Injury Control and Safety Promotion*, vol. 10(3), pp. 173–180, Sep 2003.

[2] T. Sundstrøm, S. Sollid, T. Wentzel-Larsen, and K. Wester, "Head injury mortality in the nordic countries," *Journal of Neurotrauma*, vol. 24(1), pp. 147–153, Jan 2007.

[3] M. Faul, L. Xu, M. M. Wald, and V. G. Coronado, "Traumatic brain injury in the united states," *U.S. Department of Health and Human Services*, pp. 1–74, March 2010.

[4] J. A. Langlois, W. Rutland-Brown, and M. M. Wald, "The epidemiology and impact of traumatic brain injury," *J Head Trauma Rehabil*, vol. 21(5), pp. 375–378, 2006.

[5] A. A. Hyder, C. A. Wunderlich, P. Puvanachandra, G. Gururaj, and O. C. Kobusingye, "The impact of traumatic brain injuries: A global perspective," *NeuroRehabilitation*, vol. 22, pp. 341–353, 2007.

[6] R. M. Bullock, R. Chesnut, J. Ghajar, D. Gordon, R. Hartl, D. W. Newell, F. Servadei, B. C. Walters, and J. E. Wilberger, "Surgical management of traumatic brain injury," *Neurosurgery*, vol. 3, pp. S2–1–S2–3, 2006.

[7] E. N. Marieb, J. Mallatt, and P. B. Wilhelm, *Human Anatomy*, 5th ed., S. Beauparlant, Ed. Pearson International Edition, 2008.

[8] Y. Toyama, T. Kobayashi, Y. Nishiyama, K. Satoh, M. Ohkawa, and K. Seki, "CT for acute stage of closed head injury," *Radiation medicine*, vol. 23(5), pp. 309–316, 2005.

[9] A. A. Malik, "Detecting traumatic intracranial bleedings in a brain phantom using microwave technology," Master's thesis, Chalmers University of Technology, 2012.

[10] A. D. Gean and N. J. Fischbein, "Head trauma," *Neuroimaging Clinics of North America*, vol. 20, pp. 527–556, 2010.

[11] B.-M. Bellander, S. Sollid, C. Kock-Jensen, N. Juul, V. Eskesen, T. Sundstrøm, K. Wester, and B. Romner, "Prehospital handläggning av patienter med svår skallskada," *Läkartidningen*, vol. 105, pp. 24–25, 2008.

[12] J. M. Hardman and A. Manoukian, "Pathology of head trauma," *Neuroimaging Clinics of North America*, vol. 12, pp. 175–187, 2002.

[13] B. Haas, D. Gomez, B. Zagorski, T. A. Stukel, G. D. Rubenfeld, and A. B. Nathens, "Survival of the fittest: The hidden cost of undertriage of major trauma," *Journal of the American College of Surgeons*, vol. 211, no. 6, pp. 804–811, Dec 2010.

[14] B. Jennett, "Assessment of the severity of head injury," *Journal of Neurology, Neurosurgery and Psychiatry*, vol. 39, pp. 647–655, 1976.

[15] J. L. Prince and J. M. Links, *Medical imaging signals and systems*, M. J. Horton, Ed. Pearson Prentice Hall, 2006.

[16] J. P. Coles, "Imaging after brain injury," *British Journal of Anaesthesia*, vol. 99(1), pp. 49–60, Jul 2007.

[17] J. Leon-Carrion, J. M. Dominguez-Roldan, U. Leon-Dominguez, and F. Murillo-Cabezas, "The infrascanner, a handheld device for screening in situ for the presence of brain haematomas," *Brain Injury*, vol. 24(10), pp. 1193–1201, Sep 2010.

[18] K. Hynynen and F. A. Jolesz, "Demonstration of potential noninvasive ultrasound brain theraphy through an intact skull," *Ultrasound in Medicine and Biology*, vol. 24(2), pp. 275–283, 1998.

[19] G. Unsgaard, A. Gronningsaeter, S. Ommedal, and T. A. N. Hernes, "Brain operations guided by real-time two-dimensional ultrasound: New possibilities as a result of improved image quality," *Neurosurgery*, vol. 51, pp. 402–412, 2002.

[20] T. Gerriets, E. Stolz, S. König, S. Babacan, I. Fiss, M. Jauss, and M. Kaps, "Sonographic monitoring of midline shift in space-occupying stroke," *Stroke*, vol. 32, pp. 442–447, 2001.

[21] D. M. Pozar, *Microwave Engineering*, 4th ed., A. Melhorn, Ed. John Wiley & Sons, Inc., 2012.

[22] S. Gabriel, R. W. Lau, and C. Gabriel, "The dielectric properties of biological tissues iii. parametric models for the dielectric spectrum of tissues," *Physics in Medicine and Biology*, vol. 41(11), pp. 2271–2293, 1996.

[23] U. Kaatze, "Complex permittivity and of water and as a function and of frequency and temperature," *Journal of Chemical and Engineering Data*, vol. 34, no. 4, pp. 371–374, 1989.

[24] S. J. Orfanidis, "Ch 5: Reflection and transmission," in *Electromagnetic Waves and Antennas*, 2008, pp. 152–158.

[25] A. Technologies, "Agilent network analyzer basics," pp. 15, 17, 22–24, August 2004. [Online]. Available: http://cp.literature.agilent.com/litweb/pdf/5965-7917E.pdf

[26] S. J. Orfanidis, "Ch 13: S-parameters," in *Electromagnetic Waves and Antennas*, 2008, pp. 525–530.

[27] J. Lantis II, K. Carr, R. Grabowy, R. Connolly, and S. Schwaitzberg, "Microwave applications in clinical medicine," *Surgical Endoscopy*, vol. 12(2), pp. 170–176, 1997.

[28] S. Y. Semenov and D. R. Corfield, "Microwave tomography for brain imaging: Feasibility assessment for stroke detection," *International Journal of Antennas and Propagation*, pp. 1–8, 2008.

[29] H. Trefná and M. Persson, "Antenna array design for brain monitoring," pp. 1–4, 2008.

[30] S. J. Orfanidis, "Ch 18: Aperture antennas," in *Electromagnetic Waves and Antennas*, 2008, pp. 743–748.

[31] ICNIRP, "ICNIRP guidelines, for limiting exposure to time-varying electric, magnetic and electromagnetic fields (up to 300 GHz)," *Health Physics*, vol. 74(4), pp. 494–522, 1998.

[32] ICNIRP, "ICNIRP statement on the "guidelines for limiting exposure to time-varying electric, magnetic and electromagnetic fields (up to 300 GHz)"," *Health Physics*, vol. 97(3), pp. 257–258, 2009.

[33] D. L. Hamblin, A. W. Wood, R. J. Croft, and C. Stough, "Examining the effects of electromagnetic fields emitted by gsm mobile phones on

human event-related ppotential and performance during an auditory task," *Clinical Neurophysiology*, vol. 115, pp. 171–178, 2004.

[34] D. C. Lay, *Linear Algebra and Its Applications*, 3rd ed. Tobin, Greg, 2006.

[35] J. A. Rice, *Mathematical Statistics and Data Analysis*, 3rd ed., C. Crockett, Ed. Thomson Brooks/Cole, 2007.

[36] C. S. Robertson, E. L. Zager, R. K. Narayan, N. Handly, A. Sharma, D. F. Hanley, H. Garza, E. Maloney-Wilensky, J. M. Plaum, C. H. Koenig, A. Johnson, and T. Morgan, "Clinical evaluation of a portable near-infrared device for detection of traumatic intracranial hematomas," *Journal of Neurotrauma*, vol. 27, no. 9, pp. 1597–1604, Sep 2010.

[37] P. Swahn, "Creating realistic phantoms of intracranial bleedings to evaluate detection accuracy with microwave technology," Master's thesis, University of Gothenburg, 2013.

Appendix A

Measurement protocol

A.1 Create phantom

A.1.1 Blood phantom mass

If the phantom contains a bleeding, a blood phantom mass should be prepared. The amount of blood phantom mass needed depends on the desired bleeding size, but the basic recipe can be seen in Table A.1 where the volumes are for 100 vol% = 3 dl.

Blood	Vol%	Volume
Deionised water	66	2 dl - 2 pinches = 198 ml
Salt	1	3 pinches = 3 ml
Sugar	26	5 tbs + 3 pinches = 78 ml
Red food colour	1	3 pinches = 3 ml
Agar	6	1 tbs + 3 pinches = 18 ml

Table A.1: Recipe for the blood phantom mass when the volumes are for 100 vol% = 3 dl.

1. If you are doing an **EDH**, build a wall using tape and plastic wrapping around the area where the bleeding should be placed, see Figure A.1. Continue with point 5–12 before continuing with, point 2–4, the wrapping of the cranium.

2. **Tape together the cranium using one layer of fabric tape, see Figure A.2.** Also tape the inside of the eyes and other small holes with masking tape, not the foramen magnum. Put some paper in the eye sockets, in the nose and between the foramen magnum and the teeth. This makes less agar flow out from the cranium, and makes it easier to remove the agar after solidification.

Figure A.1: The cranium before adding an EDH.

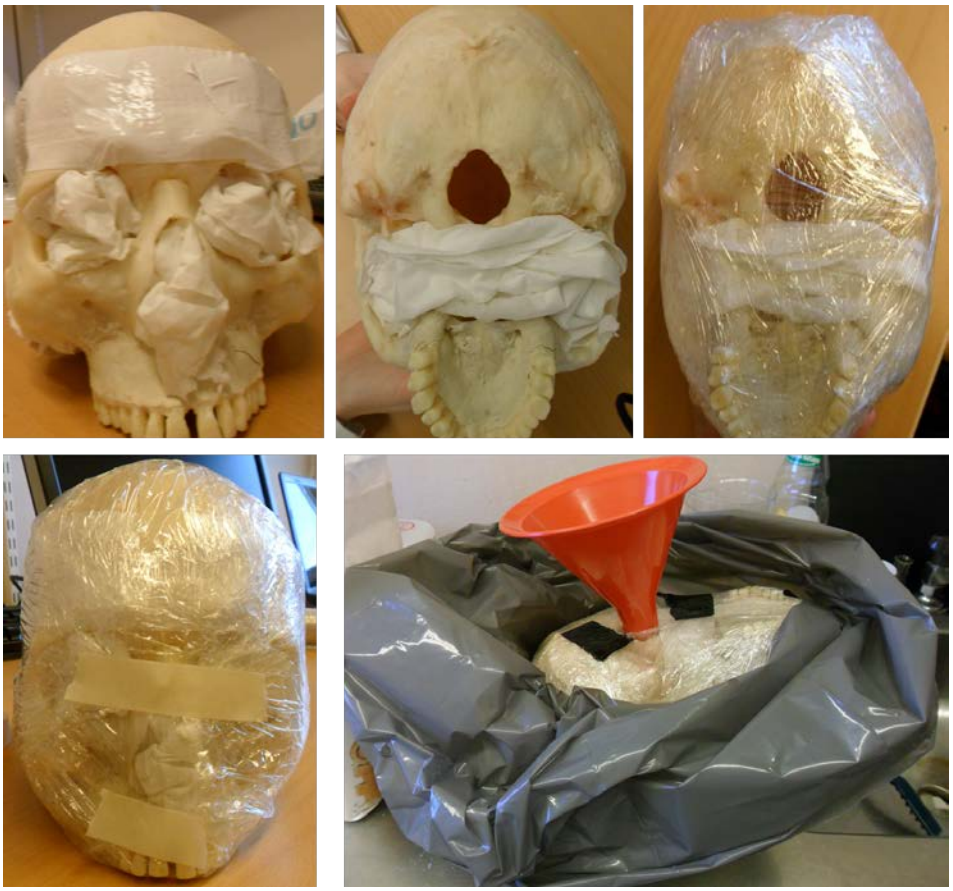

Figure A.2: Preparation of cranium before adding the agar solution.

3. **Cover the skull** with several layers of plastic wrapping and fix it with more masking and fabric tape. The plastic should be wrapped

several times around the skull in different angles so nothing can come out, see Figure A.2.

4. Put the plastic-wrapped cranium in a **plastic bag in a bowl**. This will make it easier to make a water-bath with the water close to the head, see Figure A.2.

5. **Mix sugar, salt, food colour and deionised water in a pot.** Mix the salt in a small amount of deionised water first (otherwise it may not dissolve completely). Add sugar, food colour and the rest of the water, let the sugar dissolve completely in the water, this can be done by heating the liquid. Avoid air-bubbles!

6. Remove 6 cl of the water-sugar-salt-colour mixture and put it in two shot glasses and measure the **dielectric properties**. Put the glasses in the refrigerator if it is not possible to measure the dielectric properties immediately. Mark the glasses with name and date and cover it with plastic wrapping.

7. **Add the agar**. Since 6 cl have been removed the **new agar amount** where the volumes are for 100 vol% = 3 dl is 13.5 ml (2 tsp + 3.5 pinches)! This volume is calculated from the fact that the total solution volume is not 3 dl, but around 2.4 dl (since sugar is dissolved). Stir the mixture and avoid air-bubbles!

8. **Heat the liquid** to 70 °C, keep the temperature between 70-80 °C for five minutes, otherwise it will not solidify properly [9].

9. Let the agar mass rest for 5-10 minutes **until it starts to thicken**, evaluate the consistency by eye.

10. Connect the syringe with the tube.

11. Suck up the blood phantom mass with the syringe, try to avoid air bubbles and boiling due to suppression. Remove air bubbles by turning the syringe upside down and push the air out.

12. If you are doing an **EDH**, fill the shielded area with the desired amount of blood mass, let it solidify and remove the wall. Continue with point 2–4 and afterwards with 14–16.

13. If you are doing an **SDH**, place the cranium in the plastic bowl at an angle and place the bleeding at the side of the head using the tube, make sure the bleeding stays on one side of the midline.

14. **Clean the syringe and tube** immediately to avoid clogging.

15. Save some of the left-over blood mass in two shot glasses. Mark the glasses with name and date and cover it with plastic wrapping. Let it solidify and measure the **dielectric properties**

16. Let the bleeding solidify before making the measurements.

A.1.2 Brain phantom mass

When the bleeding is solid, it is time to make the grey matter phantom mass. The amount of mass needed to fill the head can be seen in Table A.2 where 100 vol% = 2.5 l.

Grey mass	Vol%	Volume
Deionised water	50.1	12 dl + 3 tbs + 1.5 tsp = 1252.5 ml
Salt	0.1	0.5 tsp = 2.5 ml
Sugar	43.8	10 dl + 6 tbs + 1 tsp = 1095 ml = 940 g
Agar	6	1.5 dl = 150 ml

Table A.2: Recipe for the grey matter phantom mass when 100 vol% = 2.5 l.

1. **Mix sugar, salt and deionised water in a pot.** Mix the salt in a small amount of deionised water first (otherwise it may not dissolve completely). Add sugar and the rest of the water, let the sugar dissolve completely in the water, this can be done by heating the liquid. Avoid air-bubbles!

2. Remove 6 cl of the water-sugar-salt mixture and put it in two shot glasses and measure the **dielectric properties**. If it is not possible to measure immediately, mark the glasses with name and date, cover it with plastic wrapping and put it in the refrigerator.

3. **Add the agar**. Since 6 cl have been removed the **new agar amount** for 100 vol% = 2.5 l is 145.5 ml (1 dl + 3 tbs + 0.5 pinches)! This volume is calculated from the fact that the total solution volume is not 2.5 l, but around 2 l (since sugar is dissolved). Stir the mixture and avoid air-bubbles!

4. **Heat the liquid** to 70 °C, take the pot of the plate to make sure it does not get too hot and keep the temperature between 70-80 °C for five minutes, otherwise it will not solidify properly [9].

5. Let the agar mass rest in the pot for 3-5 minutes to get a bit thicker, reducing the flow out from the cranium.

6. **Fill the head** with the agar mass through the foramen magnum, using a funnel. Be careful not to destroy any bleeding, don't turn the cranium back up until it is partly filled. Make sure the cranium is properly filled and add some extra solution if needed.

7. Clean the funnel and other equipment to avoid clogging.

8. Fill the bowl (outside of the plastic bag) with cold water and let the mass solidify, change the water from time to time to keep it cold. The water will also make the leakage from the phantom smaller.

A.2 Calibration of dielectric probe (Chalmers)

Calibrate the dielectric probe and perform measurements.
You need to have everything stable when you calibrate and perform measurements with the dielectric probe. You need to recalibrate if you move anything (probe, stand or cable) between the calibration and the measurements!
Make sure you have connected all the connections correctly with the special designed torque wrench. Do not turn the cables, tighten the connections!

1. **Turn on** the VNA. The VNA program will start automatically, if it does not start press the icon on the computer screen next to the START-button. To get the graph in full screen press two times on the "Scroll Lock"-key on the keyboard.

2. **Set up the dielectric probe** system, it should look like Figure A.3. (Can also measure with the electrical calibration kit, ECAL, then you put the ECAL between the adapter and the probe. Use the black plastic thing to let the ECAL rest on it (cannot rest completely on it). If the ECAL works it will calibrate more accurate.)

3. **Start the program** on the computer (VNA) after the setup of the system above is done.
   Start the program by: Program → Agilent → 85070
   The number 85070 is the name and program of the probe.

4. Run VNA-program in the background. (Use this to see that the calibration is done correctly.)

5. Start the **calibration** in the 85070 program:

   (a) Calibration → **Configure Cal** →

      i. Calibration type: Air/short
      ii. Refresh standard type: Air (change to ECAL if the electrical calibration kit is used)
      iii. Probe type: Performance
      iv. Temperature: 19 °C (This should be the temperature of the de-ionised water that is used for the calibration)

   (b) Calibration → **Set frequency**

      i. Start frequency: 100 MHz (The probe works not so good below 500 MHz, but it is ok.)
      ii. Stop frequency: 3 GHz

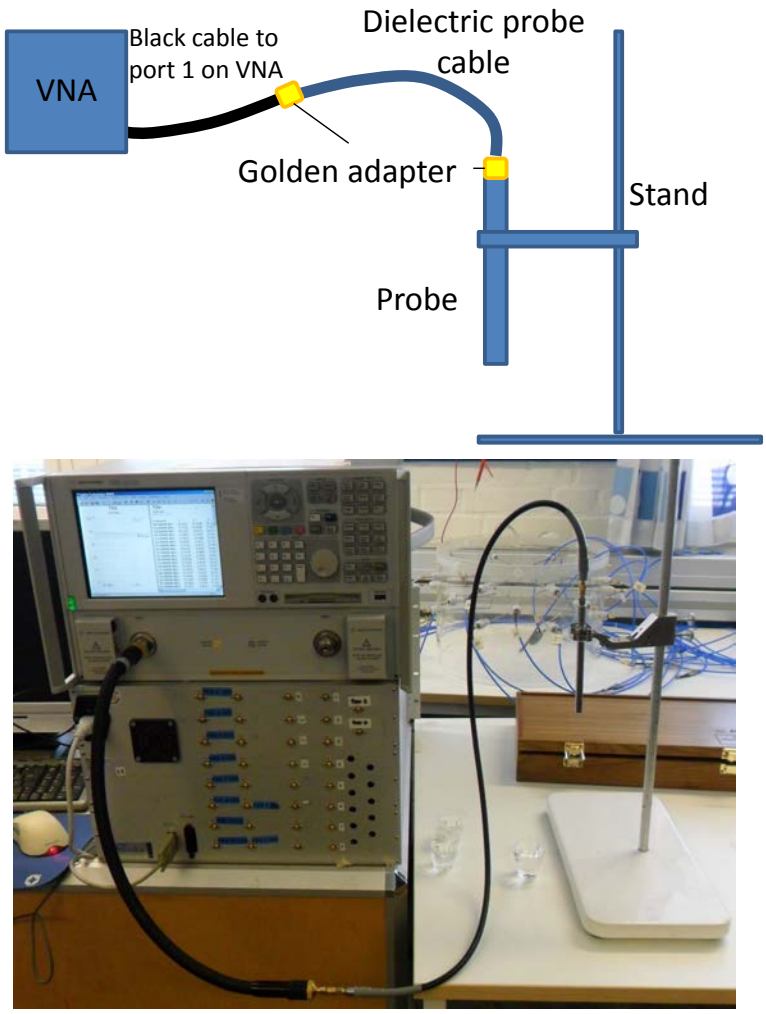

Figure A.3: Setup of dielectric probe.

iii. Number of points: 101

iv. Check the box "Set chart scale" to the right of the number of points field.

(c) Calibration → **Perform calibration**

i. First **open** is tested. The data should be on the right in the polar plot (green colour), see Figure A.4. The polar plot can be seen in the VNA program. Press OK.

ii. **Shortcut** probe by holding aluminium foil at the end of the probe. Look at the curve and press OK when the data lies

in the left part of the polar plot(red colour in Figure A.4).

iii. **Water**: Put the probe into a small cup with de-ionised water. The curve on the polar plot should look like the purple colour in Figure A.4. Press OK.

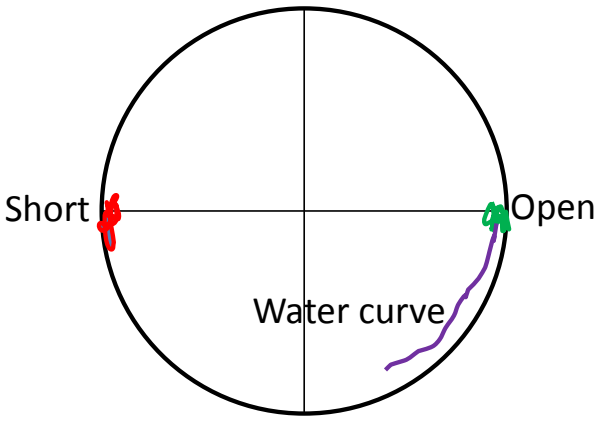

Figure A.4: Schematic polar plot for calibration.

(d) Look at the curve in the **polar plot** when you hold the water at the top of the probe and see if it measures correctly (the plot should look like the purple plot in Figure A.4).

(e) **Measure** on water, it should be an almost straight line with $\epsilon' = 80$.

i. Measure → Trigger Measurement

(f) Put the water data in the **memory**

i. Display → Data/Memory

(g) **Save data**

i. File → Save data file → Choose which one and save under disc D (in a folder with your name)

A.3 Measure with dielectric probe (Chalmers)

1. To **perform measurements** use
   (a) Measure → trigger measurement
   (b) Make sure you save the measurements.
   (c) The data can be placed on a USB-stick afterwards. (USB-connection both on the front and the back of the VNA)
   (d) Make sure you have no bubbles on the probe when you measure.
   (e) **Measure deionised in between** your measurements to see that it still looks okay. The relative permittivity of the deionised water should look like a relatively flat line at 80 over all the frequencies. Also use this to clean the probe.
   (f) **Measure liquid phantom solution**: Stir the sample before measuring to make sure it is homogeneous. Make two measurements per sample (there should be two samples), if they differ, clean the probe, stir the sample and try again.
   (g) **Measure solid phantom mass**: Press the dielectric probe into the solid phantom mass. If there is a layer of liquid on the top, remove it with a paper towel. Avoid to get air pockets in between the probe and the phantom mass. Press the sample to the probe and perform 5 measurements per slice (there should be two slices).

2. You will get the permittivity with real and imaginary parts. The conductivity, σ, can then be calculated from the imaginary part of the permittivity, ϵ'', see Equation (A.1).

$$\sigma = \omega \epsilon_0 \epsilon'' \tag{A.1}$$

   Where ω is the angular frequency and $\epsilon_0 = 8.854 \cdot 10^{-12}$ F/m.

3. Put the measured data on a USB-stick and **analyse** it in Matlab to see if it looks good compared to the desired data (the permittivity and conductivity of the real tissue) from Gabriel et al. [22].

4. At the end:
   (a) Measure water to see that you still have the same water-curve.
   (b) Clean the probe with battery water and paper so it is clean for other to use it afterwards.

A.4 Calibration of measurement equipment (Medfield Diagnostics)

How to calibrate VNA with cables to be able to measure with the MWH.

1. **Turn on the VNA**, the button is at the front left corner, behind the switch box, wait at least 1 hour before starting to measure. It is possible to have the VNA turned on for up to a week, but it will go into sleep-mode if it hasn't been used for a while.
2. Programs that should be started on the computer:
   (a) **Switch GUI**: It is a LabVIEW-file that lies on the desktop. Set the switches in the Switch GUI so the two cables and corresponding ports are connected.
      i. Green line = transmitting antenna
      ii. Blue line = receiving antenna
   (b) **NI-VNA**: Under the Start-menu, START → NI-VNA (second on the top in the menu). If it does not start, right click on it and start as an administrator.
3. **Connect all the cables** with the ports. Use the special designed torque wrench, this wrench should be used for all connections everytime they need to be tightened.
4. **Load an old calibration file** in the NI-VNA so you get the right settings. File → Recal setup → C → VNA → 20110816 (this is a good file for us to load). You only need to load the file for one connection.
5. Use a **"through"** (adapter) to connect the two cables that are going to be calibrated. It will show in the NI-VNA program when the two cables are connected. If the transmission S21 lies on 0 dB it means that it is correctly connected in the Switch GUI. (You do not need to take away the through yet.)
6. Press on **Frequency** to the right in the NI-VNA, and see that the correct frequencies are set.
7. Change **Power** on the top left to 0 dB. (Medfield Diagnostics have permission to use 0 dBm (1 mW)).
8. Perform **calibration** in the NI-VNA with the **calibration kit**, see Figure A.5.
   Calibration → Calibrate → Manual cal → choose "1 path → 2 port".

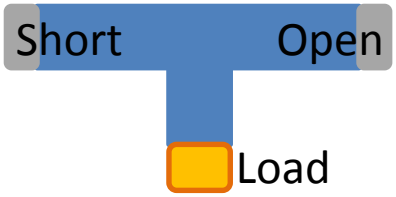

Figure A.5: Calibration kit used to calibrate the cables.

(If reflection is not needed: use "Through Update" instead of "Calibrate".)

(a) **Change the connections** in the Switch GUI to match the cables used. Redo point 5 to see if the connection in the Switch GUI is done correct.

(b) **Through**: Connect the cables with the through, put away the cables. Press on the corresponding button on the NI-VNA.

(c) Port 1 **reflection**: Connect one of the parts (short, open or load) in the calibration kit to cable 1 and calibrate (by pushing the corresponding button on the NI-VNA), do the same thing for the other two parts in the calibration kit, finish with load. Do all of this on cable 1. This part is needed only when calibrating one of the bold marked pairs in point 9. Then you should do the same thing you did for cable 1 here to the first cable number in the bold marked pairs.

(d) **Isolation**: Connect one load of 50 Ω to each of the two cable endings. Can use the load on the calibration kit for one of the cables and another load, that can be found in a box, for the other ending.

(e) Press DONE, see if it looks good on the NI-VNA. S21 should be on 0 dB when the two cables are connected with the through.

(f) If it does not look good: Press **Through Update** and see if it becomes better. It is possible to redo the calibration if it does not look good, you only have to press "Calibrate" again and redo it.

(g) **Save** when it looks good:
File → Save setup → EXJOBB (folder on the desktop) → Name the file: date_transmittingAntenna_receivingAntenna. For example: 20130204_1_2

9. **Calibrate the rest of the cables**: Redo step 8 for all the cable combinations; **1–2**, 1–3, 1–4, ..., **2–3**, 2–4, 2–5, ..., **3–4**, 3–5, 3–6, ... **12–1**, the last one is to get the reflection for cable 12. The reflection part needs to be calibrated for the bold marked pairs, but not the other pairs since they use the reflection value from the bold pairs. To calibrate the non-bold pairs, "**Through Update**" is used instead of "Calibrate".

   (a) **Switch connections** in the Switch GUI and connect the cables with the through.

   (b) Do the through update in the NI-VNA, press done and save the data as above.

10. If **only one cable** (x) needs to be calibrated, load the calibration file (1–2), do a Throug Update for cable 1–x, load the calibration file 2–3, do a Throug Update for 2–x and continue to (x-1)–x where the entire procedure needs to be done, continue with x–(x+1) and the entire procedure again, continue with Through Update for the rest of the cables but do not change calibration file.

11. When the calibrations is done: place all the **calibration files** in a folder marked with today's **date**, for example: 20130204. The date-folder should be placed in **C:\VNA**.

A.5 Preparation for measurements

The things that have to bee done before the measurements can be started.

1. **Take away** the plastic wrapping and the agar solution that has solidified outside the cranium. Try to lift in both cranium parts to avoid that they fall apart. Take away the tape that isn't needed in the eyes and over the other holes, just leave the tape that keeps the cranium together. Wipe off the cranium with a wet cloth before the measurement so it isn't so sticky. Do not turn the cranium over, there is a risk that the phantom will loosen from the cranium and air will come in between the cranium and the phantom.

2. If the upper part of the cranium is loose, add some tape around the cranium to keep it together.

3. Put **tape** over foramen magnum so the water does not evaporate.

4. Fill up the **water bags** in the MWH with some water (all the bags need to have some water in them so they don't stick together). Remove the air bubbles in the bags (it is not possible to remove all the air from the water bags).

5. Connect the **cables** to the antennas on the MWH before the cranium is placed in it. It is important which port is connected to which antenna! Follow Figure A.6. Use the special designed torque wrench to connect the cables.

   (a) Port 3 does not work, so this port needs to be terminated with a 50 Ω load.

   (b) Antenna 3 can instead be connected to port 12. The data from port 12 is normally not used since the connection between the antennas in the neck and the cranium are so bad.

   (c) Cable 8 needs to be terminated with a 50 Ω load, since antenna 8 is one of the neck antennas that have bad connection with the cranium.

6. Carefully **place** the cranium in the MWH.

7. **Hang the MWH** on a metal rod between two chairs and place a bucket with water under it, see Figure A.7. The cables have to lay still and not be stretched. It is possible to touch and move the cables after the calibration is done.

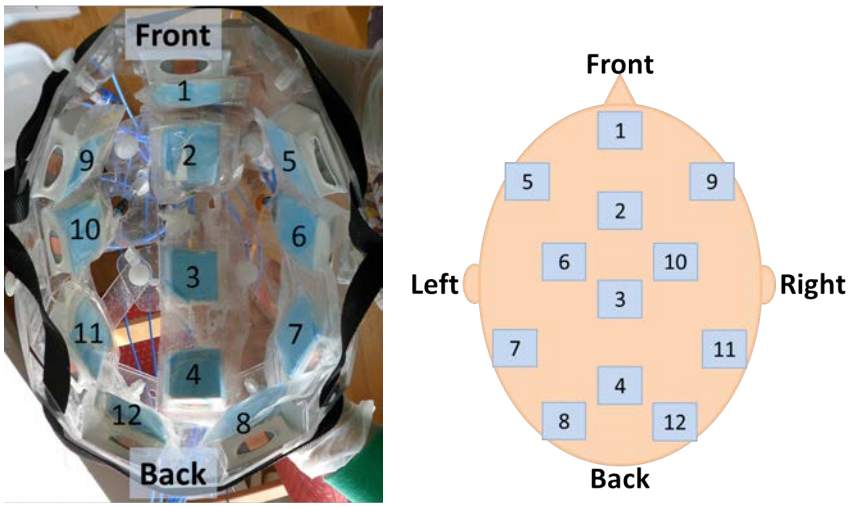

(a) Inside of the MWH with antenna numbering.

(b) Antenna placement in the MWH, seen from above.

Figure A.6: The MWH used to perform the measurements. The numbers shows the numbering of the antennas.

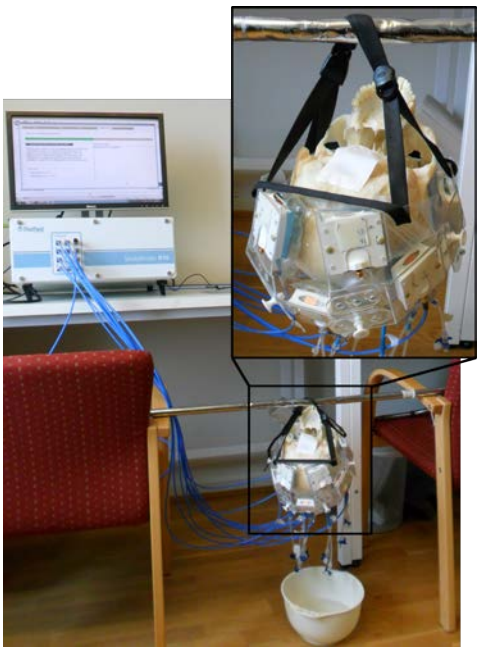

Figure A.7: Measurement setup at Medfield Diagnostics.

8. **Fill up the water bags** with water. All the bags should have approximately equal size and the cranium should lie stable in the MWH. Make sure that all the taps on the water bags are shut.

A.6 Measurements at Medfield Diagnostics

1. **Turn on the VNA**, the button is at the front left corner, behind the switch box, wait at least 1 hour before starting to measure.

2. **Change to the calibration file** that should be used: (Turn off the LabVIEW program before changing calibration file. Do not close it down, push STOP instead)

   C → Medfield SVN → LabVIEW → MedfieldConfig.ini

   (a) Change name to:
   Name = "C:\VNA\Relevant folder\Start of the file name"
   For example:"C:\VNA\20130424\20130424" (This file does not care what it says under "VNA settings", it takes all the information from the configuration file.)

3. **Turn off everything**: Turn off all the programs before starting the measurements.

4. **Open R100_Platform_Main.vi**:

   Start → LabVIEW → Medfield_R100

   R100_platform.lvclass → R100_Platform_Main.vi

   Open and run the program with the green arrow.

5. **Start Medfield Application**:

   Start → Visual Studio → Medfield Application

   Open and run the program with the arrow.

6. Check that the transmission between the antennas is not over zero, choose "Visa antenn" and look at the different antennas.

7. Choose **HJÄLM**, write comments, if any, in the program and press **Utför mätning**.

   (a) **Bekräfta**, press Ja (Yes) if everything is correct.

   (b) **Referensmätning**: Perform the reference measurements. These reference measurements are usually not used.

   (c) **Testmätning**: The test measurement tests if there are good connections with all the antennas by measuring the reflection coefficients. All antennas should get a small **"V-formed"** yellow curve in the graph, see Figure A.8. If they do not get the V-curve, then maybe the cable connections need to be tightened.

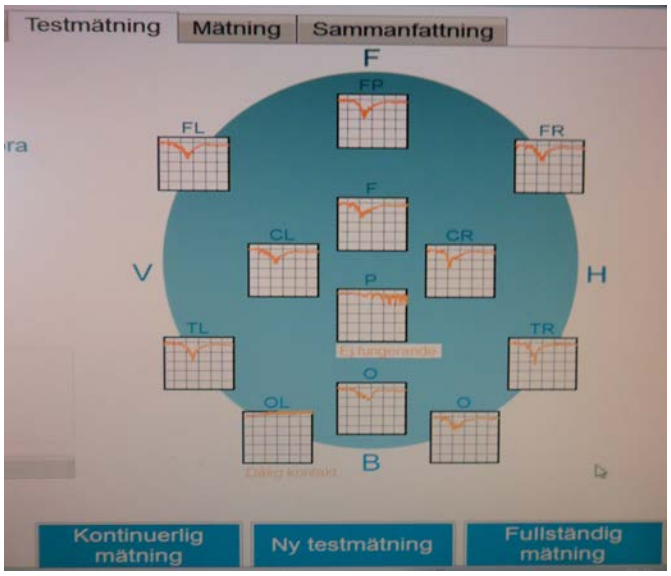

Figure A.8: Test measurements at Medfield Diagnostics, the small V-formed curves are the reflection coefficients and indicates that the connections to the antennas are good.

Antenna 3 and antenna 8 will get another curve here since they are terminated with a 50 Ω load.

(d) Choose either "**Kontinuerlig mätning**" (continuous measurement) or "**Fullständig mätning**" (complete measurement). The complete measurement measures with all the antennas one time ($\approx$ 1 min). The continuous measurement goes through all the antennas and measures over and over.

i. It can be good to write a comment during the continuous measurement if something happens.

ii. If you press "Paus/avsluta" the measurement series that is measured will continue until it is complete and then the measurements will be terminated.

iii. Stand far away from the experimental setup during the measurements to avoid interference.

iv. Better to take **Complete measurement**, since it is possible to move the cranium between the measurements then.

A. Write a note in the "Anteckningar" (notes-field) afterwards if something happened to the measurements.

B. After a complete measurement is performed press "spara anteckningar" (save the notes) and then press "ny mät-

ning" (new measurement).

C. Check out how the graphs for the antennas look. Write down if something looks weird.

8. End the measurements:

   Avsluta → Spara Anteckningar → Avsluta mätande → **Spara** resultat

   There is a short cut (2013-Shortcut) on the desktop to where the files are saved. The data is saved in a file with the date.

9. Open one of the files in Notepad and check if all values are below one.

10. Do all the measurements, see section A.6.1.

11. Put all the data on a **USB**-stick. There is a USB-port on the keyboard.

12. **Turn off** the VNA in the same way as a normal computer.

13. Analyse the data in Matlab and see if it looks good.

A.6.1 Perform measurements

1. Do the following measurements on **every phantom**:

   (a) **Ordinary measurement**: 3 x 10 measurements (lift the cranium a few cm from the MWH and put it back again between every 3 measurements).

   (b) **Hair measurements**: 3 x 10 measurements (lift the cranium a few cm from the MWH and put it back again between every 3 measurements). Take the cranium from the MWH and put the wig on it and put it back into the MWH, see Figure A.10.

   (c) **Interference of persons**: total 90 measurement, randomised. Write a note in the note field for every measurement that says which type of measurement it is (close, touching or reference). Write a note in the measurement notes document in what order the measurements come.

      i. **Person close**: 30 measurements (measure when a person stands close to the setup), see Figure A.9a.

      ii. **Holding the cables**: 30 measurements (measure when a person grips the cables ~10 cm from the switch box), see Figure A.9b.

      iii. **Reference**: 30 measurements (measure when all persons stand >1 m from the setup).

(d) **Interference of phone signal**: total 60 measurements, randomised. The person calling with the phone sits close to the setup all the time. Write a note in the note field for every measurement that says which type of measurement it is (calling or reference). Write a note in the measurement notes document in what order the measurements come.

   i. **Mobile phone call**: 30 measurements (measure when an outgoing call is made from a mobile phone close to the setup), see Figure A.9c.

   ii. **Reference**: 30 measurements (measure when a mobile phone on flight mode lies close to the setup).

(e) **Interference of movement**: total of 60 measurements, randomised. The person making the MWH move sits close to the setup all the time. Write a note in the note field for every measurement that says which type of measurement it is (shaking or reference). Write a note in the measurement notes document in what order the measurements come.

   i. **Shaking**: 30 measurements (measure when a person is moving the hanging device to make the MWH rock), see Figure A.9d.

   ii. **Reference**: 30 measurements (measure when the MWH is still).

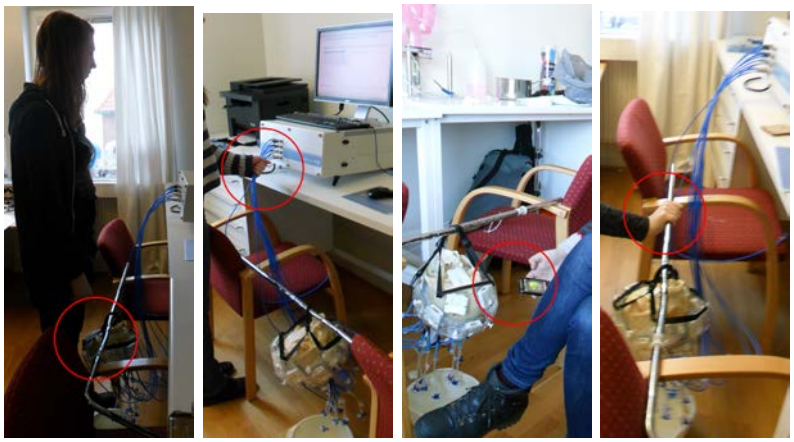

(a) Close. **(b)** Holding. **(c)** Phone. **(d)** Shaking.

Figure A.9: Different types of measurements with the MWH. A.9a: Person standing close to the MWH, A.9b: Person holding the cables, A.9c: A calling mobile phone close to the MWH during measurements, A.9d: Shaking the MWH during measurements.

Figure A.10: Cranium with wig placed in the MWH for measurement of interference from hair.

A.7 After measurements

1. Empty the waterbags in the MWH and remove the cranium.
2. Remove the tape and wipe the skull with some wet paper if it is sticky.
3. Remove the upper part of the skull.
4. Take photos of the phantom together with a ruler and a note with the date and bleeding volume/type.
5. Turn the skull upside down and shake until the phantom falls out, take some more photos.
6. Slice the phantom into 1-2 cm thick slices, make two thicker ($>$2 cm) slices, one from the front and one from the back of the phantom, without any bleeding. Wrap it carefully in plastic wrapping and mark with date and bleeding type. Save for dielectric measurements.
7. Check the phantom for air bubbles.
8. Take some more pictures of the slices where the shape of the bleeding can be seen. Take the pictures of the phantom together with a ruler and a note with the date and bleeding volume/type.

Appendix B
List of phantoms

Name in report (Our data name)	Performed measurements	Average dielectric values	Other information
Ref_0ml_1 (PhG_0226)	Ordinary (Normal) Person Phone Shake	Perm: 55 Cond: 1.5	Several air pockets
Ref_0ml_2 (PhG_0308)	Ordinary (Normal) Person Phone Shake	Perm: 58 Cond: 1.7	MWH meas. three days after production
Ref_0ml_3 (PhG_0418)	Ordinary (Normal) Phone Hair (Peruk) Shake	Perm: 51 Cond: 1.3	Might have 1 dl less sugar. Problem with antenna 1
Ref_0ml_4 (PhG_0501)	Ordinary (Normal) Phone Hair (Peruk) Shake	Perm: 48 Cond: 1.7	Bleeding with grey matter

Table B.1: Detailed list of reference phantoms in order of production. The last number in the name denotes the date it was produced. Perm and Cond denotes the relative permittivity and conductivity (S/m) of the phantom. The phantoms named Ref are the ones without bleeding, and they are numbered for identification.

Name in report (Our data name)	Performed measurements	Contrast [%]	Other information
SDH_40ml_Right (PhB40_0318)	Ordinary (Normal) Person Phone Shake	Perm: 7.73 Cond: 36.2	No problems
SDH_60m_Left (PhB60_0320)	Ordinary (Normal) Person Shake	Perm: 3.99 Cond: 37.8	Fell apart during meas. Shake values 40 dB higher
SDH_20ml_Right (PhB20_0409)	Ordinary (Normal) Phone Hair (Peruk) Shake	Perm: 23.1 Cond: 40.9	Pulpy consistency. 40 dB higher transmission
SDH_60ml_Right (PhB60_0411)	Ordinary (Normal) Phone Hair (Peruk) Shake	Perm: 23.2 Cond: 33.2	Slightly bilateral. 40 dB higher transmission
EDH_40ml_Right (PhB40_0415)	Ordinary (Normal) Hair (Peruk) Shake	Perm: 21.8 Cond: 26.7	Might have small air pocket
EDH_20ml_Left (PhB20_0417)	Ordinary (Normal) Phone Hair (Peruk) Shake	Perm: 10.0 Cond: 32.9	Leaky waterbags problem with antenna 1
SDH_40ml_Left (PhB40_0422)	Ordinary (Normal) Phone Hair (Peruk) Shake	Perm: 20.8 Cond: 34.1	No problems
EDH_60ml_Left (PhB60_0424)	Ordinary (Normal) Phone Hair (Peruk) Shake	Perm: 12.6 Cond: 36.4	Pulpy bleeding
SDH_20ml_Left (PhB20_0425)	Ordinary (Normal) Phone Hair (Peruk) Shake	Perm: 10.3 Cond: 36.0	More leakage than usual

Table B.2: Detailed list of bleeding phantoms in order of production, EDH and SDH indicates epidural or subdural bleeding, the name also include the volume and location of the bleeding. The last number in the name denotes the date it was produced. Perm and Cond denotes the difference in relative permittivity and conductivity in percent between the grey matter and blood phantom masses.